

THE EFFECT OF ANNEALING ON
MAGNETIZATION AND MAGNETOSTRICTION
IN AMORPHOUS RIBBONS

BY

SHIBENDRA SHEKHER SIKDER
B.Sc.(Hons.), M.Sc.



A THESIS PRESENTED TO THE DEPARTMENT OF PHYSICS,
BUET, DHAKA IN PARTIAL FULFILMENT FOR THE DEGREE
OF MASTER OF PHILOSOPHY.



BANGLADESH UNIVERSITY OF ENGINEERING & TECHNOLOGY

DHAKA

JULY 1988

BANGLADESH UNIVERSITY OF ENGINEERING & TECHNOLOGY
DEPARTMENT OF PHYSICS
CERTIFICATION OF THESIS WORK

A THESIS ON

"THE EFFECT OF ANNEALING ON MAGNETIZATION AND
MAGNETOSTRICTION IN AMORPHOUS RIBBONS."

By

SHIBENDRA SHEKHER SIKDER

has been accepted as satisfactory in partial fulfilment
for the degree of Master of Philosophy in physics and
certify that the student demonstrated a satisfactory
knowledge of the field covered by this thesis in an
oral examination held on 7th August, 1988.

Board of Examiners,

(1) Dr. Ali Asgar
Professor
Dept. of Physics, BUET



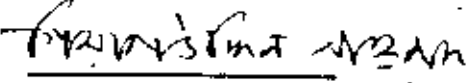
Supervisor
and
Chairman

(2) Dr. Tafazzal Hossain
Head, Dept. of Physics, BUET




Member

(3) Prof. Gias uddin Ahmad
Dept. of Physics, BUET



Member

(4) Dr. Mominul Huq
Assistant Professor
Dept. of Physics, BUET



Member

(5) Dr. A. K. Roy
Professor,
Dept. of Physics
Dhaka University, Dhaka



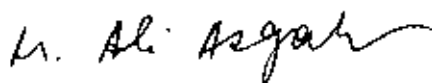
Member
(External)

538.3
1988
Sik

CERTIFICATE

This is to certify, that this work was done by me
and it has not been submitted elsewhere for the
award of any degree or for the publication.

Countersigned



Dr. Ali Asgar
Supervisor.

Signature of the Candidate



Shibendra Shekher Sikder .

ACKNOWLEDGEMENT






I would like to express my sincere thanks to Dr. Ali Asgar, Professor of Physics, Bangladesh University of Engineering & Technology, Dhaka, who gave so freely of his time to supervise this work and whose guidance, assistance and encouragement have been invaluable during the past years.

I have deep sense of gratitude to Professor Tafazzal Hossain, Head, Department of Physics, Bangladesh University of Engineering & Technology, Dhaka and Professor Gias uddin Ahmad of the same department for their encouragement and keen interest in my work.

My thanks are also due to M.A. Mazid, P.S.O. and M. Amanullah Chowdhory, P.S.O Magnetic Materials Division, Atomic Energy Centre, Dhaka, for their generous help in doing measurements of magnetization.

I am really grateful to Dr. Shaim Jahangir Ahmed, C.S.O, Mrs. Nasrin Farooque, S.O., Glass and Ceramic division, BCSIR Laboratory, Dhaka for their generous help in doing the Differential Thermal Analysis.

I  express my cordial thanks to  Dr. Mominul Haq, Dr. Nazma Zaman and  post graduate fellows of physics department, Bangladesh University of Engineering & Technology for their help in the completion of this thesis.

There are people too numerous to mention individually, whose interesting discussions have prompted much thought on various aspects, whom I would also like to thank.

Finally I record my sincerest gratitude to Bangladesh University of Engineering & Technology, Dhaka for providing me with the financial assistance during the period of this work.

ABSTRACT

Amorphous ribbons of Iron Boron prepared by melt spinning technique were studied experimentally, for their magnetization, magnetostriction and ^{to determine} the effect of annealing on these magnetic parameters. The glass transition temperature and phase transformation temperature were also determined by Differential Thermal Analysis.

A vibrating sample magnetometer was used for measuring magnetization of iron boron ribbons of different composition and thickness at room temperature to look for the composition dependence of magnetization. The sample with composition $Fe_{82} B_{18}$ was chosen for the study of magnetization process as effected by annealing and is interpreted in terms of domain reorganization by heat treatment. The effect of annealing on magnetostriction has also been measured using strain gauge and a systematic decrease in magnetostriction from its maximum value of 31.86×10^{-6} to 18.08×10^{-6} is observed. This is explained in terms of atomic ordering and domain reorganization.

C O N T E N T S

		<u>Page</u>
CHAPTER I	INTRODUCTION	1
1.1	Present Work	4
1.2	Applications of amorphous ribbons	6
CHAPTER II	REVIEW	8
2.1	Magnetostriction	10
2.2	Magnetization	11
2.3	Differential Thermal Analysis	13
CHAPTER III	THE STRUCTURE AND PREPARATION TECHNIQUE OF AMORPHOUS RIBBONS	
3.1	The structure of an amorphous ribbon	15
3.2	Preparation of amorphous ribbon	17
3.3	Melt spinning technique	17
3.4	Magnetic characteristics of amorphous ribbon	20
3.5	Experimental details of the preparation of amorphous ribbon	21
3.6	Factors contributing to glass formation	22
3.7	Examining the amorphousity	25

	<u>Page</u>
CHAPTER IV	THEORIES OF MAGNETIZATION
4.1	Magnetization of metallic glass 26
4.2	Measurement of magnetization 32
4.3	The vibrating sample magnetometer 36
4.4	Vibrating sample magnetometer coil arrangement and field distribution 39
4.5	Working procedure of vibrating sample magnetometer . 43
CHAPTER V	THEORIES OF MAGNETOSTRICTION
5.1	Physical origin of magnetostriction 46
5.2	Expression for linear magnetostriction 48
5.3	Magnetostriction in amorphous ribbon 51
5.4	Direction of linear magnetostriction 52
5.5	Magnetostriction arising from domain rotation 54
5.6	Magnetostriction measurement technique 56
5.7	Strain measurements using strain gauges 59
5.8	Gauge factor . 61
5.9	Magneto-resistance 61

CHAPTER VI	THE DIFFERENTIAL THERMAL ANALYSIS	
6.1	Introduction	63
6.2	Differential Thermal Analysis principle	63
6.3	Apparatus	66
CHAPTER VII	EXPERIMENTAL SET UP	
7.1	Experimental set up for measurements of magnetization	
7.1.1	Electronic circuits of V.S.M	71
7.1.2	Sensitivity limits	73
7.1.3	Stability tests differential measurements	74
7.1.4	Vibration amplitude	75
7.1.5	Image effects	75
7.1.6	Vibration frequency	75
7.1.7	Vibration problems	76
7.2	Experimental set up for measurements of Magnetostriction	
7.2.1	The D.C. Bridge	77
7.2.2	The D.C. Amplifier	77
7.2.3	Sensitivity and calibration of the D.C. Bridge	79
7.2.4	The choice of dummy material	81
7.2.5	The specimen holder	81

	<u>Page</u>
7.2.6 Rotator for the measurements of angular position of specimen	83
7.2.7 Specimen mounting	85
7.2.8 The gauge cementing	86
CHAPTER VIII MEASUREMENT OF MAGNETIZATION	
8.1 Calibration of the V.S.M.	87
8.2 V.S.M. Calibration data	88
8.3 Calculation of calibration constant	92
8.4 Calibration curves for magnet-1 assembly and power supply	93
8.5 Measurements of magnetization	96
CHAPTER IX MEASUREMENT OF MAGNETOSTRICTION	
9.1 Calibration curves for magnet-2	108
9.2 Bridge Circuit, sensitivity and calibration	112
9.3 Calibration curve for angle correction	117
9.4 Measurements of magnetization	120
CHAPTER X DTA RESULTS FOR AMORPHOUS IRON BORON RIBBON	132
CHAPTER XI CONCLUSION	137
REFERENCES	142

CHAPTER - I

INTRODUCTION



INTRODUCTION

The aim of this work is to investigate magnetization, magnetostriction, glass transition temperature and crystallization temperature of iron boron alloys in the form of amorphous ribbons.

The amorphous atomic structure affects all of the magnetic characteristics, e.g. the magnetization, curie temperature, temperature dependence of magnetization, magnetostriction, spin wave, magnetocrystalline anisotropy etc.

There are two technologically important classes of magnetic amorphous alloys, the transition metal metalloid alloys and the rare earth-transition metal alloys. The transition metal-metalloid alloys typically contain about 80% Fe, Co or Ni with the remainder being B, C, Si, P or Al. These materials are useful as soft magnetic materials. These amorphous alloys with high magnetizations may compete with materials used for power transformation applications. Magnetostriction is closely related to magnetic anisotropy and plays an important role in the understanding of ferromagnetic and antiferromagnetic phenomena like magnetization processes, permeability and magnetoelastic interactions. Studies of magnetostriction also have

technological utility in the production of electro-mechanical transducers, magnetostriction oscillators and filters and in removing transformer noises caused by magnetostrictive vibrations of the core.

A good deal of effort has, therefore, been made to investigate in detail, the preparation of amorphous ribbons, measurements of magnetization, magnetostriction and differential thermal analysis of amorphous ribbons and the associated difficulties in measuring these quantities. This is described in Chapter - II.

The methods of preparation of iron boron ribbon with compositions $Fe_{82}B_{18}$, $Fe_{81}B_{19}$ and $Fe_{80}B_{20}$ having special properties that can be exploited technologically is described with emphasis on melt spinning technique which was used by M.A. Asgar^(1,2) to make the amorphous ribbons, used in the present work. This is described in Chapter - III.

The variation of magnetization with the number of electrons donated by the glass forming material is listed, based on theoretical considerations. The case of boron as the glass forming material can be observed from this general relationship with iron as the base. A comparative study of the different methods of magnetization measurement is included in Chapter - IV.

The physical origin of magnetostriction and magnetoelastic co-efficients is explained from phenomenological and thermodynamic considerations. The theoretical understanding, the experimental techniques and the technological implication of magnetoelastic interaction in relation to the development of amorphous ribbons are described in Chapter-V in short.

The differential thermal analysis, principle and measurement apparatus for this are narrated in Chapter-VI. The experimental setup for measurements of magnetization and magnetostriction are discussed Chapter-VII.

The measurement of magnetization at room temperature and the study of its variation with ^{magnetic} field and annealing temperature are important for the understanding and characterisation of amorphous iron-Boron ribbons. Magnetization is measured by using a highly sensitive vibrating sample magnetometer (V.S.M). A V.S.M is used for measuring saturation magnetization of iron boron ribbons of different composition. The sample with composition $Fe_{82}B_{18}$ was chosen for the study of magnetization process as effected by annealing and is interpreted in terms of domain reorganization by heat treatment. This is reported in Chapter-VIII.

The strain-gauge technique has been used successfully for measurement of magnetostriction of amorphous ribbons with composition $Fe_{82}B_{18}$ at room temperature. Results concerning variation of magnetostriction constant with annealing temperature is reported in Chapter-IX.

The differential thermal analysis of the thin iron-boron ribbons with compositions $Fe_{80}B_{20}$ and $Fe_{82}B_{18}$ was done to find the anomalies in temperature versus time curve to obtain glass transition temperature and phase transformation temperature. This is reported in Chapter-X.

In the conclusion we would like to emphasize the fact that large gaps between theoretical and experimental results themselves exist, which demand more careful experiments in this field specially with more varied composition and temperature variation.

1.1 PRESENT WORK

The present work is aimed at the experimental determination and analysis of magnetization, magnetostriction and differential thermal analysis (DTA) of amorphous iron boron ribbon is presented.

The magnetization of thin ribbons is measured as a function of magnetic field using vibrating sample magnetometer. Magnetization is also evaluated for its dependence on annealing. The magnetization curves were obtained for samples which were annealed at different temperatures and for different durations. The effect of annealing is explained on the basis of the removal of local defects, strains, concentration gradients etc.

The problems associated with strain gauge technique as applied to thin magnetic ribbons are discussed. Magnetostriction measurements as a function of applied field are evaluated for its dependence on annealing to see the effect of heat treatment on the domain structure affecting magnetostriction.

The differential thermal analysis of the thin ribbon was taken to find the anomalies in the temperature versus time curve at the curie temperature, glass transition temperature and crystallization phase transformation.

There are four phases in our work. These are as follows :

(a) Development and calibration of equipment which include.

- (i) Setting and calibration of an electromagnet.
 - (ii) Construction of a DC Bridge.
 - (iii) Construction of a specimen holder
 - (iv) Construction of a Rotator for the measurements of angular position of specimen.
 - (v) Calibration of vibrating sample magnetometer.
- (b) Measurement of magnetization using vibrating sample magnetometer. —
- (i) As a function of field at room temperature.
 - (ii) As a function of field for different specimens annealed at different temperature.
- (c) The use of strain gauge technique for the measurements of magnetostriction of Amorphous iron-boron ribbons.
- (i) Measurements as function of field at room temperature.
 - (ii) Measurements due to the effect of annealing.
 - (d) Differential thermal analysis

1.2 APPLICATIONS OF AMORPHOUS RIBBONS

The absence of crystallinity, lack of grain boundaries and line defects and also its chemical homogeneity provide metallic and chemical properties that can be technologically exploited.

Iron-base, copper-base and titanium base amorphous ribbon and exhibit strengths in excess of those exhibited by forged materials. Amorphous ferromagnets have interesting magneto-elastic coupling and magnetic softness due to absence of crystalline anisotropy. Glassy metals are unusually ^{corrosion} free because of the absence of local electrochemical potential difference. Thus by a recently developed technique called laser glazing, surfaces of expensive metallic equipments are made amorphous to avoid corrosion. Amorphous ribbon has many other refined applications like development of magnetic bubbles for computer memory, amorphous super conductors etc.

Research in the development and application of amorphous ribbon can thus be profitable, specially at its present new phase.

CHAPTER - 11

REVIEW

REVIEW

It was believed for many years that because of the lack of atomic ordering ferromagnetism could not exist in amorphous solids. However, in 1960 Gobrecht^(2.1) predicted the possible existence of ferromagnetic ordering in non-crystalline solids on the basis of theoretical analysis. The first report of an amorphous metallic alloy appears to have been made by Brenner^(2.2). The present interest in amorphous metals research stems from reports by Duwez^(2.3) on the preparation technique of amorphous metallic alloys. Miroshnichenko^(2.3) and Salli^(2.4) almost simultaneously reported a device for preparing amorphous materials spreading alloy samples in liquid stage between two mutually approaching pistons. The theoretically expected ferromagnetic behaviour in amorphous solids was first demonstrated by Mader^(2.5) and Nowick^(2.5) in their works on vacuum deposited Co-Au alloys.

A real technological interest developed after Pond^(2.6) and Maddin^(2.6) reported on the preparation of continuous ribbons of amorphous alloys. Amorphous alloys of Fe-Ni-P-B prepared by the melt-quenching technique into ribbons by solidification on the surface of a rapidly rotating drum exhibited even lower coercivities of the order of 8 A/m.

In the past few years there have been a large contribution to both theoretical and experimental results on amorphous magnetic alloys. Many series of alloys have now been reported which are composed of transition metal alloys with a wide variety of metalloids.

Zero magnetostrictive alloys have been reported in Fe-Co system. The study of the effect of the electron donor characteristics of the metalloids on magnetization and curie temperature have led to the development of high moment and high curie temperature alloys. The studies of the mechanisms responsible for the low temperature embrittlement and magnetic anneal instability have led to the prediction and preparation of alloys of appropriate compositions possessing greatly improved stability. By annealing amorphous alloys of different compositions these materials have been demonstrated to have dynamic losses, permeabilities and magnetizations, which make them competitive in quality to existing commercial alloys. The magnetic and structural stability of these alloys have been evaluated at higher temperature's and found to be adequate for most foreseeable applications.

Increased attention is being given to the production of wide ribbons and the preparation of alloys for particular applications and for understanding the origin of the

extrinsic properties. These are important for the practical applications of magnetic materials and for evaluating and understanding the longterm stability of these alloys.

2.1 MAGNETOSTRICTION

The literature on magnetostriction of amorphous alloys is not very extensive. Simpson^(2.7) and Brambley^(2.7) prepared $Co_{91}P_9$ by electrodes deposition and reported a value of linear magnetostriction of -4.3×10^{-6} , for the as deposited alloy. This value of magnetostriction increased on annealing with out destroying the amorphous nature of the material.

The single phase crystalline alloy developed by further annealing had a value for λ of -11×10^{-6} Sherwood^(2.8) reported on the magnetostriction within the ternary region of the transition metals for roller quenched amorphous ribbon with composition $(Fe-Ni-Co)_{75}P_{16}B_6Al_3$. A zero magnetostrictive composition occurred at $(Fe_{0.04}Co_{0.96})_{75}P_{16}B_6Al_3$. This has approximately $\lambda = 0$ in crystalline alloys i.e Fe_8Co_{92} . Magnetostriction was also studied by Arai^(2.9) in three series of amorphous alloys $Fe_{80-x}Ni_xP_{13}C_7$ ($0 \leq x \leq 40$), $(Fe_{1-x}Co_x)_{80}P_{13}C_7$ ($0 \leq x \leq 0.7$) and $(Fe_{1-x}Co_x)_{75}S_{15}B_{10}$ ($0.75 \leq x \leq 1$). In

these ribbons the values of λ_s were found to be not quite isotropic. The value of λ_s decreased nearly monotonically with increase in Ni from 31×10^{-6} for $Fe_{80} B_{13} C_7$ to 15×10^{-6} for $Fe_{40} Ni_{40} P_{13} C_7$. In the Fe - Co system the magnetostriction went through zero near 96 at % Co. The magnetostrictions of the complete series of $(Fe - Ni)_{80} B_{20}$ and $(Fe - Co)_{80} B_{20}$ amorphous alloys were also reported by O'Handley. However the effect of annealing on these alloys has not been studied. O'Handley has discussed the possible origin of magnetostriction in amorphous alloys. The preparation of the amorphous ribbons of the complete series of Fe-B and Gd-Y-Ag systems was reported by M.A. Asgar^(2.11). The samples prepared by him have been used in the present work.

2.2 . MAGNETIZATION

The literature on the saturation magnetization of a material at a temperature of $0^\circ K$ is one of its basic properties. Measurements are usually expressed as average moment in units Am^2/Kg . A brief discussion of this approach, applied to amorphous alloys, may be obtained from Alben^(2.12) which follows from ideas of local chemical bonding. In atomic states of high spin the magnetic systems have low electron-electron coulomb repulsion energies. Apparently a small amount of impurity was necessary to stabilize the strong ferromagnetism in the amorphous $FeSi$ reported by Felsch^(2.13). But this was not confirmed by the results of Shimada and Kojima^(2.14).

wright^(2.15) has recently reviewed the status of the information available on pure' amorphous elements. Becker^(2.16) studied the moment and curie temperature of amorphous alloys of $(\text{Fe} - \text{Ni})_{80} (\text{P} - \text{B})_{20}$. The reduction in moment is greatest for $-P_{14} B_6$. Less for $-P_{13} B_8$ and least for $-B_{20}$ alloys.

The results for $\text{Fe}_x \text{Ni}_{1-x} P_{13} B_8$ reported by Durand^(2.17) show a pronounced change in slope. A very detailed investigation of the moment and curie temperatures of amorphous alloys in the entire accessible region of Fe-P-B alloys was reported by Durand and Young^(2.18). The magnetic moments for a wide variety of transition metal - alloys with $-P_{10} B_{10}$ glass formers are reported in the work of Mizoguchi^(2.19). The room temperature saturation magnetization is of more practical importance. The effect of additions of the transition metal to amorphous Co-SiB is observed by Fujimori^(2.20). The number of electrons donated can be listed as $-P_{13} C_7 > -S_{15} B_{10} > -P_{16} B_6 Al_3 > -P_{14} B_6 > -Si_9 B_{13} > -B_{20}$ based on the relative magnitudes of M_s . The effect of pressure on the moment of amorphous iron alloys was reported by Mizoguchi^(2.21). Such an approach has been described by Harris^(2.22) and by Gubernatis and Taylor^(2.23).

In the second approach to treating this problem a distribution of exchange integrals is assumed in order to reflect the structural fluctuations in the amorphous alloys. This approach has been developed by Handrich^(2.24), Kobe^(2.25), Montgomery^(2.26), Kaneyoshi^(2.27), Richter^(2.28) and Yamada and Wohlfarth^(2.29). Both approaches predict that the $\ln VST$ curve will fall below that for the crystalline counterpart.

2.3 DIFFERENTIAL THERMAL ANALYSIS

The DTA technique was first suggested by Le Chatelier^(2.30) in 1887 and was applied to the study of clays and ceramics. The study of thermal behaviour of carbonising materials by DTA was first introduced at the 4th carbon Conference by Nakamura and Altas^(2.31). DTA is the process of accurately measuring the difference in the temperature between a thermo-couple embedded in a sample and a thermo-couple in a standard inert material such as aluminium oxide while both are being heated at the uniform rate. The nematic mesophase has been considered by Brooks and Talor^(2.32), Dubois^(2.33) et al, Honata^(2.34) et al, and Marsh^(2.35) et al in their studies on carbon production.

The crystallization temperature of amorphous $Fe_{80}B_{20}$ has been studied by calorimetric method by

Luborsky^(10.4) and others used the same principle to look for curie temperature, glass transition temperature and crystallization phase transition in our DTA. Curie temperature could not, however, be observed because of the low sensitivity and small magnetic specific heat.

The study of DTA results for the amorphous thin iron Boron ribbon was taken to find the temperature Vs time curve. Received at the curie temperature, glass transition temperature and crystallization phase transformation temperature.

CHAPTER - III

*THE STRUCTURE AND PREPARATION
TECHNIQUE OF AMORPHOUS RIBBONS*

3.1 THE STRUCTURE OF AN AMORPHOUS RIBBON

The details of the magnetic properties and structures of Amorphous alloys have been given by Cargill^(3.1) and also a detail discussion is given by Asger^(3.3).

Structure can be discussed on many levels. For example, in terms of the external size and shape of the solid; in terms of cracks, voids, inclusions, Composition gradients and other heterogeneities resolvable by optical microscopy or other technique.

An amorphous material is analogous to a frozen-in liquid structure, there is no periodicity in the arrangement of atoms, although there may be some short-range order in the sense that certain values of the interatomic distance are more common than others. However, a metallic glass is distinct from a liquid and solid, because of its deviation from thermodynamic equilibrium while both melt and its corresponding crystalline phase have minimum free energy. An amorphous material because of its non-equilibrium state is at a higher values of free energy.

occurs as the crystals become progressively smaller.
data due to the well-known line broadening effect which
these models is still not possible by x-ray diffraction
recently. However, an unambiguous differentiation between
between the above two models have also been considered
"Noncrystallographic Cluster" model intermediate

liquid like fashion.
model in which the atoms are packed in a continuous
The other one is the Topologically disordered

regions.
at random, providing no surface to the microscopic
grain polycrystalline system in that, these are oriented
this micro crystalline model is distinct from the fine
the order of 15 Å in which the atoms are ordered. However,
In this model it is assumed that there are regions of
One is microcrystalline or nano-crystalline model.

metallic glass.

Two basic models are usually used to describe
equilibrium configuration become inaccessible.
internal equilibrium can no longer be maintained and the
and relaxation time increase to the point where the
When a melt is cooled too rapidly, its viscosity

As shown in a schematic diagram in Fig. (3.1), the melt spinning technique apparatus consists mainly of a copper roller, the induction heater and crucible.

3.3 MELT SPINNING TECHNIQUE

Although the different methods used in preparing amorphous metallic ribbons are mentioned here, only the melt spinning technique which was used (3.3) to prepare the specimens for the present work will be discussed.

- (a) The twin roll technique
- (b) The melt spinning technique
- (c) The melt extraction technique

The other techniques are: process. The other techniques are: of melt include gun technique use of hammer and anvil The methods using the principle of fast cooling

- (a) Electrodeposition
- (b) Chemical deposition and
- (c) Deposition by sputtering

The atomic deposition methods include condensation of a vapour on a cooled substrate by

- i) The atomic deposition methods
- ii) The fast cooling of the melt

The different experimental techniques developed to produce metallic glass can be grouped under

3.2 PREPARATION OF AMORPHOUS RIBBON

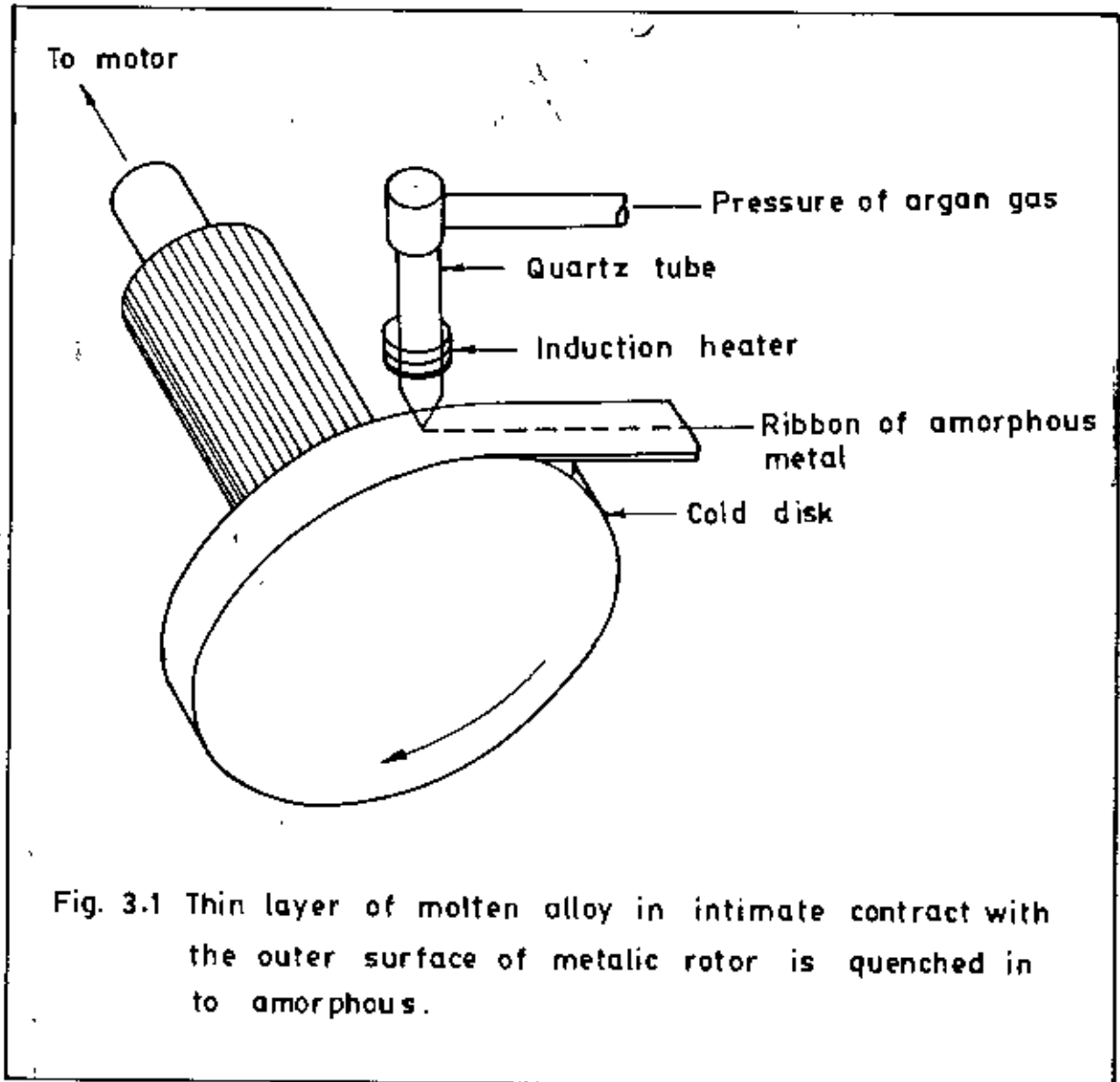


Fig. 3.1 Thin layer of molten alloy in intimate contact with the outer surface of metallic rotor is quenched in to amorphous.

The roller was driven by a variable speed motor via a tooth belt. The angular velocity could be varied in the range 0 - 2000 rev./min. Use of log wheel rotation enable one to vary the surface velocity continuously from 10 to over 60 ms^{-1} . The diameter of the copper for the roller material was chosen for its good conductivity and mechanical softness, which allowed cleaning and polishing to be carried out easily. For room temperature work, it showed no contamination of the ribbon from the roller material and the careful preparation of the surface was more important than the material of the roller.

In this process one has to consider that vibration of the roller should be well below the high frequency vibration of the melt puddle to avoid any influence of it on the geometry and uniformity of the ribbon. One has to be careful to see that the ribbon does not remain in contact with the surface of the roller for a whole revolution and be hit, from the back, A bigger diameter is thus preferred for the roller. The induction heater coil is made of hollow copper tubing which is cooled simultaneously by circulating water through its inner hole. The shape and diameter of the induction heater as also its winding is to be adjusted to produce proper temperature gradient.

This is to avoid, sudden cooling of the melt in its way out of the crucible and blocking the nozzle. The crucible used is made of quartz tubing having outer diameter 10 mm and narrowed down conically to 0.9 to 1.0 mm hole for the nozzle. The nozzle geometry is selected to minimize the contraction in the cross-sectional area of the molten jet as it leaves the nozzle orifice. Quartz crucible is suitable for repeated use in several successful runs and should be transparent to make the melting process visible. It should withstand the sudden fast changes in temperature.

3.4 MAGNETIC CHARACTERISTICS OF AMORPHOUS RIBBON

The intrinsic properties of amorphous ferromagnets are still not quantitatively understood. The basic problem is to incorporate the existing theoretical approaches the structural distribution of atoms in the glassy state, for example, in the radial distribution function of atoms. The intrinsic properties of amorphous ribbon are magnetic moment, curie temperature and magnetostriction and the extrinsic properties are coercive force, remanence-to-saturation ratio permeability, losses as a function of frequency. These magnetic properties can all be understood using the same underlying physical principles as applicable to crystalline alloys with appropriate modifications to take into account the differences in structure and composition.

3.5 EXPERIMENTAL DETAILS OF THE PREPARATION OF AMORPHOUS RIBBON^(3.3)

The amorphous ribbons are prepared in an Arc-furnace in an argon atmosphere. The buttons prepared are about 12 grams each. Care is taken to ensure thorough mixing and homogeneity of the alloy compositions, by turning over and remelting each button few times.

The mother alloys which are formed in the form of buttons in an arc furnace are cut into small pieces and is introduced in the crucible. The crucible is connected from the top by rubber 'O' rings and metal rings to the argon cylinder through a valve and a pressure gauge.

After proper cleaning of the roller surface and adjusting its speed to the desired value, as measured by stroboscope, the induction furnace is powered. When the melting temperature is reached as observed through a protective spectacle, the injection pressure is applied by opening the pressure valve. To avoid the turbulence of the wind, arising from the high speed of the roller in disturbing the melt puddle, cotton pad and metallic shield are usually used just beneath the roller. To avoid oxidation of the ribbon during its formation an inert atmosphere can be created around the roller by a slow stream of helium gas.

The speed of the roller, the volumetric flow rate, the orifice diameter, the substrate orifice distance, the injection angle etc. are adjusted by trial and error to get the best result in respect of the quality and the geometry of the ribbon.

3.6 FACTORS CONTRIBUTING TO GLASS FORMATION

There are three interrelated factors that determine glass forming tendency. These are thermodynamic conditions that favour the liquid phase relative to the crystalline phase, the kinetic conditions that inhibit crystallization and the process factors that arise due to experimental conditions.

The thermodynamic factors for glass formation are liquidus temperature, T_m at which the alloy melts, the heat of vaporization and the free energy of all the phases that arise or could potentially arise during solidification process. Viscosity of the melt the glass transition temperature T_g and the homogeneous nucleation rate belonging to kinetic parameters. The glass transition temperature is defined as the temperature at which the supercooled liquid takes on the rigidity of a solid, or more specifically at which the viscosity approaches 15 poise.

Processing parameters are the cooling rate, the heterogeneous nucleation rate and the supercooling temperature interval. The temperature of the glass transition is slightly dependent on the cooling rate. For each cooling rate the glass will freeze in a different state of internal energy. This is shown in Fig.(3.2).

At the melting point T_m , the enthalpy H of a crystal includes latent heat of fusion due to long range order and that due to short range order. In the case of rapid melting the energy decreases since long range order do not take place, thus leaving the system at a higher energy state. Heat treatment, relaxation and stability are thus important consideration in metallic glass. The glass forming tendency also arises from as size difference between the constituent elements. It appears that appreciable size difference between the components in the glassy alloy is necessary condition for ready glass formation.

A single parameter that expresses glass forming tendency is the ratio of the glass transition temperature to the melting temperature defined as

$$T_{gr} = \frac{T_g}{T_m}$$

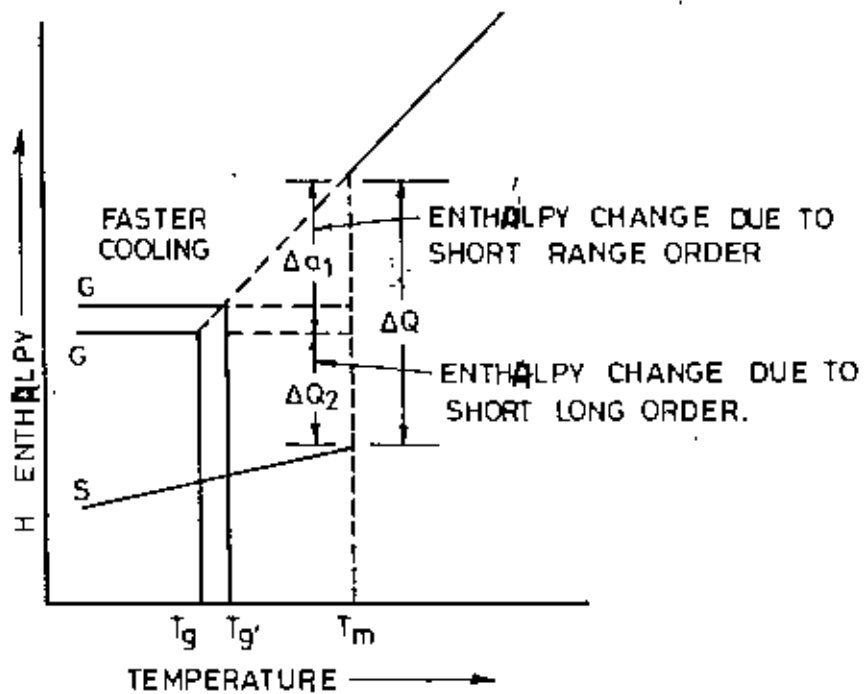


FIG 3.2 TEMPERATURE DEPENDANCE OF ENTHALPY
 H G & G' corresponds to glass & S
 CORRESPONDS TO CRYSTALLIN STATE.

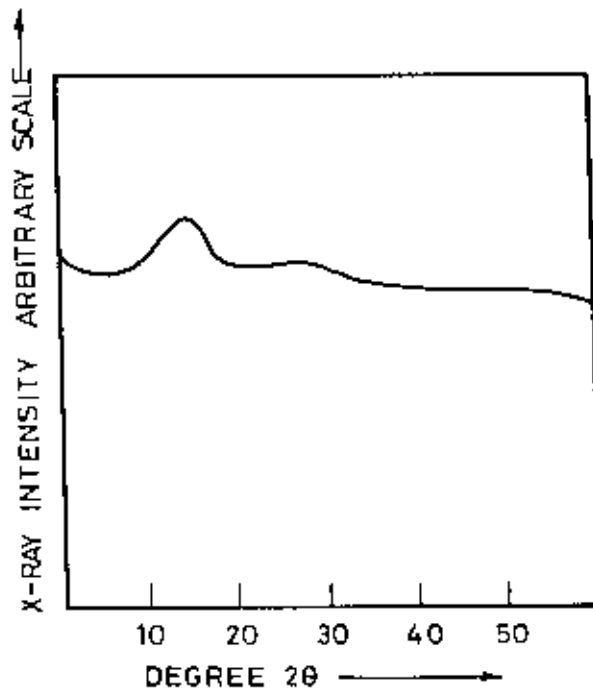


FIG.3.3 X-RAY DIFFRACTION FROM THE TOP SURFACE
 OF $Fe_{80}B_{20}$ AMORPHOUS RIBBON.

Higher values of T_{gr} obviously favour glass formation. For metallic glass to be formed by rapid cooling, T_{gr} should be greater than 0.45. Based on alloy compositions there are two major groups that readily form glasses. In one of these groups the metal is from Fe, Co, Ni, Pd or Pt and the metalloid is B, C, Si, Ge or P. These metallic glasses constitute soft amorphous magnetic materials. Our working sample prepared from Fe-B system belongs to this metal-metalloid group.

3.7 EXAMINING THE AMORPHOUSITY

The amorphous nature of the melt spun ribbons of Fe-B systems is checked by X-ray diffraction using $Cu K_{\alpha}$ radiation. It is observed that the ribbons showed broad diffraction maximum and no low angle scattering. These ribbons were also ductile and could be bent without breaking.

In these cases for which low angle scattering did appear and the broad diffraction peak are subdued showing the presence of micro crystalline phase, the speed of the roller is increased. This however, produces thinner ribbons. The nature of the broad diffraction peak as observed is shown in Fig.(3.3).

CHAPTER - IV

THEORIES OF MAGNETIZATION

4.1 MAGNETIZATION OF METALLIC GLASS

The theoretical treatment of spin ordering in amorphous solids is quite complex. The topological disorder on the amorphous alloys, affect the magnetic moment of the transition metal atoms, because of the change of environment of each magnetic atom. The exchange integral also varies at each point because of the varying interatomic distance and the overlap of the electronic wave functions. The third factor determining the magnetization processes is the single ion magneto-crystalline anisotropy, which also changes because of the changing crystalline field. However, the magnetization of amorphous alloys is computed by introducing some drastic simplifying assumptions which are applicable in regular crystalline lattices. If the molecular field approximation is used, even though its use is doubtful, the paramagnetic curie temperature can be expressed as

$$T_c = \left[\frac{2s(s+1)}{3k} \right] \sum_{ij} J_{ij} \dots (4.1)$$

where s is the spin number, k is Boltzmann's constant and J_{ij} is the exchange interaction between atoms at the position r_i and r_j and can be expressed in terms of the radial distribution function.

Mizoguchi^(4.1) has reported the exchange interaction term in equation (4.1) for various crystalline and amorphous alloys. For $\text{Co}_{80}\text{B}_{10}\text{P}_{10}$. Taking into account the change in spin $S_{(\text{cryst.})} = 0.86$ and $S_{(\text{amorp.})} = 0.5$

We can write
$$\frac{J_{ij}(\text{amorp.})}{J_{ij}(\text{cryst.})} = 1.1$$

Assuming only the short-range exchange interaction neighbor Co atoms seems to be the same in both pure $\left(\begin{smallmatrix} h \\ cp \end{smallmatrix}\right)$ Co and in the amorphous alloy, since the co-ordination number is almost the same in both case, i.e $Z = 12$. However this is not the case for Fe For $\text{Fe}_{80}\text{B}_{10}\text{P}_{10}$.

$$\frac{J_{ij}(\text{amorp.})}{J_{ij}(\text{cryst.})} = \frac{12J(\text{amorp.})}{8J(\text{cryst.})} = 0.7$$

The nearest neighbor interaction J is estimated to be roughly half in the amorphous Fe compared to that in pure bcc Fe, taking into account the difference in co-ordination number.

The saturation magnetization of a material at a temperature of 0°K is one of its basic properties. The moment of most amorphous alloys are lower than those of the pure crystalline transition metals. The direct effect of the structural disorder on the moment is ~~considered~~ considered to be very small according to Gubanov^(4.3).

Metallic glasses are rather poor conductors¹ but their 3d electrons are just as "itinerant" as in crystalline transition metal alloys. The moment of the transition metal decreases linearly with additions of metalloids; approximately $3\mu_B$ for each P-atom, $2\mu_B$ for each Si or C atom and $1\mu_B$ for each B atom. The result for the amorphous cobalt alloys all appear to follow approximately linearly as expected. The behaviour of the amorphous iron alloys is very different. Apparently a small amount of impurity was necessary to stabilize the strong ferromagnetism in the amorphous FeSi reported by Felsch^(4.4), but this was not confirmed by the results of Shimada and Kojima^(4.6). Wright^(4.6) has recently reviewed the status of the information available on 'pure' amorphous elements. In all cases it appears that the saturation moment is the same or less than its value in the crystalline state.

The magnetic moment of the transition metal (TM) atoms in the general amorphous alloys $(TM)_{1-z-y}F_zG_y$ to be expressed as

$$\mu = [m(1-z-y) - fz - gy] / (1-z-y) \dots (4.2)$$

or for the moment per atom of alloy as

$$\mu = m(1-z-y) - fz - gy .$$

Where F and G represent the metalloids or glass forming atomic species, m is the original number of unpaired spins in the transition metal alloys, f and g are the number of electrons transferred from the F and G atoms respectively.

Using the rigid band model with the transition metal alloy compositions and assuming $\mu_{Ni} = 0.6$ Bohr magnetons $\mu_{Fe} = 2.1$ Bohr magnetons and assuming that each phosphorus atom reduced the moment by 1.0 and each boron by 0.3 Bohr magnetons, the moment per atom of alloy found out to be

$$\mu = 2.1x + 0.6b - 1.0z - 0.3y \dots (4.3)$$

in Bohr magnetons. The model was proposed by Becker^(4.7).

For our iron Boron composition $Fe_{0.82} B_{0.18}$ by using the same model, we find

$$\begin{aligned} \mu &= 2.1 \times 0.82 - 0.3 \times 0.18 \\ &= 1.722 - 0.054 = 1.668 \text{ Bohr magneton.} \end{aligned}$$

The room temperature saturation magnetization is of more practical importance. These are shown in fig.(4.1) for a variety of alloys as a function of composition for transition metals. The effect of the transition metal

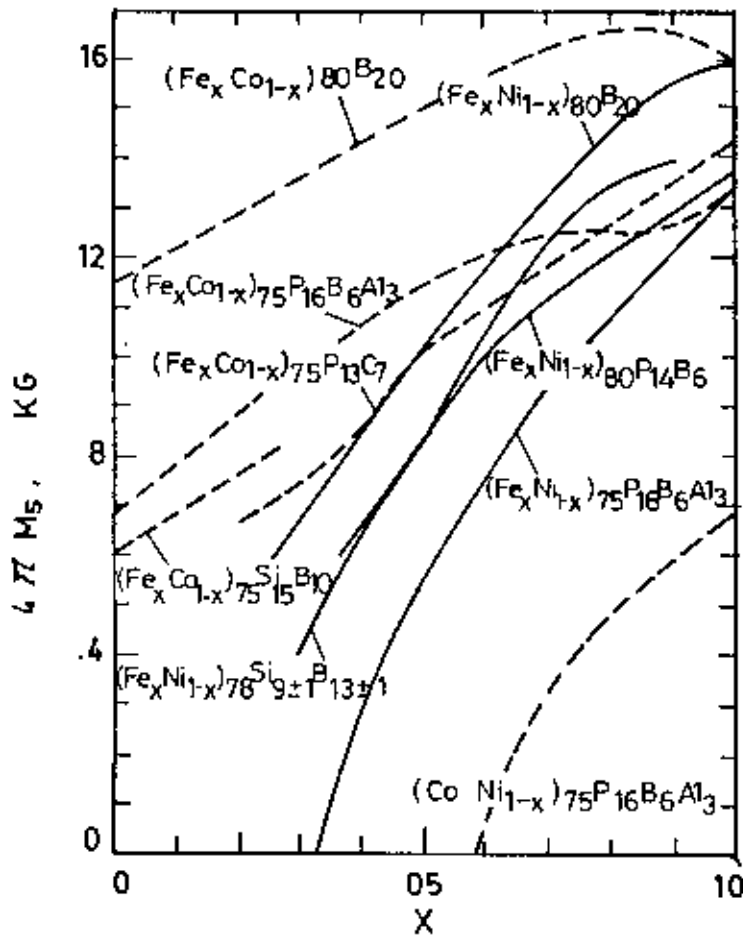


Fig. 4.1 Saturation magnetization at room temperature as a function of composition for Fe-Co-Ni amorphous alloys. FeNiRB Becker et al. (1977); FeNiSiB Masumoto et al. (1977); FeNiB FeCoB O'Handley et al. (1976a; 1976b); FeCoPC, FeCoSiB Fujimori et al. (1976b); CoNiPBA1, FeCoPBA1, FeNiPBA1 Gyorgy et al. (1976).

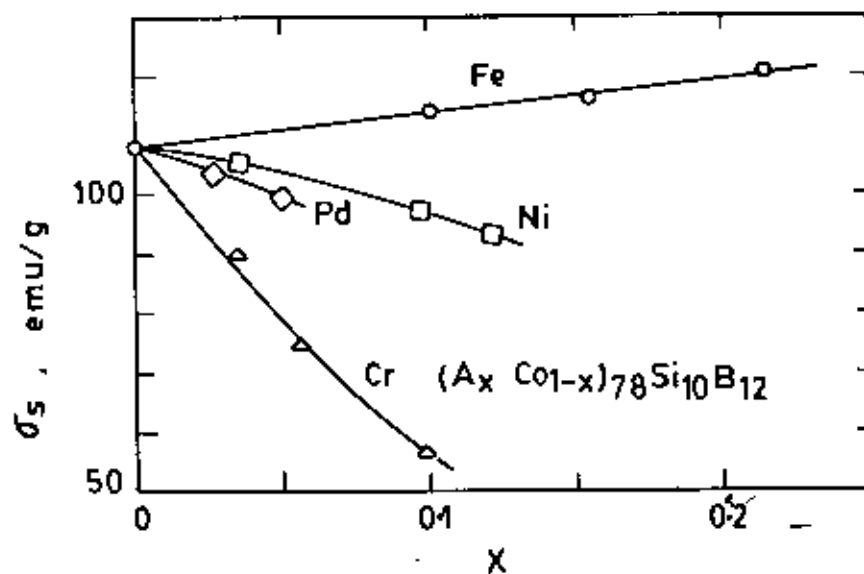


Fig.4.2 Saturation magnetization per gram at room temperature for some amorphous - SiB alloys, Fujimori et al. (1977).

additions to amorphous Co-Si-B is shown in Fig.(4.2). from Fujimori (4.8). The relative number of electrons donated can be obtained from Fig.(4.1). The number of electrons donated can be listed as

$$\begin{aligned}
 & \sim P_{13}C_7 > \sim S_{15}B_{10} > \sim P_{16} B_6 Al_3 > \\
 & \sim P_{14}B_6 > \sim Si_9 B_{13} > \sim B_{20} > \sim B_{18}
 \end{aligned}$$

based on the relative magnitude of magnetization.

4.2 MEASUREMENT OF MAGNETIZATION

The usual methods of measuring magnetic moment can be divided into three major classes.

- i) Measurement of a force on a material in a non-uniform magnetic field.
- ii) Measurement of magnetic induction in the vicinity of the sample.
- iii) Indirect measurements of phenomena which involve the magnetic properties.

In the Force method, the change in Force exerted on the sample in a magnetic field is measured using a sensitive balance. This includes Goucy method, Faraday method and Torsion pendulum using force method. It is of course, difficult to observe the magnetization in a truly uniform magnetic field, since the field gradient

is essential for the production of the force. Moreover, this method is not easily adaptable to routine measurements of magnetization versus applied field for crystals with magneto crystalline anisotropy.

Objections to the use of force methods for magnetic measurements of highly anisotropic materials have recently been raised by wolf^(4.9).

There are various methods for the measurement of magnetization by the indirect methods. These include measurements using the Faraday effect, analysis of galvanomagnetic effects, ferromagnetic resonance measurements etc. The advantage and disadvantage of indirect measurements are illustrated by microwave ferromagnetic resonance experiments where by the magnetization may be obtained from a detailed knowledge of the sample shape.

The general problem of indirect techniques is that they are limited to particular phenomena which are observable in a limited class of materials about which considerable prior knowledge is required.

Despite many limitations in particular instances these indirect techniques are capable of extremely high sensitivity.

All the magnetic induction measurements involve observation of the voltage induced in a directional coil by a flux change when the applied magnetic field, coil position or sample position is changed. Recently, oscillatory coil or sample techniques have been used to observe the magnetization of a sample by an ac method. All of these techniques have employed an arrangement in which the detection coil is symmetrically distributed about the sample with the axis of the detection coil parallel to the applied magnetic field. One major disadvantage of such a method is that unless an air-core solenoid type magnet is used the usual laboratory magnet must be extensively modified. The most convenient arrangement is to drive either the sample or the detection coil with a vertical rod, which passes between the pole faces of the magnet. The vibrating coil technique has been developed by D.O. Smith (4:10) and this technique has been used by M.A. Mazid and M.A. Chowdhury (4:11) to build the present V.S.M. in AECB which all have used.

In the vibrating sample magnetometer, the sample is vibrated perpendicular to the field direction. The flux change induces an e.m.f. (signal) proportional to the magnetization of the sample in two pick-up coils placed symmetrically on either side of the sample and connected in series to add up the e.m.f.'s. The axes of

the coils are parallel to the direction of vibration of the sample. A reference signal is obtained by vibrating a permanent magnet of known magnetic moment inside a coil with the frequency and amplitude similar to the sample. Then the reference signal is brought in phase with the sample signal and divided using a decade divider and compared in a null-detector, i.e lock-in amplifier.

The magnetic moment produced by a current I through the primary coil is given by

$$\mu = \pi r^2 N_1 I \dots\dots\dots (4.4)$$

Where r is the radius of the primary coil and N_1 is the number of turns.

The flux through one of the secondary coils of radius R and at a distance Z from the dipole is given by

$$\begin{aligned} \phi &= \frac{\mu_0 \mu}{4\pi} \int_0^R \left[\frac{3Z^2 x}{(Z^2 + x^2)^{5/2}} - \frac{x}{(Z^2 + x^2)^{3/2}} \right] 2\pi dx \\ &= \frac{\mu_0 \mu}{2} \frac{R^2}{(Z^2 + R^2)^{3/2}} \dots\dots\dots (4.5) \end{aligned}$$

The induced e.m.f. in the secondary coils (N_2 turns) in add-up configuration is given by

1) The magnetic sample vibrates perpendicular to the applied field.

short is as follows :

The principle of vibrating sample magnetometer is

4.3 THE VIBRATING SAMPLE MAGNETOMETER

sample.

Thus current is a measure of the magnetization of the sample signal to the primary of the reference signal coil. The device which sends a current proportional to the amplifier is fed to a proportional integrating differentia-current range and compare the sample signal in a lock-in divided in a decade transformer to obtain a suitable angular frequency of vibration. The reference signal is ΔZ_0 is the amplitude of vibration and ω is the

$$Z = Z_0 + \Delta Z_0 \sin \omega t \dots \dots \dots (4.7)$$

coil is given by

where the instantaneous position of the primary

$$= \frac{2}{3} \mu \mu_0 R^2 z_0 \omega^2 \cos \omega t \frac{(z_0^2 + R^2)^{3/2}}{\dots \dots \dots} \dots \dots \dots (4.6)$$

$$= - \left[\mu \mu_0 \left\{ \frac{\partial}{\partial z} \left(\frac{z^2 + R^2}{R^2} \right)^{3/2} \right\} \right]_{z=z_0} \frac{\partial z}{\partial t}$$

$$E = - \left(\frac{\partial \phi}{\partial z} \right)_{z_0} \frac{\partial z}{\partial t}$$

11) Detection Coil Configuration with effective

area turns is non-symmetrically distributed

about the axis of vibrations, which permit

this oscillating dipole field to be observed.

The basic instrument, briefly described is shown

in Fig. (4.3). The sample is vibrated perpendicularly to

the applied field by the vibration of a loud speaker. The

oscillating magnetic field of the vibrating sample induces

a voltage in the pick-up coils and from measurements of

this voltage the magnetic properties of the sample are

deduced in a similar stationary set of reference coils

by a reference sample, which in our coil was a small

permanent magnet. Since the sample and reference magnet

are driven synchronously by a common vibrator the phase

and amplitude of the resulting voltages are directly

related. The known portion of the voltage from reference

coil, phased to balance the voltage from pickup coil, is

then proportional to the magnetic moment of the sample by

this procedure the measurements can be made insensitive

to change of vibration amplitude, vibration frequency

small magnetic field instabilities, non-uniformity in the

magnetic field in amplifier gain. The associated electronic

circuits serve the function of a null detector.

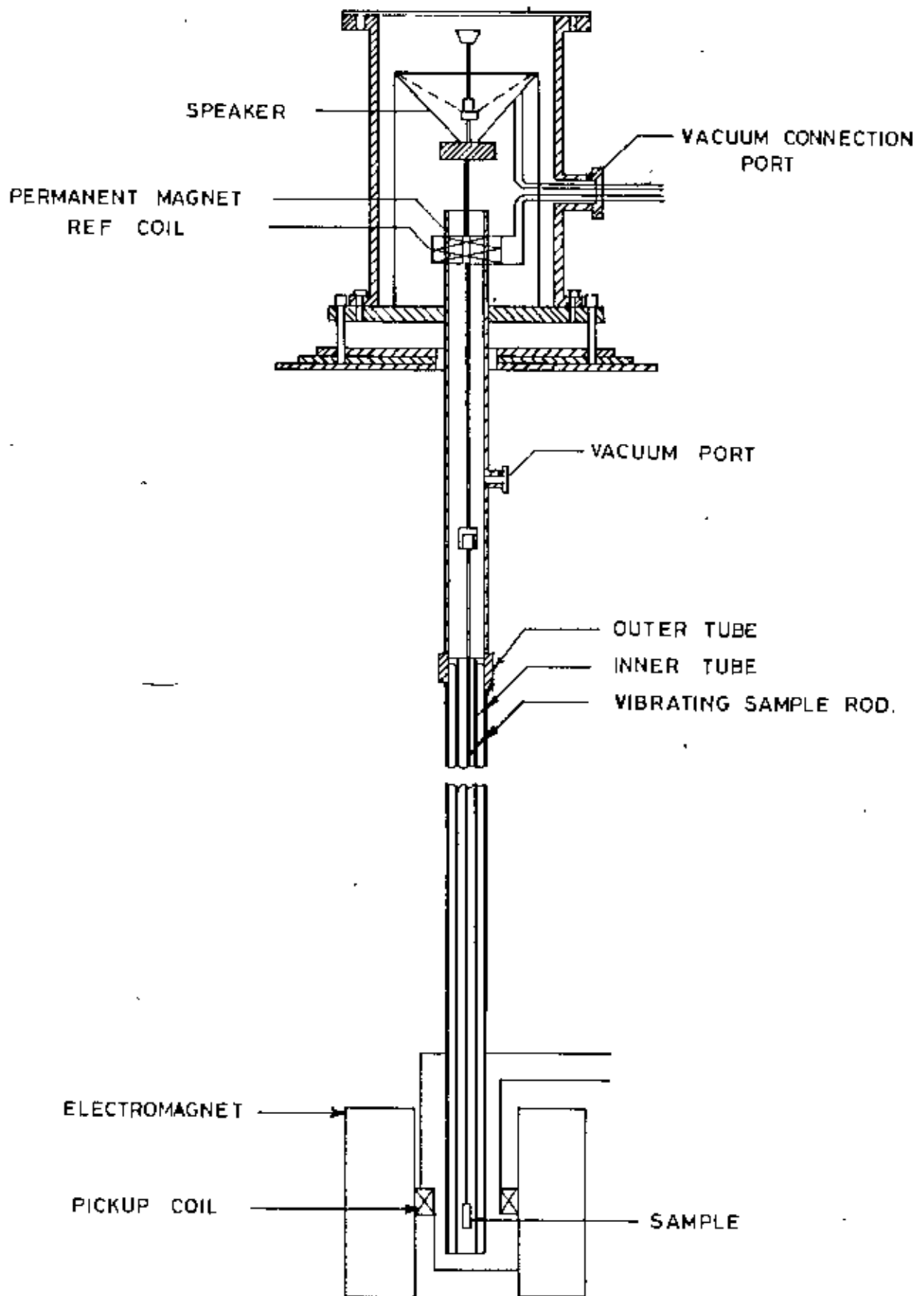


Fig. 4.3 Simplified from of vibrating sample magnetometer.

4.4 VIBRATING SAMPLE MAGNETOMETER COIL ARRANGEMENT AND FIELD DISTRIBUTION

The advantage of sample vibration perpendicularly to the applied field can be fully utilized only if a suitable detection coil arrangements can be devised as part of the vibrating dipole field. The scalar potential of fixed dipole M at the origin and pointed along the x -direction is

$$\phi = \frac{Mx}{r^3} \dots (4.8)$$

If M is vibrated in the Z -direction with sufficiently small amplitude a , the time varying potential in the surrounding space coil be $\phi_1 e^{i\omega t}$

$$\begin{aligned} \text{where } \phi_1 &= -a \left(\frac{\partial \phi}{\partial z} \right) \\ &= \frac{qMxz}{r^5} \dots (4.9) \end{aligned}$$

The flux pattern of the time varying part of the field is given by $-\text{grad } \phi_1$. Its configuration in the xz plane is shown in Fig(4.3a) with coils at 45° .

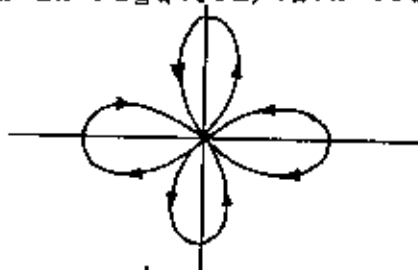


Fig.4.3a Time varying part of dipole field in x - z plane for vibration parallel to z and dipole moment parallel to x .

The arrangement of a single coil, useful when very high fields are required, is shown Fig. (4.4b). The output voltage in such a case can be maximized for position in

and Fig. (4.6) :

whose characteristics have the general features of Fig. (4.5) convenient in operation oval-shaped coils, shown in Fig. (4.4c), arrangement has proved both easy to assemble and most extensively for almost all our magnetic measurements. This The coil configuration shown in Fig. (4.4a) has been employed double coil assemblies are plotted in Fig. (4.5) and (4.6) . variations of relative output signal for two typical is the use of double-coil, shown in Fig. (4.4a) . A special One of the most convenient detection coil arrangements

causes H to vary during vibration. slight non-uniformities of the magnetizing field, which effects of change of sample position and the effect of or external field variation. This is also to minimize employed in order to minimize effects of sample position about the axes of vibration pairs of coils which are each effective area turn is nonsymmetrically distributed feature of all the useful coil configurations is that occupies part of the volume in the Z-direction. A general The later case may require 4 coils, if the instrument

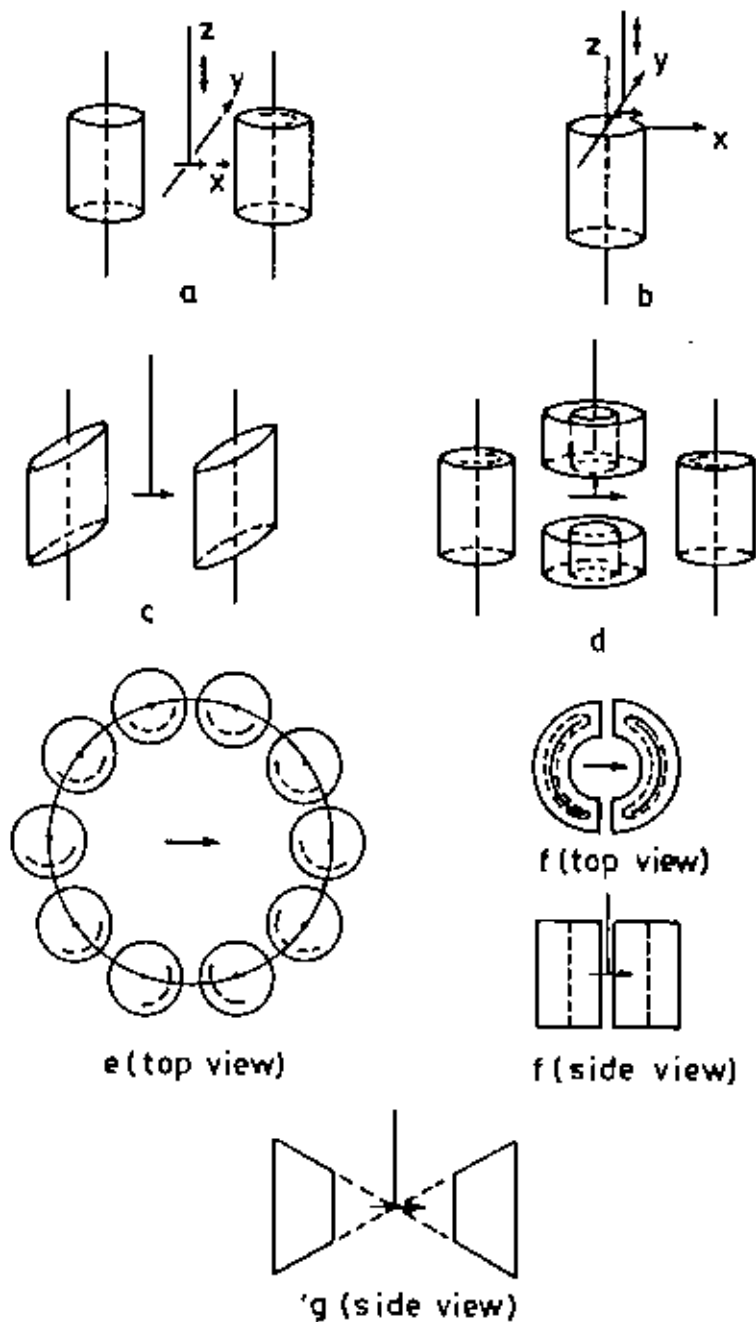


Fig. 4.4 Examples of useful detection coil arrangements described in the text. The sample, indicated by the heavy arrow, is vibrated along the Z direction.

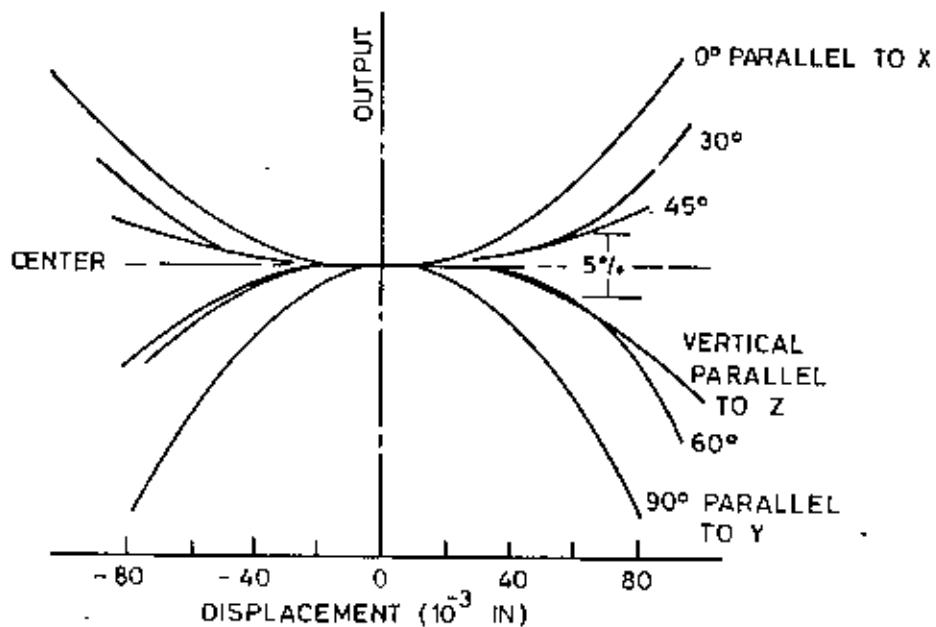


Fig 4.5 Relative output signal from a double-coil system vs. sample position. The contours of the "saddle point" are illustrated by measurements along various directions in the XY plane.

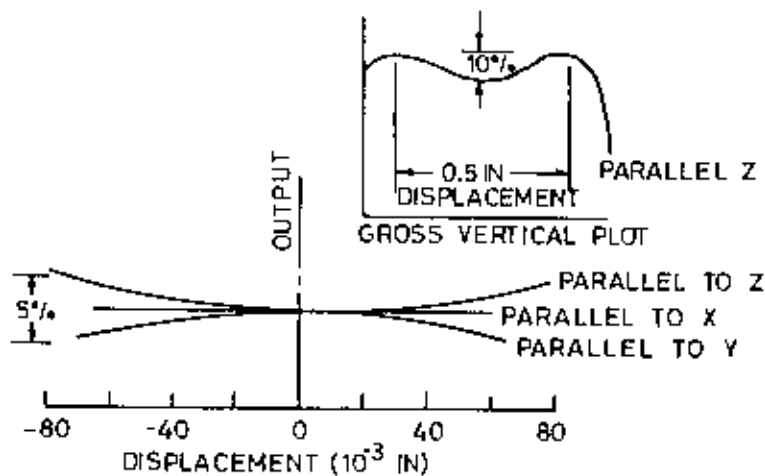


Fig.4.6 Relative output signal from a double-coil system vs. sample position. Bottom curves show relative output vs. displacement along the three orthogonal directions in neighborhood of "saddle point." Upper right insert shows relative output for large sample displacement along the Z direction.

the X or Y-direction. So that the output signal is then insensitive to small sample displacements in these direction's. This arrangement suffers, however, from a strong Z dependence of the output signal. Fig.(4.4a) shows the addition of a pair of coils co-axial with the Z-axis. With such an arrangement the magnitude and direction of the magnetic moment vector in space can be determined. The Z-component is detected by the co-axial pair and the component in the XY plane is determined by rotating the double coil. Fig.(4.4c) shows a multiple coil arrangement which attempts to intercept a maximum of the sample dipole field but at the expense additional thermal noise of the coils. An efficient modification of(4.4e) is shown in Fig.(4.4f) This coil geometry, however, is not easy to fabricate. Finally, the cross-section of a coil geometry which reflects most of the dipole field symmetry properties is shown in Fig.(4.4g).It is directly derived from Fig.(4.4f) and Leads to rather simple computation of output voltage versus geometric parameters.

4.5 WORKING PROCEDURE OF VIBRATING SAMPLE MAGNETOMETER

This is a sensitive equipment and it should be handled carefully. The following procedure may be followed. The sample is fitted to drive rod assembly and then positioned at about the mid-point of the sample coils by

eye estimation. The switches of the electromagnet power supply unit, the signal generator, the audio amplifier and the phase shifter are then turned on. At least half an hour is spent for the warming up of all the component units. The frequency of the sine-wave from the signal generator is set at 80 Hz.

The gain of the audio amplifier is adjusted to make the output signal driving the speaker to about 3 volts peak to peak. This signal makes the rod assembly vibrate with sufficiently large amplitude. The signal leveling produced in the reference coil-system is found to be about 5 mV_{pp} . The rod assembly is made vertical by adjusting the levelling screws. About 2 amperes or more current is passed through the electro-magnet depending on the size and material of the specimen. The sample signal alone is first seen on the d.c. meter of the lock-in amplifier. The meter reading is maximised by changing the phase of the locking signal in the reference channel. The sample signal is then optimised it is maximised by moving the sample in the Z-direction (vertical) and in the Y-direction and then minimised by moving it in the X-direction (Field direction).

The locking signal in the reference channel is brought in exact quadrature with the sample signal to give a correct null-reading on the meter. The two signals are then brought in the same phase to give a maximum reading on the meter to the right. Similarly, the reference coil signal alone is next seen on the meter. This signal is first brought in quadrature with the locking signal with the help of the external phase-shifter in such a manner that it gives a deflection to the left on the meter where it is again brought in phase with the sample signal. The lock-in amplifier is then set in the differential mode. The null-reading is obtained by correctly equalising the decade transformer when multiplied by calibration constant gives the sample moment.

CHAPTER - V

THEORIES OF MAGNETOSTRICTION

The physical origins of magnetostriiction is explained by Asgar (5.1) along the following lines:

For non-S-state ions the orbital angular momentum

has non-zero value of l with $(2l+1)$ degeneracy in the

lowest energy ground state. The orbital charge distribution

for these ions is highly asymmetrical. When these paramagnetic

ions are surrounded by crystalline electric field within a

crystal, the orbital degeneracy is removed and the resultant

wave function form new linear combinations, which reflect the

local symmetry of the crystal. The rotation of the charge

distribution lobes alters the orbital angular momentum,

because of spin orbit coupling. The magnetization associated

with spin will thus be related.

Spin-orbit coupling also contributes to the

anisotropy by way of another mechanism called anisotropic

exchange introduced by van Vleck (5.2). From s-state ions the

orbital angular momentum is zero and the charge distribution

is some what distorted by the crystal field. The spin-orbit

coupling thus contributes to the anisotropy energy and the

magnetostriiction in this case as well, although of much

smaller magnitude. Exchange energy can make contributions

to magnetoelastic energy due to the strain dependence of the

exchange integral J_{ij} . When the magnetic moments of



(a). CRYSTAL FIELD ANISOTROPY



(b). EXCHANGE ANISOTROPY



(c). EXCHANGE STRICTION

Fig. 5.1 Physical origins of Magnetostriction.

neighbouring ions are rotated away from parallelism. The exchange energy while increasing the elastic energy gives rise to magnetostriction.

There are three mechanisms of anisotropy:

- (i) Crystal field anisotropy
- (ii) Exchange anisotropy and
- (iii) Exchange striction

which is shown schematically in Fig.(5.1a),(5.1b) and(5.1c) respectively.

5.2 EXPRESSION FOR LINEAR MAGNETOSTRICTION

The origin of magnetostriction along the lines of Neels^(5.3) theory, which was developed in his paper on magnetic annealing and surface anisotropy, is as follows. When the distance between the atomic magnetic moments is variable, the interaction energy is expressed by

$$W(r, \cos \phi) = g(r) + L(r) \left(\cos^2 \phi - \frac{1}{3} \right) + q_2(r) \left(\cos^4 \phi - \frac{6}{7} \cos^2 \phi + \frac{3}{35} \right) + \dots \quad (5.1)$$

If the interaction energy is a function of r , the crystal lattice must be deformed upon the generation of a ferromagnetic moment, because such interaction tends to change

the bond length in a different way depending on the bond direction. The first term $g(r)$ is the exchange interaction term and is of relevance only when volume magnetostriction is considered as manifested in thermal expansion anomaly at the magnetic ordering temperature.

If $\bar{\alpha}$ denotes the direction of domain magnetization and that of the bond direction, we can write

$$W = g(r) + l(r) \left\{ (\alpha_1 \gamma_1 + \alpha_2 \gamma_2 + \alpha_3 \gamma_3)^2 - \frac{1}{3} \right\} + q(r) \left[(\alpha_1 \gamma_1 + \alpha_2 \gamma_2 + \alpha_3 \gamma_3)^4 - \frac{6}{7} (\alpha_1 \gamma_1 + \alpha_2 \gamma_2 + \alpha_3 \gamma_3)^2 + \frac{3}{35} \right] + \dots \quad (3.2)$$

Considering a deformed cubic lattice and relating the direction cosines γ_i to the strain tensor L_{ij} , we can get the expansion for magnetoelastic energy. Since the magnetoelastic energy has a linear dependence on strain the crystal will deform without limit unless it is counter balanced by the elastic energy which increases rapidly because of its quadratic dependence on strain.

By differentiating the

$$\text{Total energy} = E_{\text{mag. elastic}} + E_{\text{elastic}}$$

with respect to the strain components, and setting the partial derivatives equal to zero, for minimum energy

condition, one can obtain the relation for the fractional change in length of the crystal in any arbitrary direction

$\bar{\beta}$ as

$$\lambda_{\beta} = \sum_{i,j=1} e_{ij} \beta_i \beta_j \dots \dots (5.3)$$

Substituting the values of strain components as obtained by minimizing total energy coming from magnetoelastic and elastic terms, we can get an expression for

$$\begin{aligned} \lambda_{\beta} = & h_0 + h_1 \left(\sum \alpha_i \beta_i^2 - \frac{1}{3} \right) + 2h_2 C_{ij} (\alpha_i \alpha_j \beta_i \beta_j) \\ & + h_3 s + h_4 \left(\sum \alpha_i^4 \beta_j^2 + \frac{2}{3} s - \frac{1}{3} \right) + 2h_5 C_{ij} \\ & [\alpha_i \alpha_j (1 - \alpha_i^2 - \alpha_j^2) \beta_i \beta_j] + \dots \dots \dots (5.4) \end{aligned}$$

Where C_{ij} indicates a summation over terms with cyclic permutation of the indices and $h_0 \rightarrow h_5$ are the magnetostriction constant defined by

$$\begin{aligned} h_0 = \frac{-b_0}{C_{11} + 2C_{12}}, \quad h_1 = \frac{-b_1}{C_{11} - C_{12}}, \quad h_3 = \frac{-b_3}{C_{11} + 2C_{12}} \\ h_4 = \frac{-b_4}{C_{11} - C_{12}} \quad \text{and} \quad h_5 = \frac{-b_5}{2C_{44}} \dots \dots \dots (5.5) \end{aligned}$$

Where the co-efficients b_n are magnetoelastic coupling co-efficients.

For hexagonal crystals the relations become modified due to different symmetry conditions and have been treated in detail by Mason and Lewis^(5.4).

For ~~hexagonal~~ cubic crystals

$$\lambda_{\beta} = \frac{3}{2} \lambda_{100} (\alpha_1^2 \beta_1^2 + \alpha_2^2 \beta_2^2 + \alpha_3^2 \beta_3^2 - \frac{1}{3}) + 3 \lambda_{111} (\alpha_1 \alpha_2 \beta_1 \beta_2 + \alpha_2 \alpha_3 \beta_2 \beta_3 + \alpha_3 \alpha_1 \beta_3 \beta_1) \dots (5.6)$$

where λ_{100} and λ_{111} indicates strains along (100) and (111) direction respectively.

5.3 MAGNETOSTRICTION IN AMORPHOUS RIBBON

For amorphous material we can apply the same approximation as in the case of Poly crystalline magnetic material. Such that $\lambda_{100} = \lambda_{111} = \lambda_s$

We get eqⁿ (5.6).

$$\begin{aligned} \lambda_{\beta} &= \frac{3}{2} \lambda_s (\alpha_1^2 \beta_1^2 + \alpha_2^2 \beta_2^2 + \alpha_3^2 \beta_3^2 - \frac{1}{3}) + 3 \lambda_s (\alpha_1 \alpha_2 \beta_1 \beta_2 + \alpha_2 \alpha_3 \beta_2 \beta_3 + \alpha_3 \alpha_1 \beta_3 \beta_1) \\ &= \frac{3}{2} \lambda_s \left[\alpha_1^2 \beta_1^2 + \alpha_2^2 \beta_2^2 + \alpha_3^2 \beta_3^2 + 2 \alpha_1 \alpha_2 \beta_1 \beta_2 + 2 \alpha_2 \alpha_3 \beta_2 \beta_3 + 2 \alpha_3 \alpha_1 \beta_3 \beta_1 - \frac{1}{3} \right] \\ &= \frac{3}{2} \lambda_s \left[(\alpha_1 \beta_1 + \alpha_2 \beta_2 + \alpha_3 \beta_3)^2 - \frac{1}{3} \right] \dots (5.7) \end{aligned}$$

Hence $\alpha_1 \beta_1 + \alpha_2 \beta_2 + \alpha_3 \beta_3 = \cos \theta$

where θ is the angle between the direction of magnetization and that of observation. When the domain magnetization rotates toward the direction of the applied field, the fractional change is given by

$$\lambda_{\theta} = \frac{\Delta l}{l}$$

Becomes eqⁿ (5.7)

$$\frac{\Delta l}{l} = \frac{3\lambda_s}{2} \left(\cos^2 \theta - \frac{1}{3} \right) \dots \dots \dots (5.8)$$

5.4 DIRECTION OF LINEAR MAGNETOSTRICTION

Experiments have shown that the deformation depends upon the direction of the magnetization. For a cubic crystal magnetized in the direction given by the direction cosines α_1 , α_2 and α_3 (defined with respect to the cube axes). This deformation expressed in strain components ϵ_{ij} ($i, j = x, y, z$) become in first approximation.

$$\epsilon_{xx} = \frac{3}{2} \lambda_{100} \left(\alpha_1^2 - \frac{1}{3} \right) \dots \dots \dots (5.9)$$

$$\epsilon_{yy} = \frac{3}{2} \lambda_{100} \left(\alpha_2^2 - \frac{1}{3} \right) \dots \dots \dots (5.10)$$

$$\epsilon_{zz} = \frac{3}{2} \lambda_{100} \left(\alpha_3^2 - \frac{1}{3} \right) \dots \dots \dots (5.11)$$

$$\epsilon_{xy} = \frac{3}{2} \lambda_{111} \alpha_1 \alpha_2 \dots \dots \dots (5.12)$$

$$\epsilon_{yz} = \frac{3}{2} \lambda_{111} \alpha_2 \alpha_3 \dots \dots \dots (5.13)$$

$$\epsilon_{zx} = \frac{3}{2} \lambda_{111} \alpha_3 \alpha_1 \dots \dots \dots (5.14)$$

The extra terms ($-\frac{1}{3}$) make the total change of volume nil (Trace of the matrix is zero). The factors $\frac{3}{2}$ ensure that the strain in the direction of magnetization with respect to the non-magnetized state ($\alpha_1^2 = \alpha_2^2 = \alpha_3^2 = \frac{1}{3}$) is λ_{100} and λ_{111} in the $[100]$ and $[111]$ directions respectively. The strain in a direction perpendicular to is $-\frac{1}{2}\lambda_{100}$ and $-\frac{1}{2}\lambda_{111}$ respectively.

In an arbitrary direction we then have parallel to the magnetization

$$\lambda(\alpha_1, \alpha_2, \alpha_3) = \lambda_{100} + 3(\lambda_{111} - \lambda_{100})(\alpha_1^2\alpha_2^2 + \alpha_2^2\alpha_3^2 + \alpha_3^2\alpha_1^2) + \dots \dots \dots (5.15)$$

For the ferromagnetic metals the values of λ at room temperature are found to be

Fe	Ni
$\lambda_{100} = + 25 \times 10^{-6}$	$\lambda_{100} = - 46 \times 10^{-6}$
$\lambda_{111} = - 19 \times 10^{-6}$	$\lambda_{111} = - 25 \times 10^{-6}$

In discussing the effect of a unidirectional stress it is convenient to divide materials into two classes which have.

- (i) Positive magnetostriction
- (ii) Negative magnetostriction

$$\lambda = -\lambda_s/2$$

(Transverse effect) $\theta = 90^\circ$ and the change in length

at right angles to the direction of magnetization

λ_s , when $\theta = 0$ at saturation. When the length is measured

so that it is equal to the longitudinal change in length

change in volume is zero. The zero point of λ_1 is chosen

is zero. The zero point of λ_1 is chosen so that the

direction of magnetization and that the change in volume

magnetostriction is independent of the crystallographic

the change in length is measured. It is assumed now that

Here θ is the angle between the direction in which

$$\lambda_1 = \frac{2}{3} \lambda_s \left(\cos^2 \theta - \frac{1}{3} \right) \dots \dots \dots (5.16)$$

magnetization in the domain as follows

simple quantitative way to change in direction of

The change in dimension of a single domain can be rotated in

Magnetostriction is associated with domain orientation.

5.5 MAGNETOSTRICTION ARISING FROM DOMAIN ROTATION

contracts when magnetized.

magnetization is decreased by tension and the material

materials expands when magnetized in class (ii) the

increased by tension (except at $I = 0$ or I_s) and the

In materials of class(i) the magnetization is in

For polycrystalline or amorphous material the domains are initially oriented at random. The same relation is applicable if one uses the average of $\cos^2 \theta$ overall the domains. When the material is unmagnetized, $\langle \cos^2 \theta \rangle_{av} = \frac{1}{3}$ and $\lambda = 0$. upon application of a strong field θ becomes zero and $\lambda = \lambda_s$.

If the domains are not initially random, one can use the relation

$$\begin{aligned} \lambda &= \frac{3}{2} \lambda_s [\langle \cos^2 \theta \rangle_{av} - \frac{1}{3}] - \frac{3}{2} \lambda_s [\langle \cos^2 \theta \rangle_0 - \frac{1}{3}] \\ &= \frac{3}{2} \lambda_s [\langle \cos^2 \theta \rangle_{av} - \langle \cos^2 \theta \rangle_0] \dots\dots\dots(5.17) \end{aligned}$$

where

$\langle \cos^2 \theta \rangle_0$ = initial domain distribution

$\langle \cos^2 \theta \rangle_{av}$ = domain distribution at any time

If the domain are oriented originally so that $\theta = 0$ for half of them and $\theta = 180^\circ$ for other half $\langle \cos^2 \theta \rangle_0 = \langle \cos^2 \theta \rangle_{av} = 0$ and $\lambda = 0$. (The reference point); in a strong field $\theta = 0$ and there is no change in $\cos^2 \theta$ and again $\lambda = 0$. When used in this sense, λ depends decidedly on the initial domain distribution while λ_s is a constant of the material. The constant λ_s can be determined in any specimen by measuring λ when a saturation field is applied first parallel and then at 90° to the

direction of measurement of λ . The total change in length caused by the change in field in the polycrystalline or amorphous material is then

$$\frac{\Delta L}{L} = \frac{3}{2} \lambda_s \quad \dots \quad (5.18)$$

independent of the initial domain distribution.

5.6 MAGNETOSTRICTION MEASUREMENT TECHNIQUE

This technique, since the time of its introduction by Goldman^(5.5) has gradually replaced almost entirely all other methods of magnetostriction measurement. The reason for this successes, as also the problems associated with this method and some of the improvement in the use of this technique as developed by Asgar^(5.6) are as follows :

Magnetostriction measurements are set with a large number of problems. Strain develops in a magnetic specimen, when magnetized. This small strain is dependent both on the direction of magnetization and its magnitude. Also the state of zero average external magnetization may not correspond to the zero magnetic strain, because the demagnetized multidomain state is neither unique nor well defined.

The X-ray technique which was first used by Rooksby and Willis (5.8) to determine spontaneous magnetostriiction, measures the distortion of crystal axes by determining $(c/a-1)$ directly from the magnitude of the splitting of X-ray reflection spots from different crystal planes.

The difficulty with this method is that one has to use a big specimen to get sufficient sensitivity. Again it is difficult to magnetize a big specimen in different direction using rotating field, maintained at uniform field and steady temperature. Again this method cannot provide the strain difference of two well defined magnetic states and one has to assume equal distribution of the domains in all the easy direction of magnetization in the demagnetized state, which may not be true.

In the displacement method Nagaoaka (5.7) combined optical and mechanical method. Here the specimen, by the displacement of its free end, the other end being fixed, rotates a spindle to which a mirror is attached. A beam of light reflected off this mirror forms optical lever.

However, X-ray method besides being less sensitive is difficult to use with different directions of magnetization. In using strain gauge technique one can get over many of these difficulties. The gauges can be used on a very small disk shaped specimen cut in a definite crystallographic plane and the gauge can be bonded in a precisely determined direction.

The strain gauge works on the principle that when a fine wire in the form of a grid or a thin foil, and embedded in a paper or epoxy film is bonded firmly on a specimen and shows a change in resistance proportional to the strain.

We can write this relation as

$$\frac{dR}{R} = G \frac{dL}{L} \dots \dots (5.19)$$

Where $\frac{dR}{R}$ is the fractional change in resistance, G is the gauge factor and $\frac{dL}{L}$ is the strain along the gauge direction.

The magnetic strain in the crystal is determined from the change in resistance of the gauge fixed on the specimen in relation to the resistance of another dummy gauge bonded on a reference specimen using a resistance bridge in the out of balance condition.

The mechanism of resistance change of the gauge wire under strain can thus be quite complex. More over, the gauge may not follow the strain of the material on which it is bound. Thus there is to be a affected bonding factor. In addition one has to consider the thermally induced resistance change, when the dummy and active gauge are at different temperature. The most important difficulty with the use of strain gauges is dummy gauge on a suitably chosen non-magnetic material which have the same thermal and thermoelastic properties as the magnetic material. This ensures that the dummy and the active gauge are subjected to the same strain and temperature except for the magnetic strain.

5.7 STRAIN MEASUREMENTS USING STRAIN GAUGES

In 1947 Goldman was the first to measure magnetostriction by the use of strain gauge a folded metal wire, which can have a resistance of the order of 100 ohms.

The strain gauge technique is based on the fact that any strain characteristic of the specimen on which the gauge is affixed is transmitted faithfully to the electrically sensitive zone of the gauge and is observed as a resistance changes which can be measured with the help of a ~~Wheatstone~~ Wheatstone bridge. When the temperature of the specimen is changed

there is a further contribution to the resistance change due to thermal expansion of the gauge wires, the gauge matrix, the bonding glue, specimen and the resistivity change and the change in gauge factor of the gauge material. Similar strain gauge known as dummy gauge is in the other arm of wheatstone bridge to compensate as far as possible for temperature influence.

The measurement can be carried out with direct current or low frequency alternating current ($f < 100$ c/s) since the magnetic material to which the current carrying wires are affixed can give rise to an inductive effect which changes during magnetization. This method is also very sensitive, being capable of measuring strains upto 10^{-8} . The minimum dimensions of strain gauges are approximately 2 mm. Additional errors that can occur in this measurements is magnetoresistance of the wire. At room temperature this is not greater than 10^{-7} .

When more than one strain gauge (active and dummy) is used in a wheatstone bridge circuit. This effect is approximately eliminated if care is taken to ensure that all the strain gauges are in the same magnetic field.

5.8 GUAGE FACTOR

It is observed experimentally that the resistance of a thin wire varies proportionately to the strain to which it is subjected, provided the temperature is constant and the applied strain is small. This provides the definition of gauge factor of the wire as the fractional change in resistance per unit strain

$$G = \left(\frac{R}{\Delta R} \right) / \left(\frac{L}{\Delta L} \right) \dots \dots (5.20)$$

5.9 MAGNETORESISTANCE

Magnetoresistance is another serious drawback of strain gauge at room temperature for measurements in the presence of a magnetic field. Magnetoresistance is very dependent on temperature, chemical composition of the gauge, particularly magnetic impurity, the strength of the magnetic field and perhaps the state of strain in the gauge. The differential magnetoresistance in the gauges we have used was less than 10^{-7} when reduced to strain. The effect of rotation of a magnetic field of 8 kililo Gauss showed an even smaller differential magnetoresistance. Measurements which require only rotation of the field, thus are not seriously affected provided that the dummy gauge is placed parallel to the active gauge.

The use of Durofix facilitated the removal of the gauges from the copper discs for subsequent use with proper glue. The possibility of bad bondage with Durofix was checked by observing the differential strain. The whole success of this method, however, lies in the proper choice of a glue which can give proper bondage throughout the temperature range and at the same time can easily be dissolved without damaging the gauges. To measure differential magnetoresistance, it is not of course essential to get as good a grip as needed for measurements of, say magnetostriction or thermal expansion, because the strain arising from the application of magnetic field is small. The purpose of the glue is mainly to keep the gauge flat on the specimen to avoid bending.

71294

CHAPTER - VI

THE DIFFERENTIAL THERMAL ANALYSIS

THE DIFFERENTIAL THERMAL ANALYSIS

6.1 INTRODUCTION

The technique of differential thermal analysis is an important tool to study the structural change occurring both in solid and liquid materials under heat treatment. These changes may be due to dehydration transition from one crystalline variety to another, destruction of crystalline lattice, oxidation, decomposition etc. The principle of differential thermal analysis (DTA) consists in measuring the heat changes associated with the physical or chemical changes occurring when a standard substance is gradually heated. This technique has been used in determining the glass transition temperature and crystallization temperature of our amorphous iron boron ribbon.

6.2 DIFFERENTIAL THERMAL ANALYSIS

The DTA technique was first suggested by Le Chatelier^(6.1) in 1887 and was applied to the study of clays and ceramics. DTA is the process of accurately measuring the difference in the temperature between a thermocouple embedded in a sample and a thermo-couple in a standard inert material such as aluminium oxide while both are being heated at the uniform rate. These

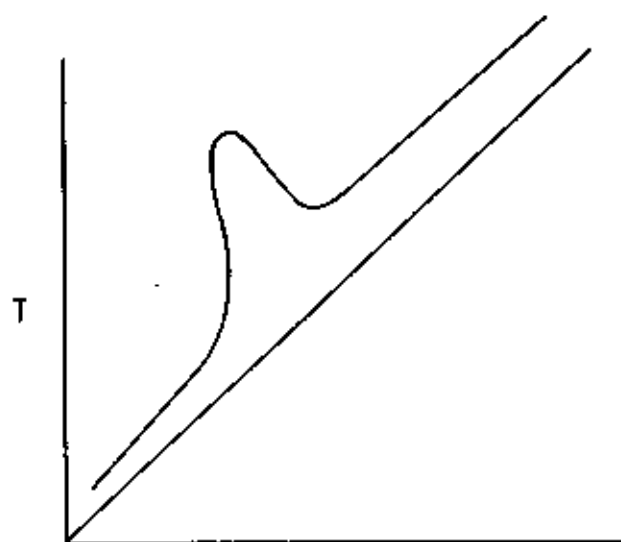


Fig. 6.1(a) Heating curve of sample and reference substance.

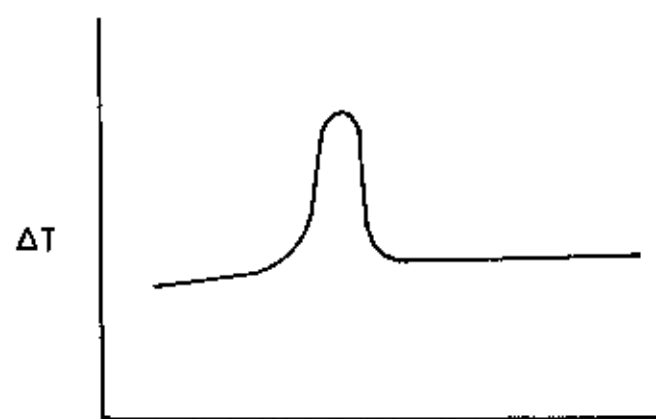


Fig. 6.1(b) DTA Curve

The temperature of the reference substance, which is thermally inactive rises uniformly when heated, while the temperature of a sample changes anomalously when there is a physical and chemical change of the active specimen at a particular temperature. When there is an exothermic reaction there is a peak in the temperature vs time curve, ^{heat} supplied from outside is consumed by the reaction. And when the reaction is over, the sample temperature is different from the ambient, and it rises rapidly to catch it up, and then it begins to change uniformly. The temperature difference ΔT is detected, amplified and recorded by a peak Fig. (6.1b).

When a sample and reference substance are heated or cooled at a constant rate under identical environment, their temperature differences are measured as a function of time or temperature (as shown by the curve in Fig. (6.1a). thermal record of reactions occurring in a sample.

respectively from a base line. So, DTA gives a continuous shown in the DTA trace as positive and negative deviations the exothermic and endothermic reactions are generally (reaction) or absorption of heat (endothermic reaction). the sample involving the evolution of heat (exothermic transitions (Transformations) or chemical reactions in differences of temperature, arise due to the phase

The temperature in the sample holder is measured by a thermocouple the signal of which is compensated for the ambient temperature and fed to the temperature controller. This signal is compared with the program signal and the voltage impressed to the furnace is adjusted. Thus the sample and reference substance are heated or cooled at a desired rate. The temperature in the sample holder is digitally displayed on the DT-30 and is also recorded on the recorder.

6.3 APPARATUS

The apparatus of the differential thermal analysis consists of a thin walled refractory specimen holder made of sintered alumina with two adjacent cubical compartments of exactly the same size, 1 cm in length Fig.(6.2). Of these one is for the reference (inert) material and the other for the test material, the compartments being separated by a 1 mm wall. The specimen holder is placed in the cavity of the heating blocks which is operated in the centre of the cylindrical refractory tube of an electrical furnace, which supplies a uniform heating rate. The furnace (9" x 6" x 9" deep) is peked with calcined China clay. The input of current into the furnace is secured through the secondary of a variac transformer, which controls the current. Fine chromelalumel wires (28 gauge) are used for thermocouples. A cold junction is used for thermocouples' leads and the e.m.f is recorded

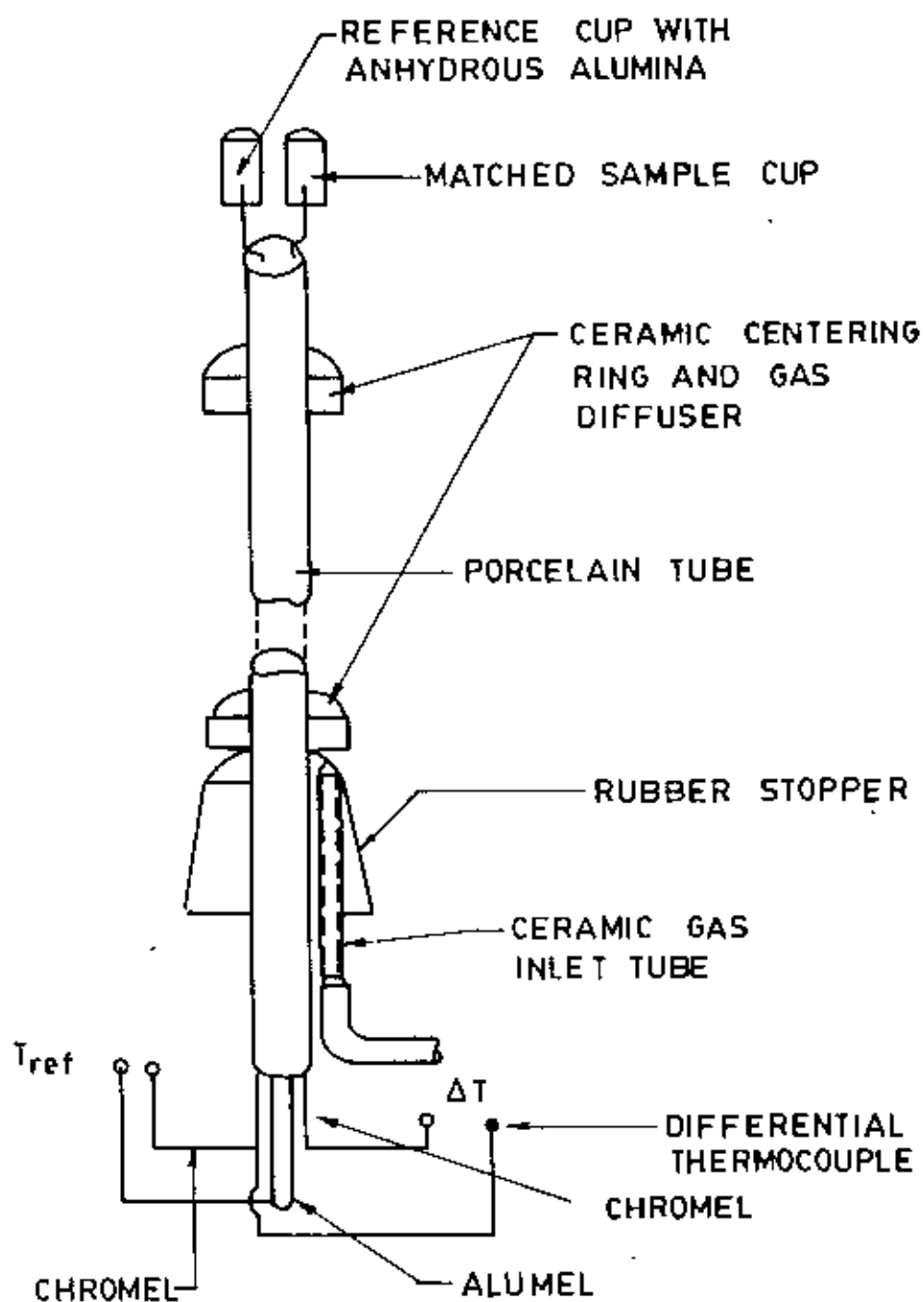


FIG. 6.2. DTA THERMOCOUPLE ASSEMBLY.

almost continuously, while the temperature of the inert material is measured at 3 minutes intervals. It is essential to use perfectly dry materials, as otherwise errors will be introduced in the analysis. Approximately 0.1 g anhydrous alumina is used in the reference cup and the sample weights varies over a range 0.05 g to 0.125 g depending on their peaked density, A heating rate of 10°C per minute (average) of the furnace is conveniently kept, and this gives satisfactory results in most cases. A block diagram of DTA is shown in Fig.(6.3).

The thermal analysis runs generally for 1 to $1\frac{1}{2}$ hrs. Thermal analysis curves are obtained by plotting heating temperature and the difference between the temperatures of the test and the reference substances. From these plots the reaction temperature could be determined. Under standard conditions of the experiment, characteristic curves for different composition iron - Boron amorphous ribbon were obtained.

Glass transition and crystallization temperature points are indicated, usually by a sharp exothermic peak. The temperatures of decomposition of phases are similarly given by exothermic peaks and in cases - typical endothermic curves afford useful information about the structural changes taking place in the compound.

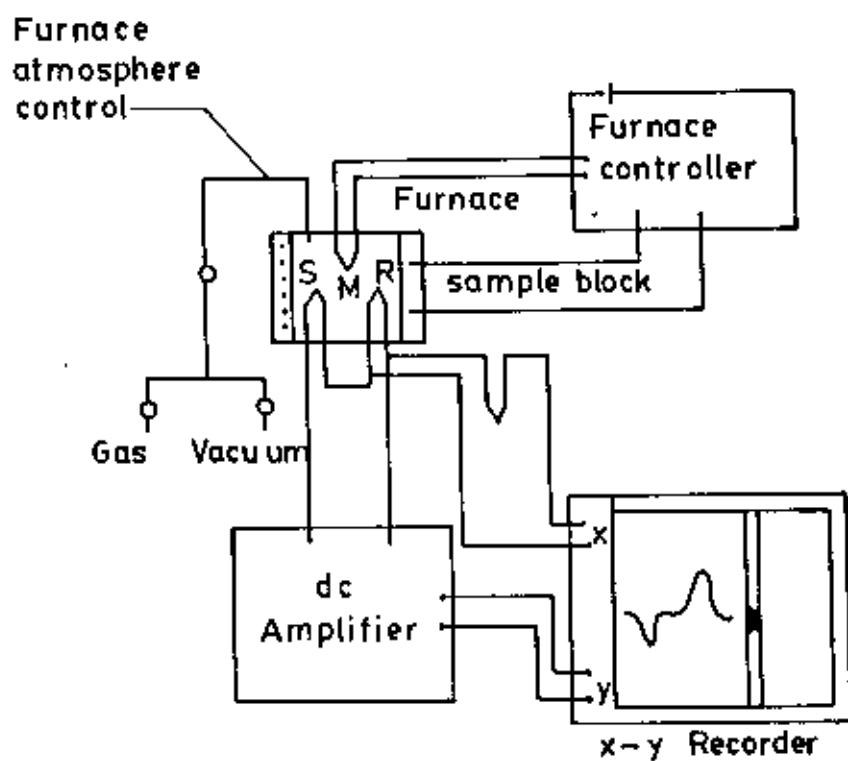


Fig. 6.3 Block diagram of a differential thermal analysis equipment, (S) sample thermocouple, (S) reference thermocouple, (M) monitor thermocouple.

All experiments are run at atmospheric pressure in a continuous flow of a purified inert gas usually argon, nitrogen or helium. Gases are normally purged into the furnace chamber at the lower end through a purification train in which oxygen and water are removed by heated copper wool and exhausted from the top into a condensate trap for collecting the condensable volatile products.

CHAPTER - VII
EXPERIMENTAL SET UP

7.1 EXPERIMENTAL SET UP FOR MASUREMENTS OF MAGNETIZATION

7.1.1 ELECTRONIC CIRCUITS OF VSM

The functions of the associated electronic circuits are

- (i) To permit accurate calibration of the signal output obtained from the detection coils.
- (ii) To produce a convenient AC output signal which is directly related to the input and which can be recorded.
- (iii) To produce sufficient amplifications for high sensitivity operation.

The block diagram of the electronic circuit used for.

The vibrating sample magnetometer consists of a mechanical vibrator, a sinewave generator, an audio amplifier, a ratio transformer, a phase-shifter, a Lock-in-amplifier, a pick-up coil system, a reference coil system and an electromagnet as shown in Fig.(7.1) .

The mechanical vibrator is a specially prepared loudspeaker which vibrates a glass rod assembly at frequency of 80 Hz. A sample s and a small permanent

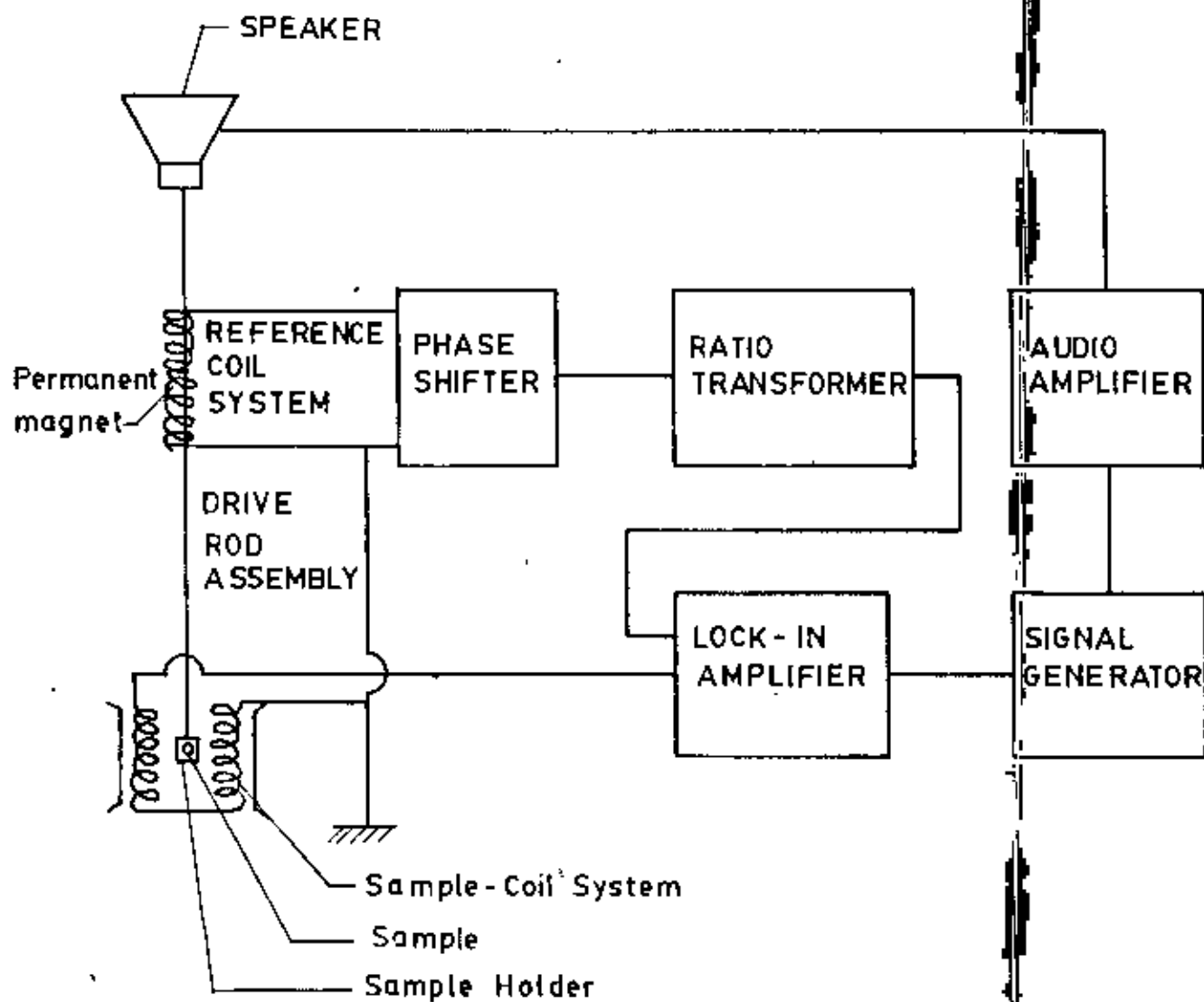


Fig. 7.1 Schematic diagram of the electronic system of the V.S.M.

magnet P attached to the glass rod assembly Fig.(7.1) also vibrate at the same frequency.

The sample magnetized by the electromagnet generates an e.m.f in the pick-up coils PC. The strength of this signal is proportional to the magnetization of the sample. The vibrating permanent magnet also generates an e.m.f of fixed amplitude in the surrounding reference coils. This reference signal is stepped down with the help of a ratio transformer so that its amplitude is equal to that of the sample signal. The two signals are then brought in phase and put to the Lock-in amplifier.

The Lock-in amplifier works as a null detector. The ratio transformer reading is to be calibrated by using spherical sample s of 99.9% pure iron.

7.1.2 SENSITIVITY LIMITS

Limits of sensitivity are determined by signal to noise ratio at the input circuit where noise is defined as any signal not arising from the magnetic moment of the sample. The major sources of noise are the Johnson noise of the wire used for the pick-up coils, and the magnetic properties of the sample holder, which superimposes undesired signals in phase with the wanted signal. Use of a minimum mass of weakly diamagnetic material for a

sample holder, carefully checked to contain no ferromagnetic impurities, is essential to minimize this coherent noise contribution. Corrections for the small magnetic contribution of the sample holder can then be made by measurements with the sample removed. This correction is much less than the equivalent case with a moving coil system.

Our standard sample used for calibration was spherically shaped specimens of mass ~~20.7~~ mg. The different field susceptibility $\Delta\chi \approx 5 \times 10^{-10}$ could be observed after synchronous phase detection with bandwidth $\approx 2 \times 10^{-2}$ cps. The other tests used was small current at 80 Hz or an alternating current at 80 Hz passed through the coil which remained stationary.

7.1.3 STABILITY TESTS DIFFERENTIAL MEASUREMENTS

With only the lock-in amplifier and the oscilloscope as a null detector, it was found that the 20.7 mg Fe-sample signal could be balanced reproducibly. Such reproducibility indicated that the long time drifts caused by the combined effects of vibration, amplitude changes and frequency changes average sample position and other effects were negligible. Chosen synchronous phase detector added differential changes about one-tenth the size that could be recorded reproducibly.

7.1.4 VIBRATION AMPLITUDE

The Peak-to-peak vibration amplitude has been varied from less than 0.1 mm upto 1.0 mm in order to examine errors caused by amplitude changes. Such tests show that the measured magnetic moment varied by less than $\pm 0.5\%$ over these range of amplitude, although a some what sharper balance is obtained at higher variation amplitudes because of the larger signals involved.

7.1.5 IMAGE EFFECTS

Image effects were also examined with a small vibrating coil carrying a dc current. The image effect was no greater than $\pm 1\%$ for fields upto 5 kilogauss produced in an air gap of 3.6 cm. Undoubtedly, there is an image induced in the magnet poles. It appears, however, that when the sample is vibrated, the effective image vibration is reduced by eddy-current shielding.

7.1.6 VIBRATION FREQUENCY

The vibration frequency is not critical. High frequency operation is limited by the driving mechanism and capacitive shunting in the detection coils. Frequencies of 100 Hz or less permit the use of inexpensive components and minimize eddy current shielding by the vacuum chamber. The measurements are completely independent of eddy currents in the surrounding parts, if measurements and

calibration are made at the same temperature. The thickness of conducting parts has been minimized, so that the temperature dependence of penetration depth is less than 1% .

7.1.7 VIBRATION PROBLEMS

Mechanical coupling between the vibrating system and the fixed detection coils must be avoided. Although the coils are arranged minimum sensitivity to external vibration, a noticeable background signal is obtained when the vacuum chamber contacts the detection coils. Such mechanical effects are difficult to eliminate electronically, because the spurious background signal has the same frequency as the sample signal and maintains a constant phase difference with respect to the sample signal. Usually the magnetometer and detection coils are both supported by the magnet, so that some mechanical coupling may be noticed at highest sensitivity.



Figure.

Arrangement of the vibrating sample magnetometer (V.S.M.).

7.2 EXPERIMENTAL SET UP FOR MEASUREMENTS OF MAGNETOSTRICTION

The experimental set up consists of a strain sensing device, i.e strain gauges, D.C bridge for strain measurements, D.C amplifier, electromagnet to produce the magnetic field, A specimen holder with an arrangement for rotating the specimen in the magnetic field by definite angles.

7.2.1 THE D.C BRIDGE

A D.C wheatstone bridge is slightly out of balance condition measured the fractional change in resistance in the active gauge. The components of the bridge are shown in Fig.(7.2). When the resistance of the active gauge was changed from R to $R + \Delta R$, a corresponding out of balance voltage developed across the input of the D.C amplifier. The output of the amplifier is recorded.

7.2.2 THE D.C AMPLIFIER

To measure the small out of balance D.C voltage, the Model 140 nano voltmeter was used, which acted as a potentiometric amplifier and had a sensitivity of 0.1 microvolt for full-scale deflection in the highest sensitivity range. A panel switch selector permitted the meter sensitivity to be altered. Any A.C signal

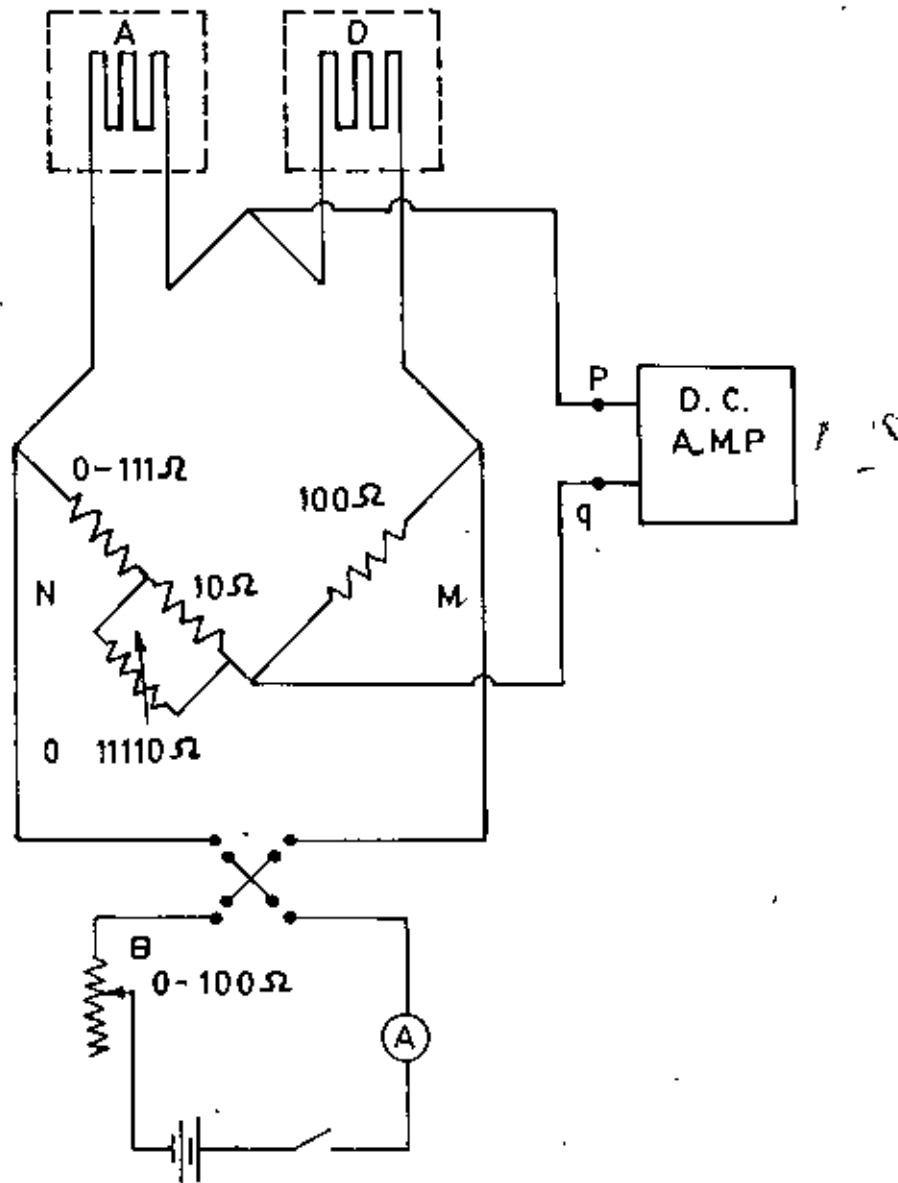


FIG. 7.2 D. C. BRIDGE

superimposed on the D.C voltage to be measured was almost entirely attenuated, the filtering factor being inversely proportional to the frequency. The zero drift was less than 0.1 μ v/hour when all sources of thermo E.M.P were reduced by using low thermal solders and protecting the metallic junctions from thermal fluctuations.

7.2.3 SENSITIVITY AND CALIBRATION OF THE D.C BRIDGE

The current in the D.C Bridge circuit, in terms of the parameters of the bridge shown in Fig. (7.2) is

$$I_g = \frac{E}{\left(B+D+A + \frac{BD}{M} \right) \left(Z+N+A + \frac{ZN}{M} \right)} \times \left(\frac{4\Delta}{1 + K\Delta} \right) \dots (7.1)$$

where

$$K = \frac{N(D+Z) + (B+N)(B+D+Z)}{M(B+D+A + \frac{BD}{M}) \left(Z+N+A + \frac{ZN}{M} \right)}$$

Eq(7.1) is an exact algebraic solution for I_g where the circuit on the right hand side of points PQ has been treated as a current measuring device of input resistance Z . since the bridge is only slightly unbalanced $K\Delta \ll 1$ and the factor $(1 + K\Delta)$ can be replaced by unity. Also, since the input resistance of the measuring unit is

of the order of one megohm, we can put $Z \rightarrow \infty$ in equation (7.1) and obtain the expression for the maximum voltage sensitivity corresponding to $B = 0$ close to the balance condition of the bridge as

$$x \left(\frac{\Delta I_g}{\Delta A} \right)_0 \approx \frac{ED}{(D+A)^2} \dots \dots \dots (7.2)$$

In our bridge D represents the resistance of the dummy gauge and A that of the active gauge. Both have the same value of 158.2 ohm in the unstrained condition. Thus the fractional change in resistance can be written as

$$\frac{\Delta A}{A} = \frac{\Delta z \Delta I_g}{E} \dots \dots \dots (7.3)$$

Thus the out of balance voltage $Z \Delta I_g$ measured by the recorder maintains a linear relationship with $\Delta A/A$, giving a constant sensitivity. The deviation from linear relationship will only occur if the condition $1 + K \Delta A = 1$ does not hold. It can be shown that the fractional error 0.01%. The bridge was calibrated by changing the resistance parallel to the 10 ohm resistor in the arm N of the bridge. The minimum voltage that could be measured without noise and drift was of the order of 10^{-6} . The gauge factor of the strain gauge we used was (\approx) 2.02 as supplied by the manufacturer and the voltage supplied to the bridge was two volts. Thus maximum strain sensitivity

was of the order of 10^{-6} from equation (7.3). The sensitivity of the bridge could be increased further either by increasing the current in the circuit or by using higher gain in the amplifier. The upper usable limit was determined by the maximum allowable joule heating in the gauges and the signal-to-noise ratio.

For minimising the noise, all the connections were made with co-axial cables, so that all parts were well screened.

7.2.4 THE CHOICE OF DUMMY MATERIAL

The identical behaviour of the active and dummy gauges is the basic necessity for justifying the use of a compensating gauge for all strain measurements. The nearest approach to this condition can be made by subjecting the two gauges to identical strain and thermal conditions used Fused silica, glass as dummy material for its negligible thermal expansion co-efficient.

7.2.5 THE SPECIMEN HOLDER

It is very important to keep the temperature of the specimen and the dummy identical for accurate measurements. Any difference in the thermal environment of the active and dummy gauges effect the result drastically.

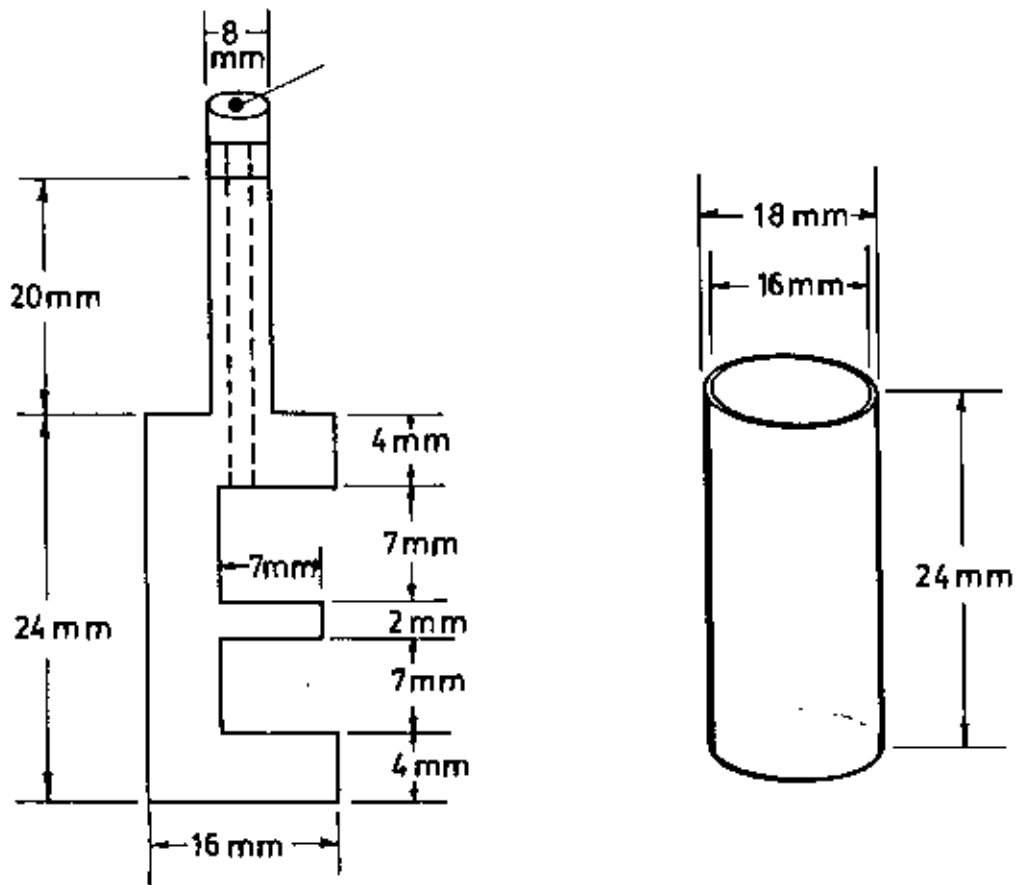


Fig. 7.3 Specimen holder .

To keep the gauges in the same thermal environment a cylindrical shaped specimen holder was made as shown in Fig.(7.3). It was made from a copper rod of 16 mm diameter. Two identical grooves of approximate thickness 7 mm and width 10 mm were cut separated by a thin section of width 2 mm. This arrangement made it assemble to keep the active and dummy specimens as close as possible.

The specimen and the dummy were fixed on the opposite faces of the thin section. Two identical strain gauges one on the face of the active specimen and other on the dummy specimen were glued. Electrical connections from the gauges were taken out through the hole of 2 mm diameter made in the centre specimen holder. The thinner section of the specimen holder of diameter 8 mm and length was glued to a glass tube of internal bore of 8 mm in diameter. This glass tube in turn hangs from the rotator. A copper hollow tube of 16 mm internal diameter was used as a jacket to keep the active and the dummy at same temperature and to isolate them ^{from} thermal fluctuations. The arrangement was found to be quite satisfactory.

7.2.6 ROTATOR FOR THE MEASUREMENTS OF ANGULAR POSITION OF SPECIMEN

In order to rotate the specimen in the magnetic field a rotating system has been constructed as shown in

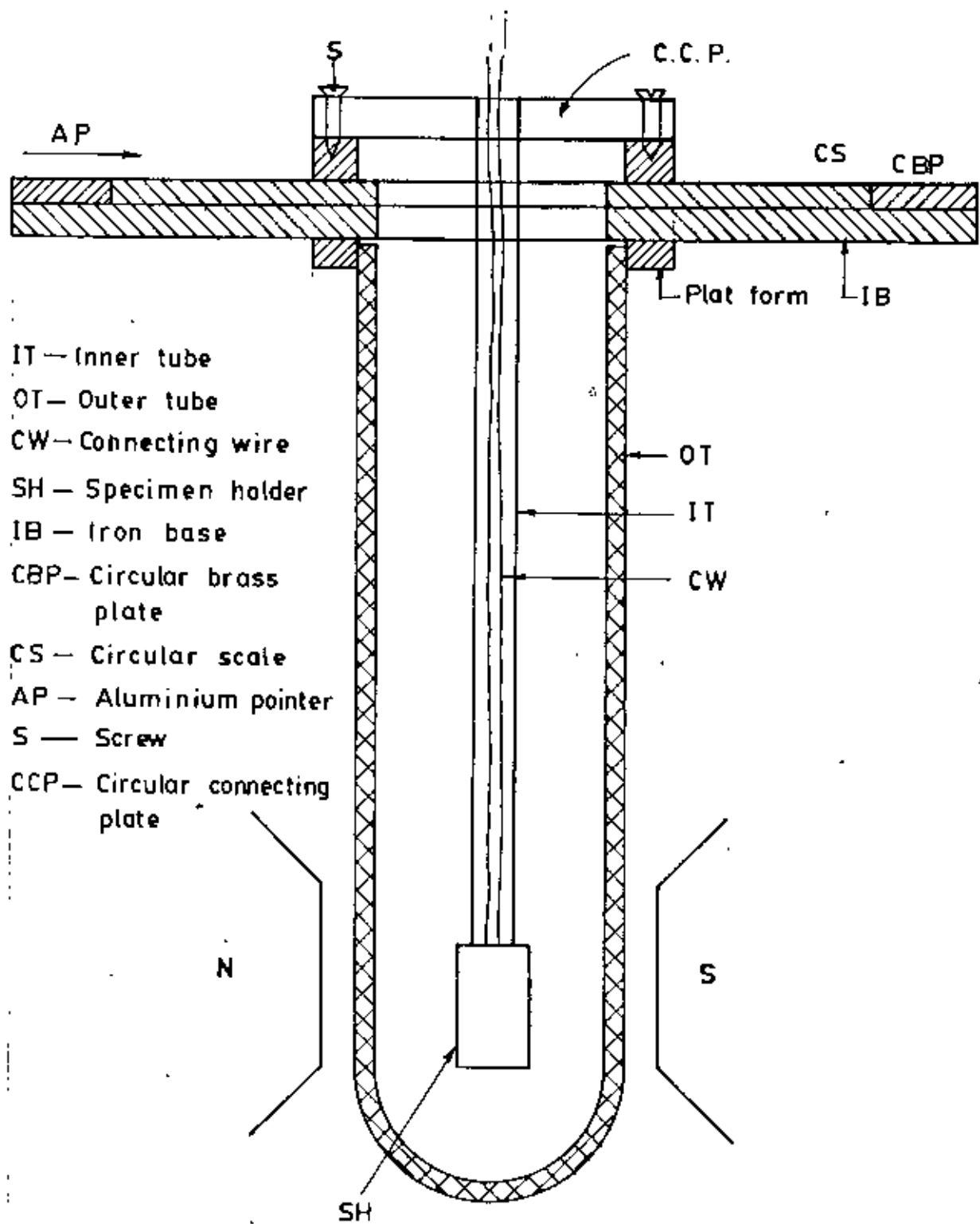


Fig. 7.4 Sample Rotating System.

in the diagram (7.4). The specimen rod along with the specimen holder was hanged from the bottom of the rotator made of brass - called circular connecting piece where it is glued firmly. The circular connecting piece is screwed to the collar of a rotatable circular brass plate having a circular scale graduated in degrees from 0° - 360° . The brass plate with circular scale just fits into a circular groove on an iron base and guarded by a thin circular brass plate. An aluminium pointer fitted to circular brass plate gives reading of any circular rotation of the specimen. The hole set up is put on a heavy wooden platform. The specimen tube was inserted inside a thin glass tube of internal diameter of 8 mm. This tube hangs from the bottom of the iron base. The thin glass tube is again surrounded by a thick outer glass tube of internal diameter 25 mm prevently from any draught from out side. The specimen holder alongwith glass tube hangs in such a manner that specimen lie in the homogenous region of the magnetic field produced by the electromagnet.

7.2.7 SPECIMEN MOUNTING

The mounting of the specimen in the specimen holder has to be flexible in order that specimen can freely change in dimension. At the same time to avoid any rotation of the specimen due to torque produced by the magnetic field, the specimen must be held sufficiently rigid. The best

compromise is made by using a thin cork spacer between the specimen and the base of the specimen holder. The specimen is glued to the cork by Durofix and the cork in turn to the specimen holder. The mosaic pattern of the cork spacer allows the specimen to expand or contract quite freely but constrains it from rotation due to body forces. Comparison of thermal expansion of a brass specimen when fixed to a cork spacer and when free showed that the constraint due to the above mentioned arrangement does not affect the result.

7.2.8 THE GAUGE CEMENTING

For perfect gauge bondage between the gauge and the surface of the specimen it is necessary to have very fine scratches on the gauges and specimen surfaces. The specimen surface is naturally left with fine irregularities of six micron order. The gauge is enclosed in a paper jacket which provides both insulation and protection. The paper base also provides good bonding surface for the gauge on to the specimen.

A thin coat of Durofix was applied to the gauge surfaces and the gauge area of the specimens. Then the gauge was placed on the specimen surface and the small pressure was applied on the gauge. The adhesive was cured for 24 hours at room temperature.

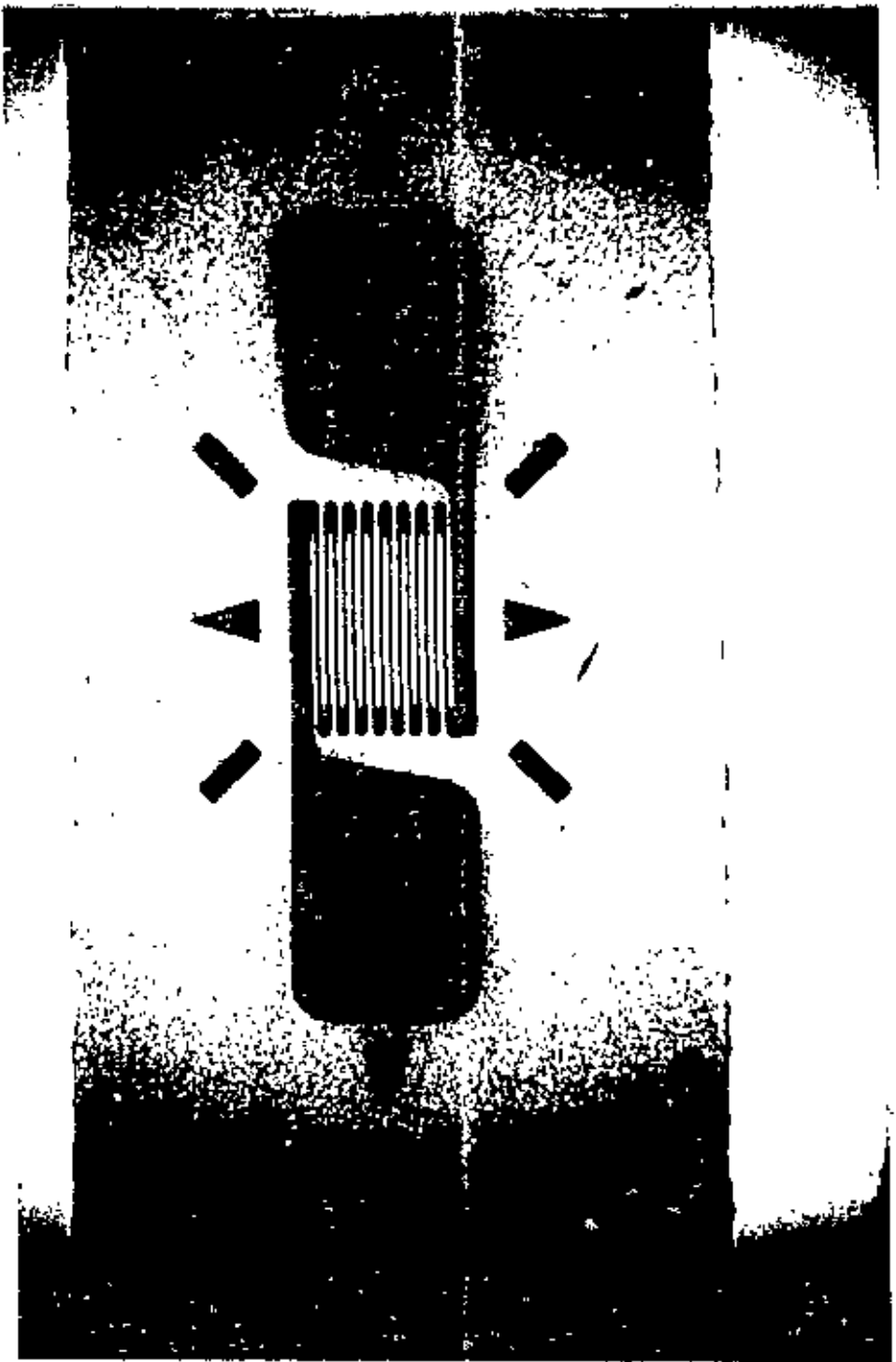
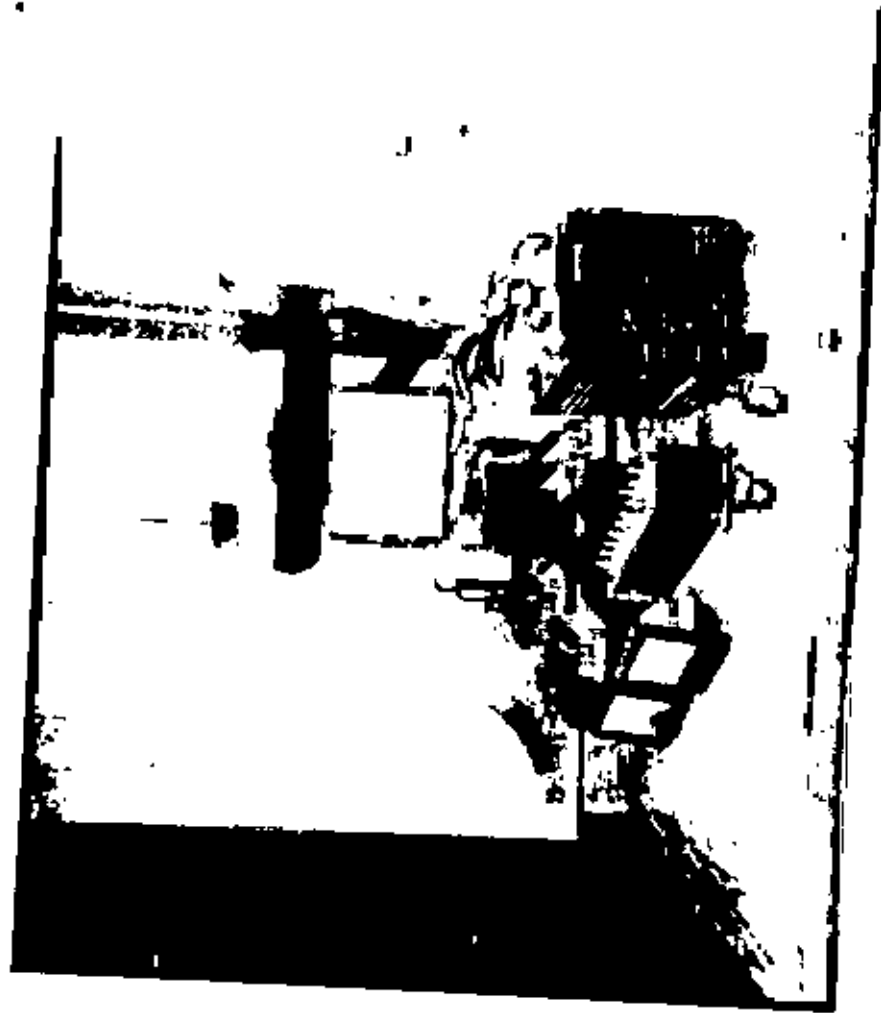


Figure
Magnified photograph of the micro-measurement strain gauge



Figure

A general view of the apparatus for measurements of magnetostriction

CHAPTER - VIII

MEASUREMENT OF MAGNETIZATION

8.1 CALIBRATION OF THE VSM

There are usually two methods of calibration of a vibrating sample magnetometer

- (i) by using a standard sample and
- (ii) by using a coil of small size whose moment can be calculated from the magnitude of the d.c current through it.

We have calibrated our V.S.M using a ~~20.7~~ mg spherical sample of 99.9% pure iron. The sample was made spherical with the help of a sample shaping device. It was then annealed in helium atmosphere at about 900°C . The sample's saturation magnetic moment has been calculated using the available data. The ratio transformer reading is obtained by actual measurement from the relation

$$M = k' k \dots \dots \dots (8.1)$$

Where M is magnetic moment, k' is saturation ratio transformer reading and k is VSM constant.

But $M = m \alpha \dots \dots \dots (8.2)$

Where α is the specific magnetization and m is the mass of the sample.

$$k k' = m \alpha$$

$$k = \frac{m \alpha}{k'} \dots \dots \dots (8.3)$$

The accuracy of this calibration however depends on the reliability of the standard iron sample; the accuracy of the ratio transformer and the gain of amplifier. The equipment has been operated repeatedly with the same standard sample and stability has been found to be within 1 part in 100.

The absolute accuracy of the instrument depends on the knowledge of the magnetic properties of the calibration standard and reproducibility of sample position. When the substitution method of calibration is used, the major error $\pm 1\%$ is introduced by the estimation of the standard iron sample. The relative accuracy of this instrument depends on accurate calibration of the precision resistor divider net work.

The total error here can be kept to less than 0.5% . A typical calibration curve of magnetic field Vs ratio transformer reading is shown in Fig.(8.1).

8.2 V.S.M CALIBRATION DATA

(1) Reference signal with phase shifter and decade transformer in connection

$$\begin{aligned} V_{\text{ref,}} &= \frac{1}{0.01} \times \frac{10 \mu V}{20} \times 19 \\ &= 9.5 \mu V \times 100 = 0.95 \text{ mv.} \end{aligned}$$

$V_{\text{ref,}}$ with variation of $0.5 \mu V \times 100 = 0.95 \text{ mv}$

(2) Reference signal with decade transformer in connection

$$V_{\text{ref}_2} = \frac{1}{0.01} \times 11 \mu\text{v} = 1.1 \text{ mv}$$

V_{ref_2} with variation of 0.1 mv

(3) Reference signal direct

$$V_{\text{ref}_3} = 13 \times 0.1 \text{ mv} = 1.3 \text{ mv}$$

V_{ref_3} with variation of 0.2 mv.

Table - 8.1

FINAL SET OF READING FOR PURE Fe- SAMPLE

Reference Frequency = 80 Hz.

Speaker voltage = 4 volts peak to peak.

Mass for pure Fe-sample = 20.7 mg = 20.7×10^{-6} Kg.

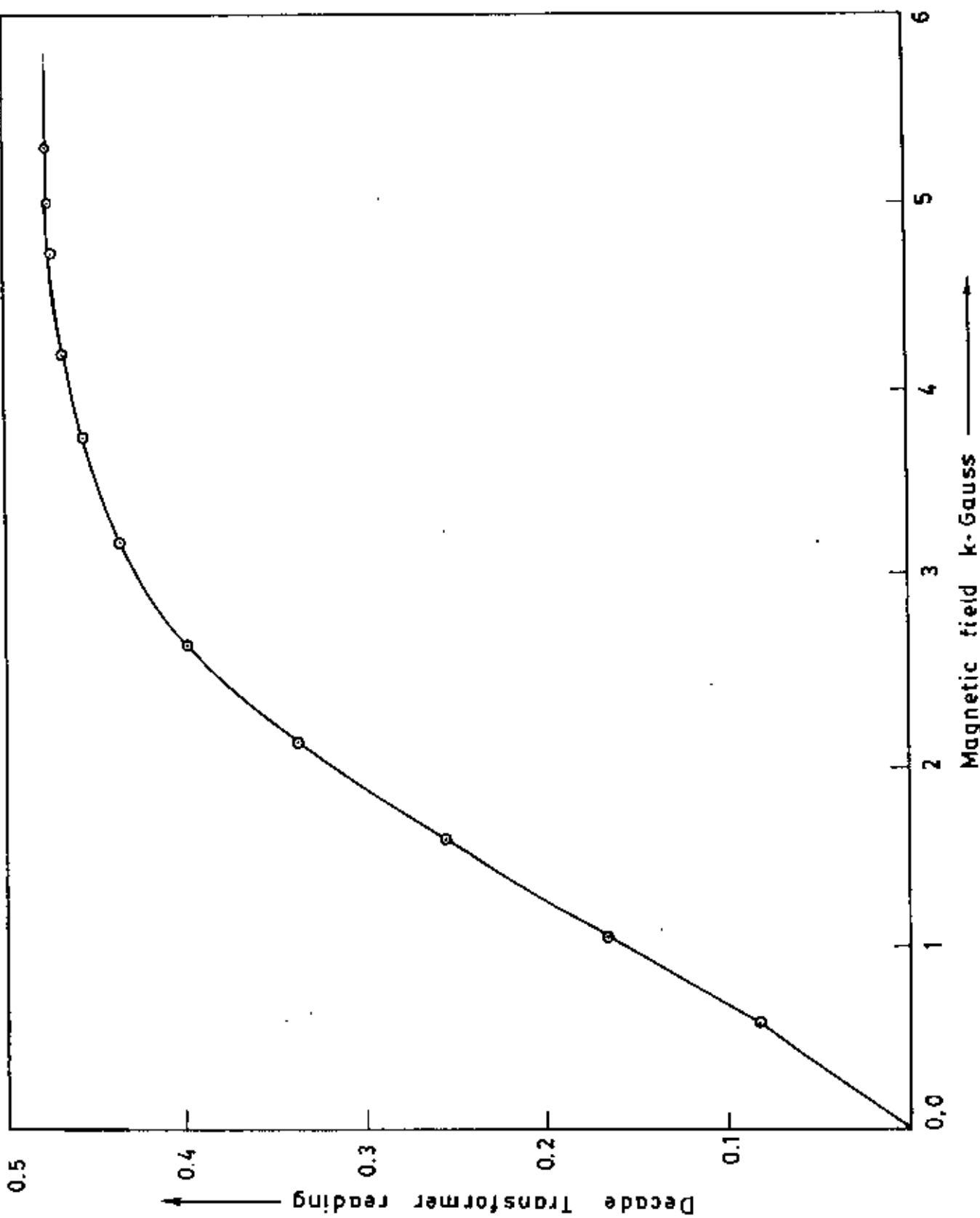


Fig. 8.1 Calibration curve of magnetic field vs. decade transformer reading (V.S.M).

<i>Field current (amp)</i>	<i>Magnetic Field H(Gauss)</i>	<i>Decade Transformer reading</i>
0	0	0.0073
1	600	0.0825
2	1075	0.1656
3	1600	0.255
4	2100	0.355
5	2625	0.397
6	3187	0.4322
7	3750	0.4526
8	4175	0.4646
9	4725	0.47
9.5	5000	0.4725
10	5300	0.4725

8.3 CALCULATION OF CALIBRATION CONSTANTStandard data on the ferromagnetic elements^(8.2)

Elements	20°C			0°K	H_B	T_c	$\frac{\alpha_s}{\alpha_0}$
	α_s emu/g	M_s emu/cm ³	$4\pi M_s$ G	α_0 emu/g			
Fe	218	1714	21580	221.9	2.219	770	0.982
Co	161	1422	17900	162.5	1.715	1131	0.991
Ni	54.39	484.1	6084	57.50	0.604	358	0.946

Saturation decade transformer reading for pure Fe at 20°C

$$K' = 0.4725$$

Specific magnetization for pure ⁵⁶Fe at 20°C

$$\begin{aligned}\alpha &= 218 \text{ emu/gm} \\ &= 218 \text{ Am}^2/\text{Kg}\end{aligned}$$

$$\begin{aligned}\text{Magnetic moment } M &= m\alpha \\ &= 20.7 \times 10^{-6} \times 218 \\ &= 4.5126 \times 10^{-3} \text{ Am}^2\end{aligned}$$

Calibration constant

$$K = \frac{4.5126 \times 10^{-3}}{0.4725}$$

$$K = 9.5505 \times 10^{-3} \text{ Am}^2$$

8.4 CALIBRATION CURVES FOR MAGNET-1 ASSEMBLY AND POWER SUPPLY

The electromagnet used for the measurement of magnetization was a Newport Electromagnet Typen 177 with 17.7 cm diameter Pole Pieces. The magnet was mounted on a graduated rotating base. The standard model was modified to provide an adjustable pole gap in order that the highest possible field strength was available. The calibration of the magnet was done with a NORMA Electronic Fluxmeter to an accuracy of about $\pm 1\%$. A Typical calibration curve of current I VS field strength H is shown in Fig.(8.2). Even with this calibration instrument a small hysteresis effect was observed.

Table - 8.2

DATA OF MAGNET TYPE ~~N~~177 [177 mm DIAMETER POLES] PLANE TIP.

pole gap = 6.5 cm.

Coil 1550 turns of copper strip.

Maximum current without water cooling

= 10 amps continuous.

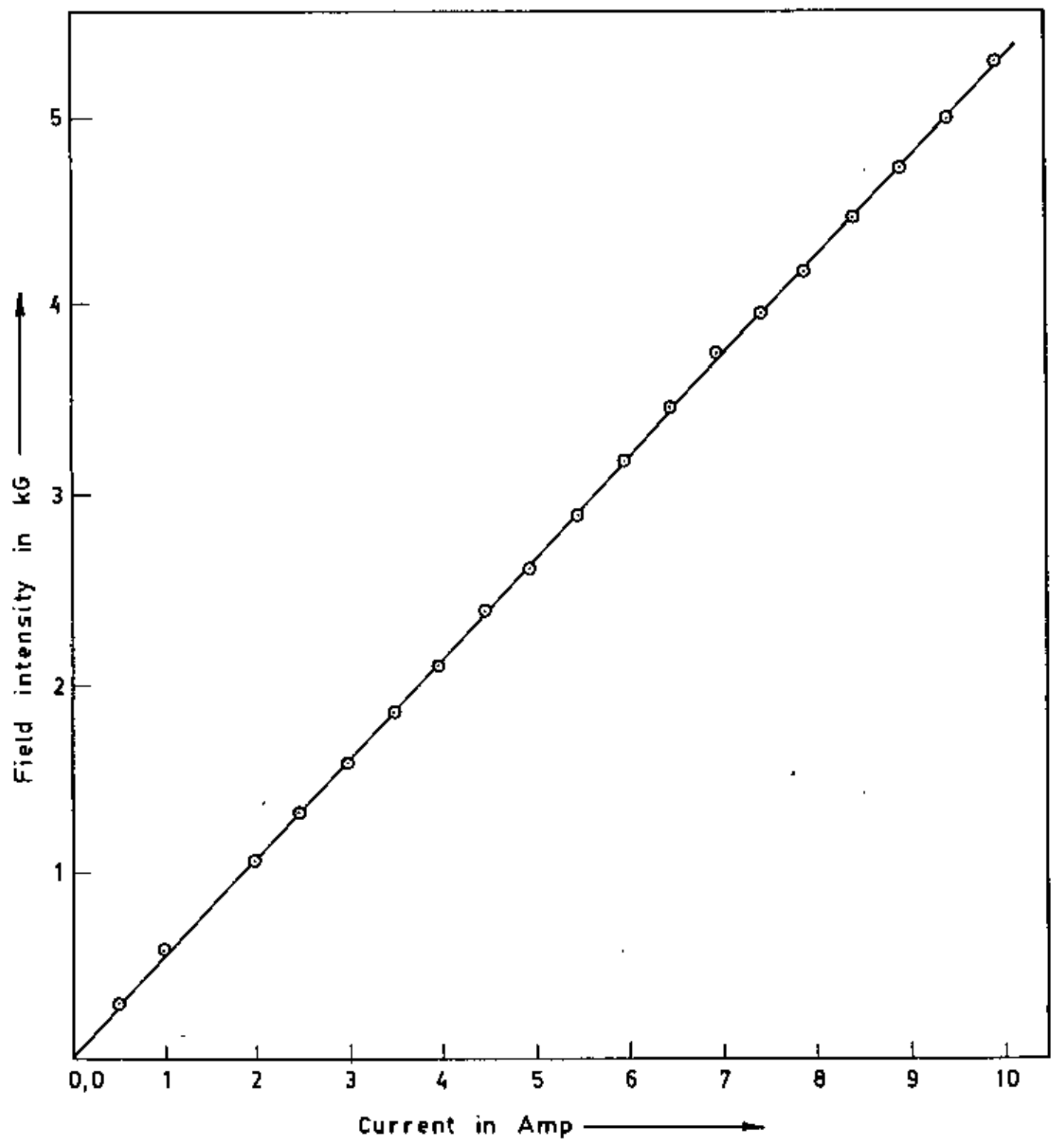


Fig. 8.2 Magnetic field vs. current electromagnet-2, pole gap-6.5cm.

Field current (Amp)	Fluxmeter deflection			Scale divider 5
	I(+)	I(-)	Average deflection	Magnetic Field (Per division 50 Gauss)
0.5	6	6.5	6.25	312.50
1.0	12	12	12	600.00
2.0	21	22	21.5	1075.00
2.5	26	27	26.5	1325.00
3.0	32	32	32	1600.00
3.5	37	38	37.5	1875.00
4.0	42	42	42	2100.00
4.5	48	48	48	2400.00
5.0	52	53	52.5	2625.00
5.5	58.5	58	58.25	2912.50
6.0	63.5	64	63.75	3187.50
6.5	69	69	69	3450.00
7.0	75	75	75	3750.00
7.5	79	79	79	3950.00
8.0	84	83	83.5	4175.00
8.5	89	89	89	4450.00
9.0	94	95	94.5	4725.00
Scale divider 10, Magnetic field per division 100 Gauss				
9.5	50	50	50	5000.00
10.0	53	53	53	5300.00

The magnetization of thin iron boron ribbon is measured as a function of magnetic field using vibrating sample

magnetometer. The iron boron ribbon samples are first weighed, then glued to a standard sample mount. The magnetometer may be used as a field measuring device by using iron boron

sample and the susceptibility is not too large and is field independent. The proportionality constant accounting for the particular coil geometry and susceptibility is obtained by

calibration with the pure iron standard above the saturation. The field standard above the saturation. The field measured is an average value over the sample volume. A relative

accuracy of about 1% is obtained with the double coils; the absolute accuracy depends on the calibration method.

A vibrating sample magnetometer was used for measuring magnetization of iron boron ribbons of different compositions $Fe_{82}B_{18}$, $Fe_{81}B_{19}$ and $Fe_{80}B_{20}$ of thicknesses 55 μm , 40 μm and 30 μm respectively at room temperature to look for the composition dependence of magnetization. This is shown in Fig. (8.5).

The sample with composition $Fe_{82}B_{18}$ was chosen for the study of magnetization process. The magnetization of thin ribbon $Fe_{82}B_{18}$ is measured as a function of magnetic field

at room temperature as shown in Fig.(8.3). Magnetization is also evaluated as a function of field to find the dependence of magnetization on the domain structure.

The sample $Fe_{82} B_{18}$ is also studied for its magnetization process as affected by annealing and is interpreted in terms of domain reorganization by the heat treatment.

The magnetization curves were obtained for sample $Fe_{82} B_{18}$ (Fig.8.7) which were annealed for 2.5 hours at temperatures $50^{\circ}C$, $100^{\circ}C$, $150^{\circ}C$, $200^{\circ}C$, $250^{\circ}C$ and $300^{\circ}C$ respectively.

These annealing temperatures were maintained constant during annealing.

Table - 8.3

Variation of Magnetization with magnetic field for sample with composition $Fe_{81} B_{19}$.

Ribbon thickness $40 \mu m$

Weight of the sample(m) $5 \times 10^{-6} Kg.$

Calibration constant(K) = $9.5505 \times 10^{-3} Am^2$.

Field current (Amp)	Magnetic Field (Gauss)	Decade Transformer Reading $\times 10^{-4}$ k'	Specific magnetization $\alpha_s = \frac{kk'}{m}$ (Am^2/Kg)
1	600	693	132.37
2	1075	860	164.27
3	1600	930	177.64
4	2100	938	179.17
5	2625	946	180.69
6	3187	946	180.69

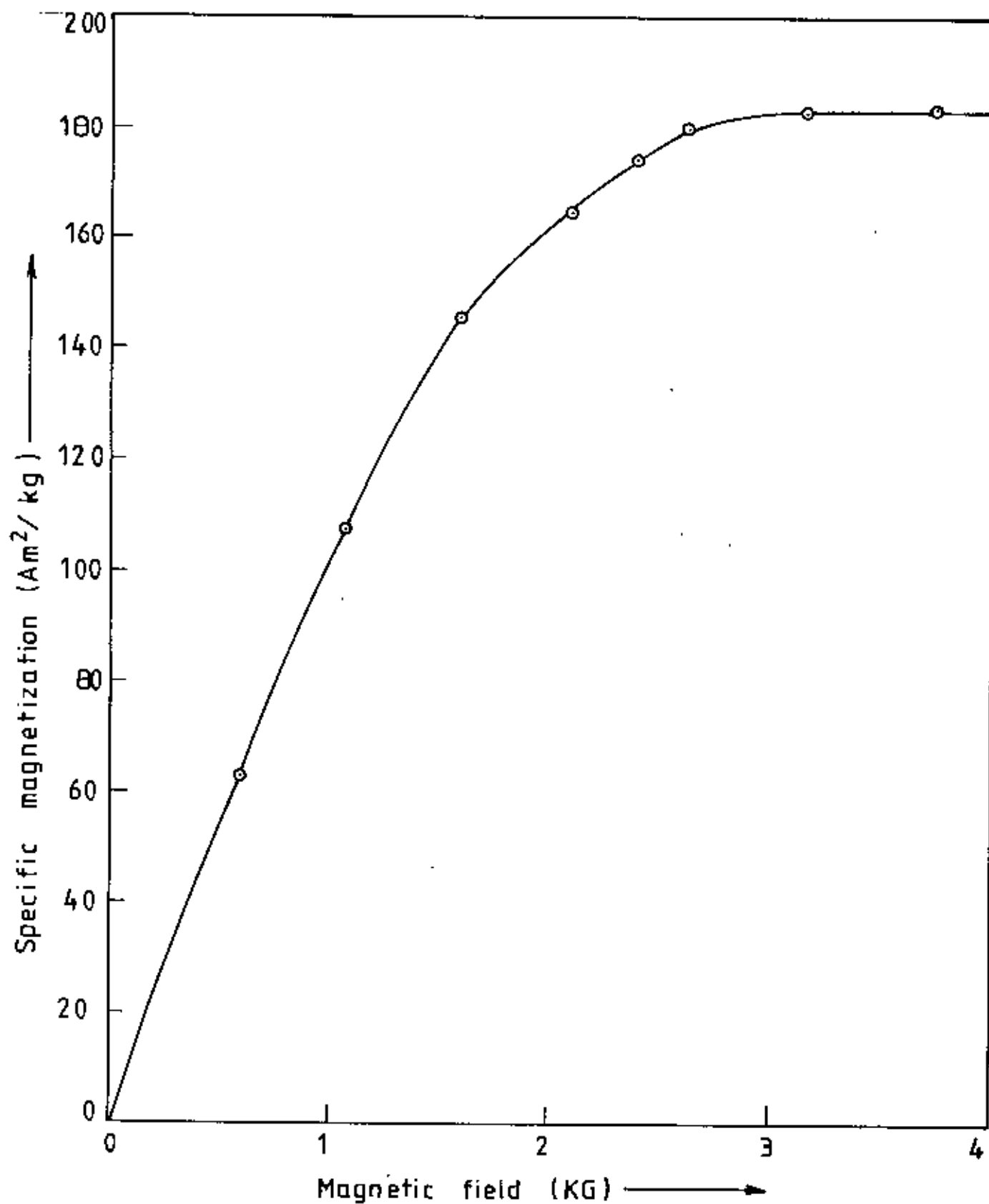


Fig. 8.3 Variation of magnetization vs. magnetic field for $Fe_{82}B_{18}$.

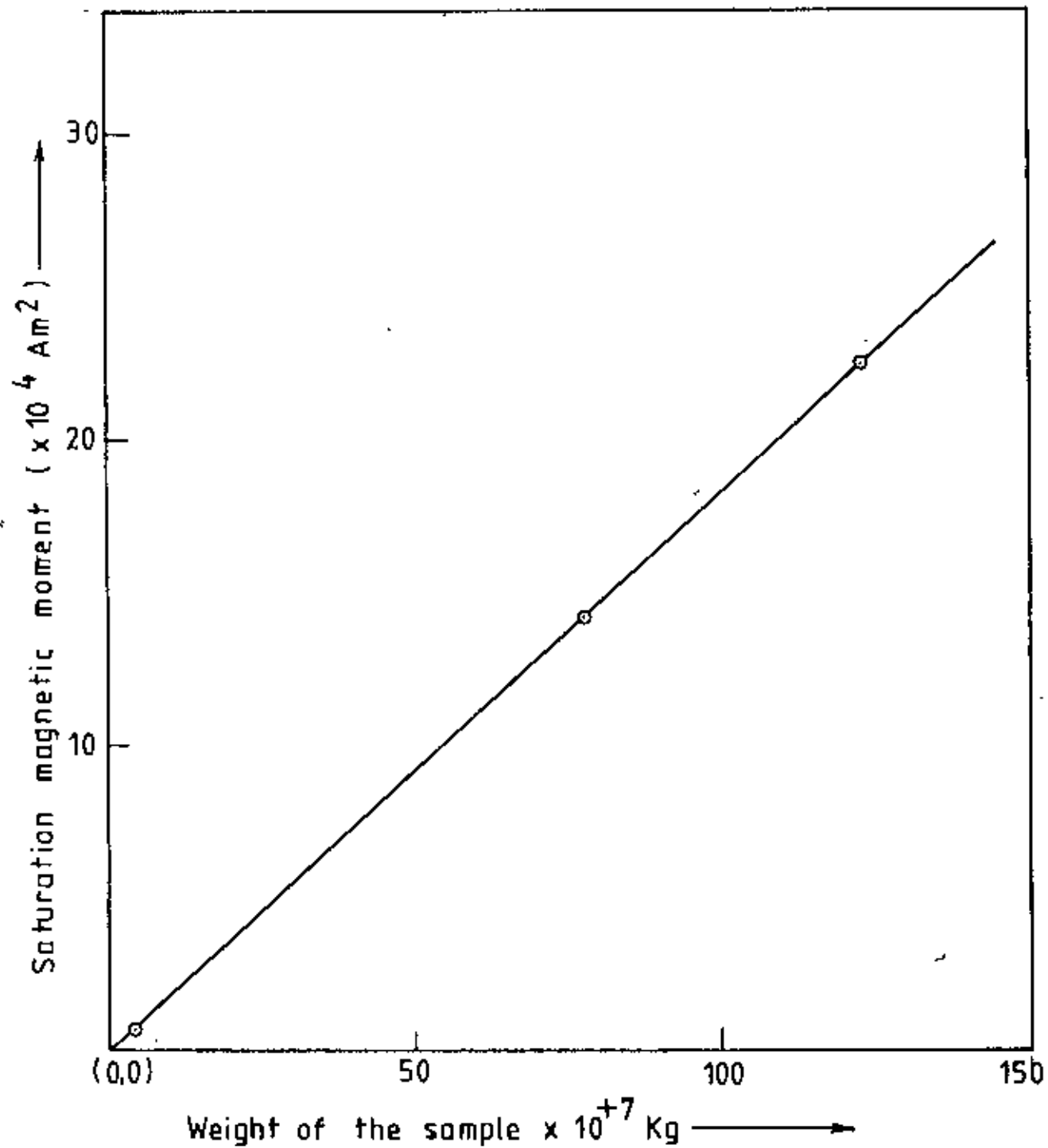


Fig. 8.4 Variation of saturation magnetic movement vs. weight of the sample $\text{Fe}_{82}\text{B}_{18}$ ribbons.

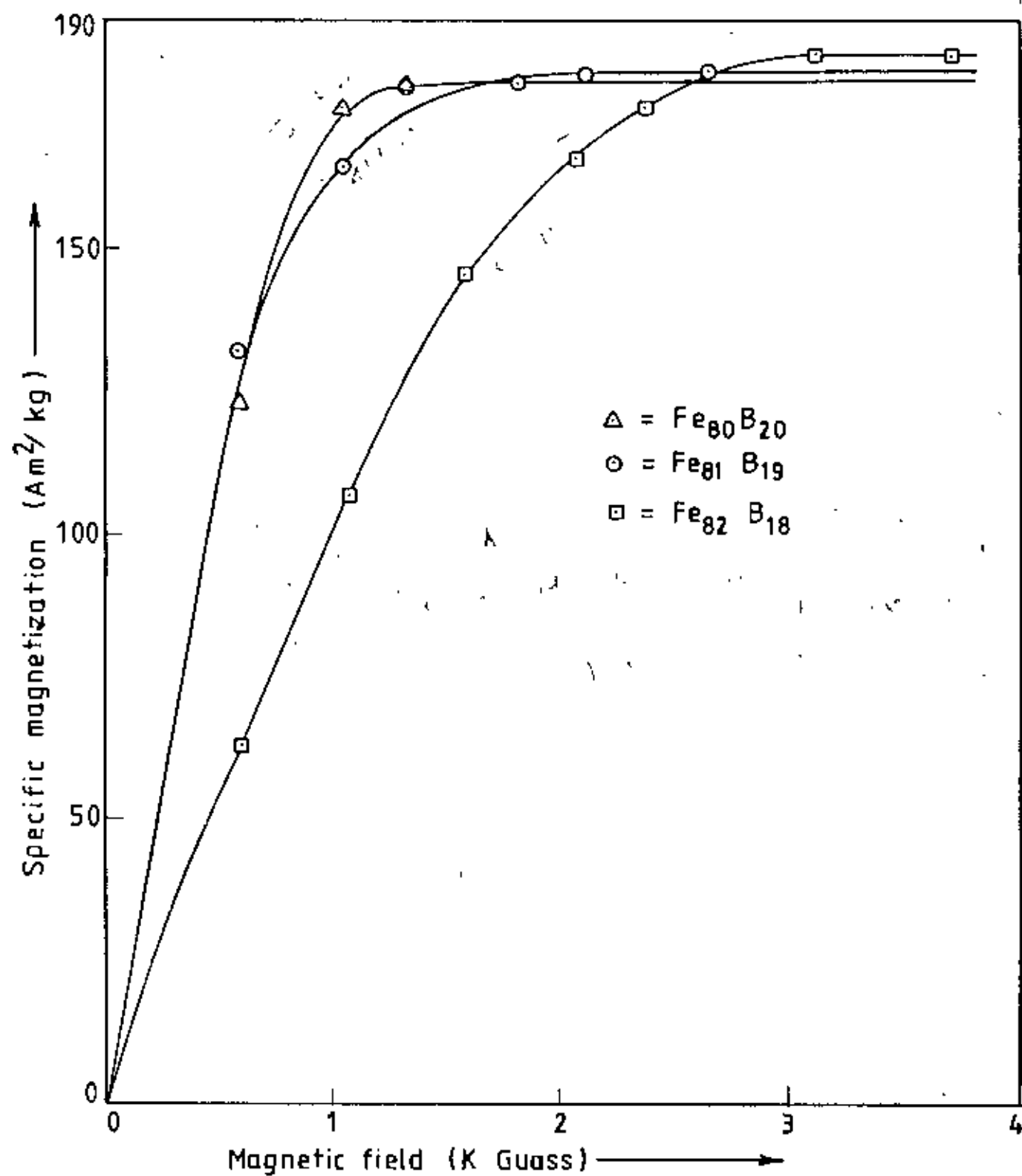


Fig. 8.5 Magnetization vs. magnetic field for different composition.

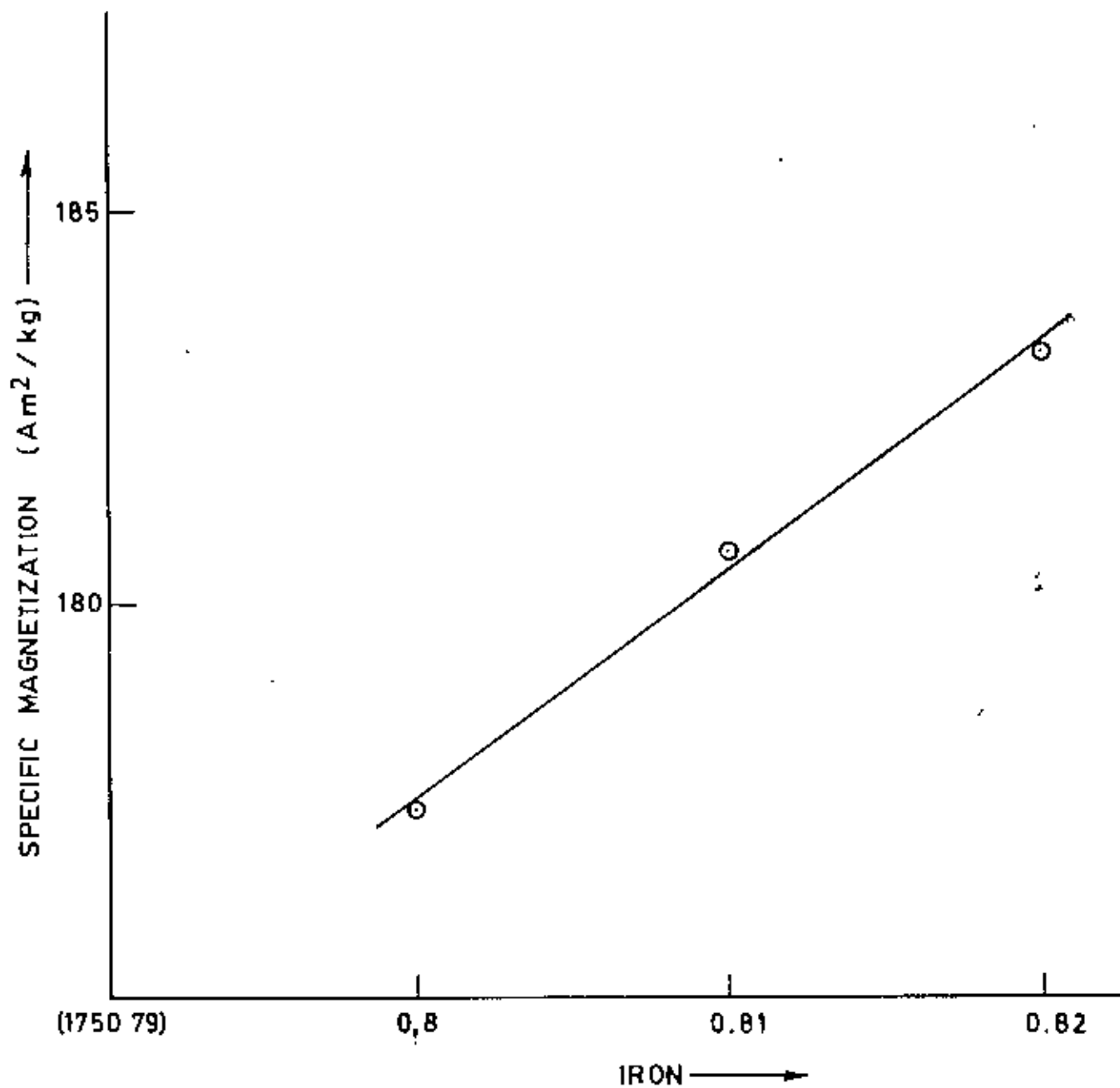


Fig. B.6 MAGNETIZATION VS. CHANGE IN IRON COMPOSITION.

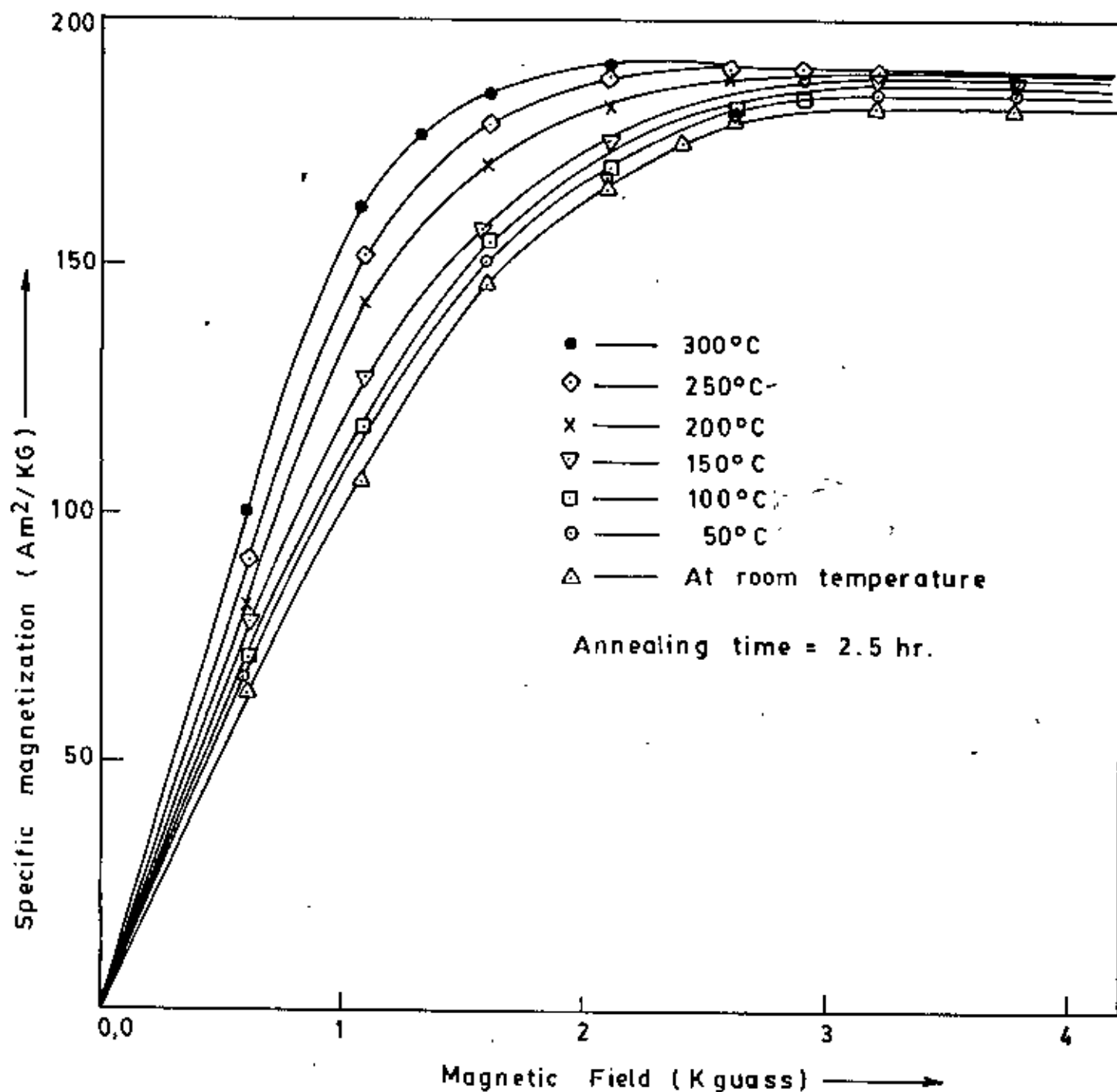


Fig. 8.7 Magnetization vs. magnetic field for different annealing temperature.

Table - 8.4

Variation of Magnetization with magnetic field for unannealed sample $Fe_{80} B_{20}$.

Weight of the sample (m) = 4.2×10^{-6} Kg

Calibration constant (k) = 9.5505×10^{-3} Am²

Ribbon thickness = 30 μ m .

Field current (Amp)	Magnetic field (Gauss)	Decade Trans-former reading $\times 10^{-4} = k^1$	Specific magnetization $a_s = \frac{kk^1}{m}$ (Am ² /Kg)
1	600	540	122.79
2	1075	770	175.09
3	1600	780	177.37
4	2100	780	177.37

Table - 8.5

Variation of Magnetization with magnetic field for unannealed sample $Fe_{82} B_{18}$.

Weight of the sample (m) = 1.23×10^{-5} Kg

Calibration constant (k) = 9.5505×10^{-3} Am²

Ribbon thickness = 55 μ m .

Field current (Amp)	Magnetic field (Gauss)	Decade Trans-former reading $\times 10^{-4} = k^1$	Specific Magnetization $a_s = \frac{kk^1}{m}$ (Am ² /Kg)
1	600	815	69.28
2	1075	1378	106.99
3	1600	1875	145.59
4	2100	2120	164.61
4.5	2400	2240	173.93
5	2625	2320	180.14
6	3187	2360	183.26
7	3750	2360	183.26

Table 8.6

Variation of Magnetization with magnetic field for Annealed sample $Fe_{82}B_{18}$.

Annealed Temperature = $50^{\circ}C$

Annealed Time = 2.5 hours

Weight of the sample (m) = $1.78 \times 10^{-5} Kg$

Calibration constant (K) = $9.5505 \times 10^{-3} Am^2$

Field current (Amp)	Magnetic Field (Gauss)	Decade Transformer reading $\times 10^{-4}$ k'	Specific Magnetization $\alpha_s = \frac{kk'}{m} (Am^2/Kg)$
1	600	1248	66.96
2	1075	2018	108.27
3	1600	2815	151.04
4	2100	3130	167.94
5	2625	3360	180.28
6	3187	3461	185.70
7	3750	3461	185.70

Table 8.7

Variation of Magnetization with magnetic field for Annealed sample $Fe_{82}B_{18}$.

Annealed Temperature. : $100^{\circ}C$

Annealed time = 2.5 hours.

Weight of the sample (m) = $8.8 \times 10^{-6} Kg$

Calibration constant (k) = $9.5505 \times 10^{-3} Am^2$.

Field current (Amp)	Magnetic Field (Gauss)	Decade Transformer reading $\times 10^{-4}$ k'	Specific magnetization $\alpha_s = \frac{kk'}{m} (Am^2/Kg)$
1	600	656	71.19
2	1075	1088	118.08
3	1600	1430	155.20
4	2100	1560	169.3
5	2625	1672	181.46
5.5	2912.5	1700	184.49
6.0	3187	1720	186.67
7.0	3750	1720	186.67

Table - 8.8

Variation of Magnetization with magnetic field
for Annealed sample $Fe_{82}B_{18}$.

Annealed Temperature : $150^{\circ}C$

Annealed Time = 2.5 hours

Weight of the sample (m) = 8.1×10^{-6} Kg

Calibration constant (k) = 9.5505×10^{-3} Am² .

Field current (Amp)	Magnetic Field (Gauss)	Decade transformer reading $\times 10^{-4}$ k'	Specific magnetization $\alpha_s = \frac{kk'}{m}$ Am ² /Kg
1.0	600	665	78.41
2.0	1075	1085	127.93
3	1600	1275	150.33
3.5	1875	1355	159.76
4.0	2100	1450	170.97
4.5	2400	1540	181.58
5.0	2625	1566	184.64
5.5	2912.5	1597	188.297
6.0	3187	1597	188.297

Table - 8.9

Variation of Magnetization with magnetic field
for Annealed sample $Fe_{82}B_{18}$.

Annealed Temperature. : $200^{\circ}C$

Annealed time = 2.5 hours

Weight of the sample (m) = 7.7×10^{-6} Kg

Calibration constant (k) = 9.5505×10^{-3} Am² .

Field current (Amp)	Magnetic Field (Gauss)	Decade Transformer reading $\times 10^{-4}$ k'	Specific magnetization $\alpha_s = \frac{kk'}{m} \text{ Am}^2/\text{Kg}$
1	600	656	81.37
2	1075	1155	143.26
3	1600	1380	171.16
4	2100	1470	182.33
5	2625	1520	188.53
6	3187	1520	188.53

Table 8.10

Variation of Magnetization with magnetic field for Annealed sample $\text{Fe}_{82}\text{B}_{18}$.

Annealed Temperature : 250°C

Annealed Time = 2.5 hours

Weight of the sample (m) = 1.08×10^{-5} Kg.

Calibration constant (k) = $9.5505 \times 10^{-3} \text{ Am}^2$.

Field current (Amp)	Magnetic Field (Gauss)	Decade Transformer reading $\times 10^{-4}$ k'	Specific magnetization $\alpha_s = \frac{kk'}{m} (\text{Am}^2/\text{Kg})$
1	600	1027	90.82
2	1075	1725	152.54
3	1600	2033	179.78
4	2100	2130	188.36
5	2625	2150	190.13
6	3187	2150	190.13

Table - 8.11

Variation of Magnetization with magnetic field
for Annealed sample $Fe_{82}B_{18}$.

Annealed Temperature : $300^{\circ}C$

Annealed Time : 2.5 hours

Weight of the sample (m) = 1.04×10^{-5} Kg

Calibration constant (k) = $9.5505 \times 10^{-3} Am^2$.

Field current (Amp)	Magnetic Field (Gauss)	Decade Transformer reading $\times 10^{-4}$ k'	Specific magnetization $\alpha_s = \frac{kk'}{m}$ (Am^2/Kg)
1	600	1098	100.83
2	1075	1765	162.08
2.5	1325	1925	176.78
3	1600	2010	184.58
4	2100	2060	189.17
5	2625	2076	190.64
6	3187	2076	190.64

CHAPTER - IX

MEASUREMENT OF MAGNETOSTRICTION

9.1 CALIBRATION CURVES FOR MAGNET-2 (FOR
MAGNETOSTRICTION MEASUREMENT)

The electromagnet used for the measurement of magnetostriiction was a Newport Electromagnet Type 126 with 12.6 cm diameter pole pieces. The calibration of the magnet was done with a NORMA Electronic Fluxmeter to an accuracy of about $\pm 1\%$. A typical calibration curve of current I VS field strength H is shown in Fig.(9.1). Even with this calibration instrument a small hysteresis effects was observed.

Table 9.1

Data of magnet (2) Typen 126 [126 mm
diameter poles] plane Tip .

Magnet face gap , = 3.5 cm

Fluxmeter scale divider position 10 (division
(100 Gauss per scale div.)

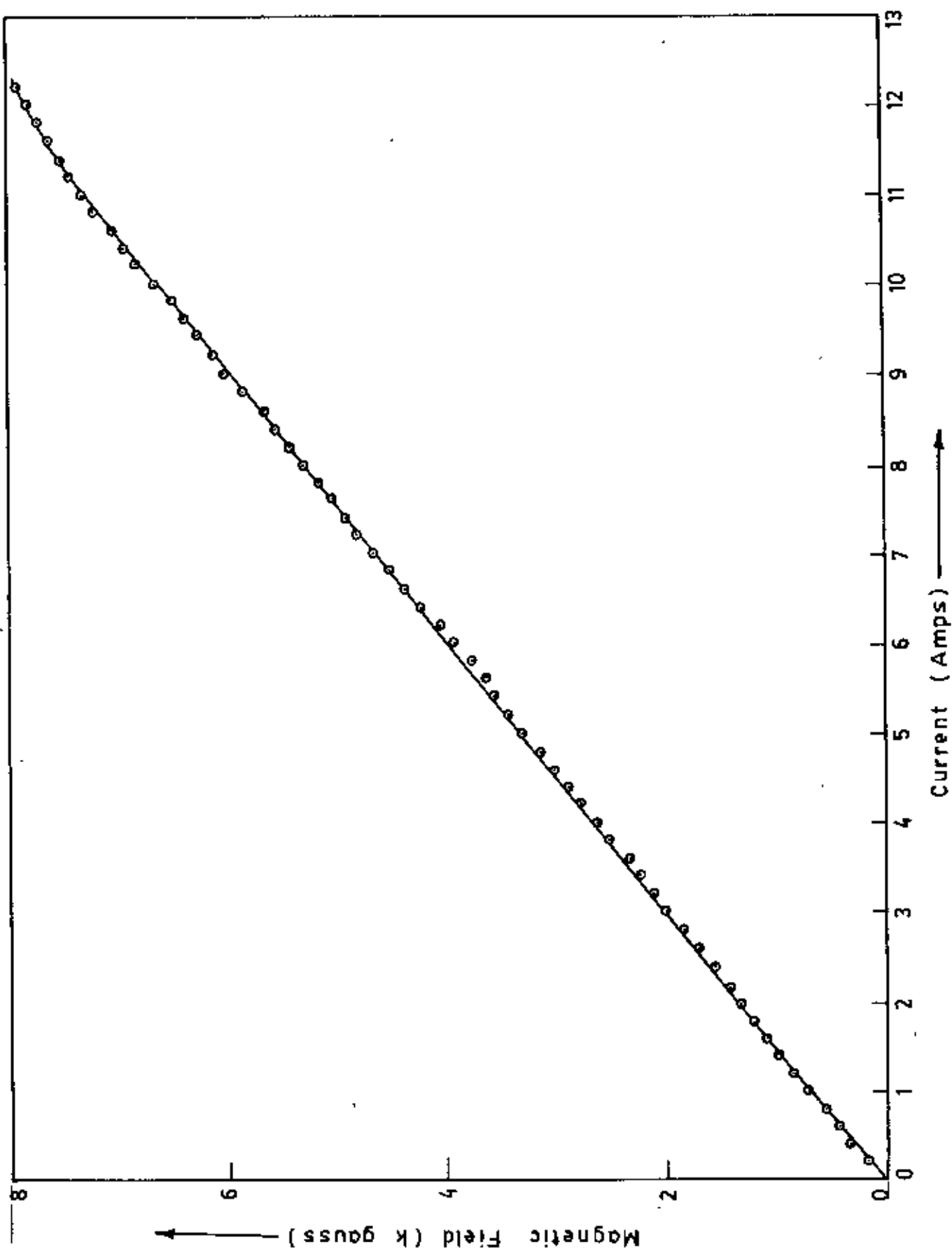


Fig. 9.1 Magnetic field vs. current electromagnet - 2, pole gap - 3.5 cm.

Field current (Amp)	Fluxmeter Reading		Average deflection	Magnetic Field (Gauss)
	I(+)	I(-)		
0.2	2	2	2	200
0.4	3	4	3.5	350
0.6	4	5	4.5	450
0.8	5	6	5.5	550
1.0	7	8	7.5	750
1.2	8	9	8.5	850
1.4	10	10	10	1000
1.6	11	11	11	1100
1.8	12	12	12	1200
2.0	13	13.5	13.25	1325
2.2	14	14	14	1400
2.4	16	15	15.5	1550
2.6	17	17	17	1700
2.8	18	18.5	18.25	1825
3.0	20	20	20	2000
3.2	21	21	21	2100
3.4	22	22	22	2200
3.6	23	23	23	2300
3.8	25	25	25	2500
4.0	26	26	26	2600
4.2	28	29	27.5	2750
4.4	29	28	28.5	2850
4.6	30	30	30	3000
4.8	31	31.5	31.25	3125

Field current (Amp)	Fluxmeter reading		Average deflection	Magnetic Field (Gauss)
	I(+)	(-)		
5.0	33	33	33	3300
5.2	34	34	34	3400
5.4	35	36	35.5	3550
5.6	36	36	36	3600
5.8	37	38	37.5	3750
6.0	39	39	39	3900
6.2	40	40	40	4000
6.4	42	42	42	4200
6.6	43	44	43.5	4350
6.8	45	45	45	4500
7.0	46	47	46.5	4650
7.2	48	48	48	4800
7.4	49	49	49	4900
7.6	50	50	50	5000
7.8	51	52	51.5	5150
8.0	52	53	52.5	5250
8.2	54	54	54	5400
8.4	55	55.5	55.25	5525
8.6	56	56	56	5600
8.8	58	59	58.5	5850
9.0	60	60	60	6000
9.2	61	61	61	6100

Field current (Amp)	Fluxmeter reading		Average deflection	Magnetic field (Gauss)
	I(+)	I(-)		
9.4	63	62	62.5	6250
9.6	64	64	64	6400
9.8	64	65	64.5	6450
10.0	66	67	66.5	6650
10.2	68	68	68	6800
10.4	69	69.5	69.25	6925
10.6	70	70	70	7000
10.8	72	72	72	7200
11.0	73	73	73	7300
11.2	74	74	74	7400
11.4	75	75	75	7500
11.6	76	76	76	7600
11.8	77	77	77	7700
12.0	78	78	78	7800
12.2	79	79	79	7900

9.2 BRIDGE CIRCUIT SENSITIVITY AND CALIBRATION

The circuit used for measurement of the resistance changes in the gauges was a D.C Wheatstones Bridge Fig.(7.2). It included a reversing switch(s) to ascertain to what extent thermal E.M.F.'s into the circuit were effecting the balance conditions of the bridge. The ¹⁰⁰⁰ Nano voltmeter used was a Model 140 of high sensitivity and a period of 2.5 seconds.

the calculation of results. drifts would be recorded and allowance made for these in the ~~the~~ voltmeter scale deflection. Also slow steady thermal bridge when measuring very small strains and to recorded is hoped to amplify small D.C. output voltages from the Work on the bridge arrangement is to continue and it

the fluctuations should be zero. these are in opposing arms of the bridge, the net effect of which occurred in gauge A also occurred in gauge B and since environment as the active gauge, any thermal fluctuations the specimen and D represents the dummy gauge in the same were A represents the active strain gauge in contact with The components of the bridge are shown in Fig. (7.2)

to prevent overheating in the gauge elements. Bridge currents were restricted to a maximum of 25 mA

bridge current Fig. (9.2) & Fig. (9.3). This low periodic time of the instrument enabled quick recording of out-of-balance deflections thus minimizing errors due to drift and fluctuations from thermal R.H.F.'s in the circuit. The bridge sensitivity changed linearly with

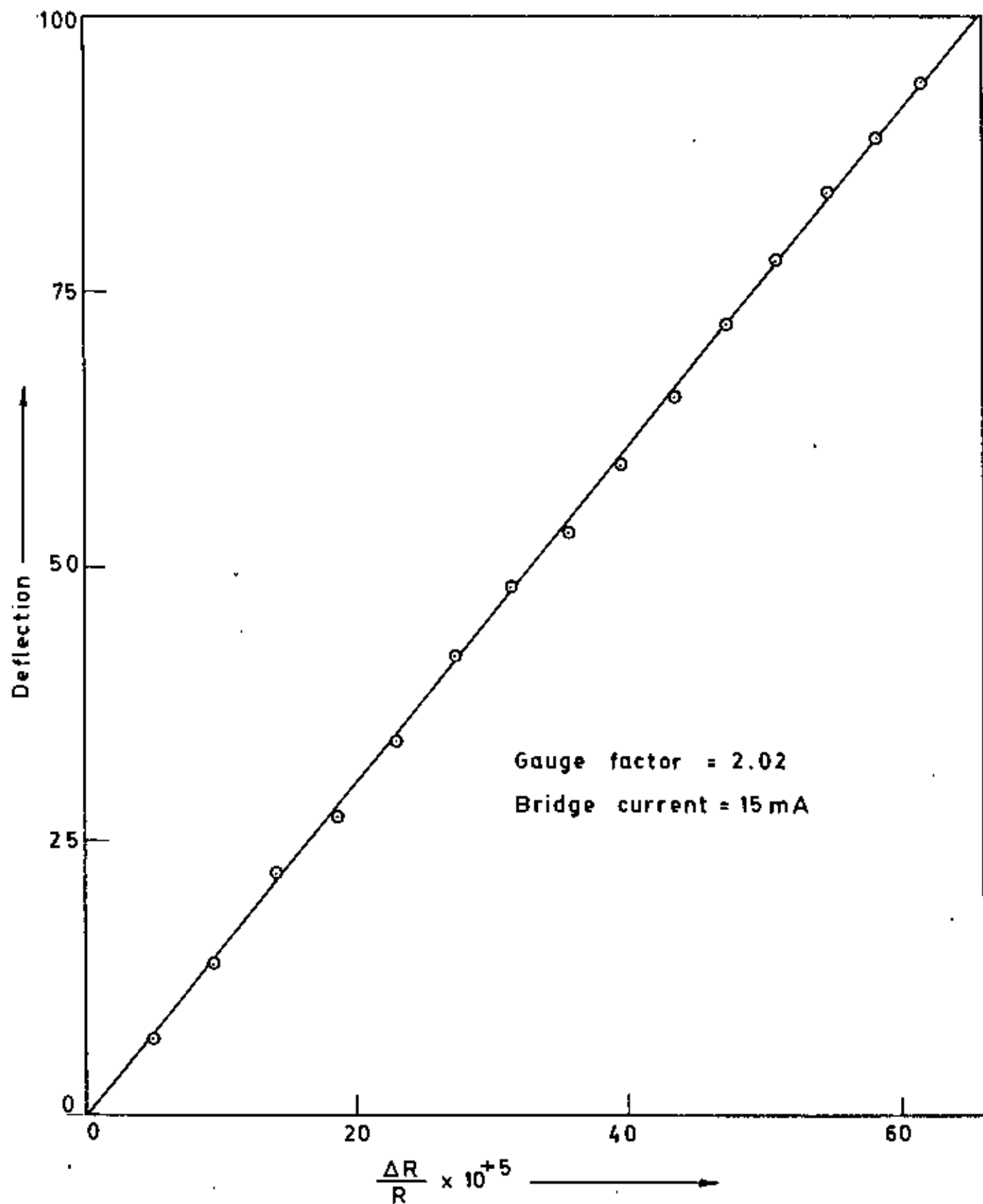


Fig. 9.2 Bridge sensitivity

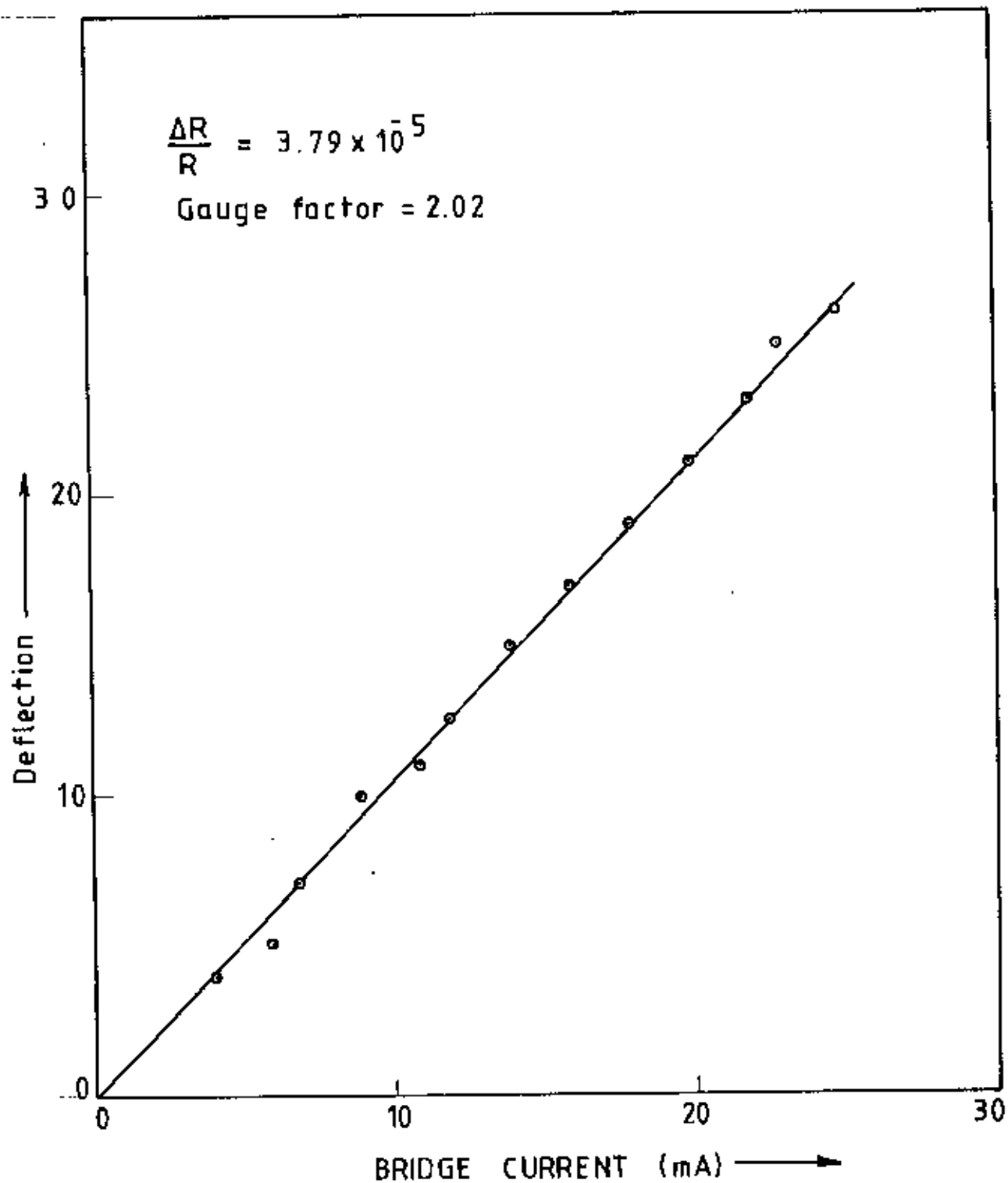


Fig. 9.3 Variation of bridge, sensitivity with bridge current.

9.3 CALIBRATION CURVE FOR ANGLE CORRECTION

In an Amorphous ribbons the magnetic domains of the the different micro crystallites having random orientations make different angles with each other in the demagnetized state. When the magnetic field is applied the magnetic domain wall movement starts. In the initial state due to 180° domain wall movement no contribution is there to the net strain of the amorphous ribbon specimen, because the reversal of the direction of magnetization has no effect on the elongation of the domain. In the second state with increased magnetic field the 90° domain wall movement begins. This gives rise to magnetostriction i,e changing lattice dimension which is in our case is positive. This magnetostriction effect can be looked at as due to predominance of the strain axes in the direction of the measurements. The angle Vs magnetostriction curve shown in Fig.(9.4). The angle Vs magnetostriction curve showed that a minimum at 133° and a maximum at 223° . The minimum at 133° is identified as the 0-position of magnetic field with respect to the gauge direction and the maximum at 123° is identified as the 90° position of the field with respect to the gauge direction.

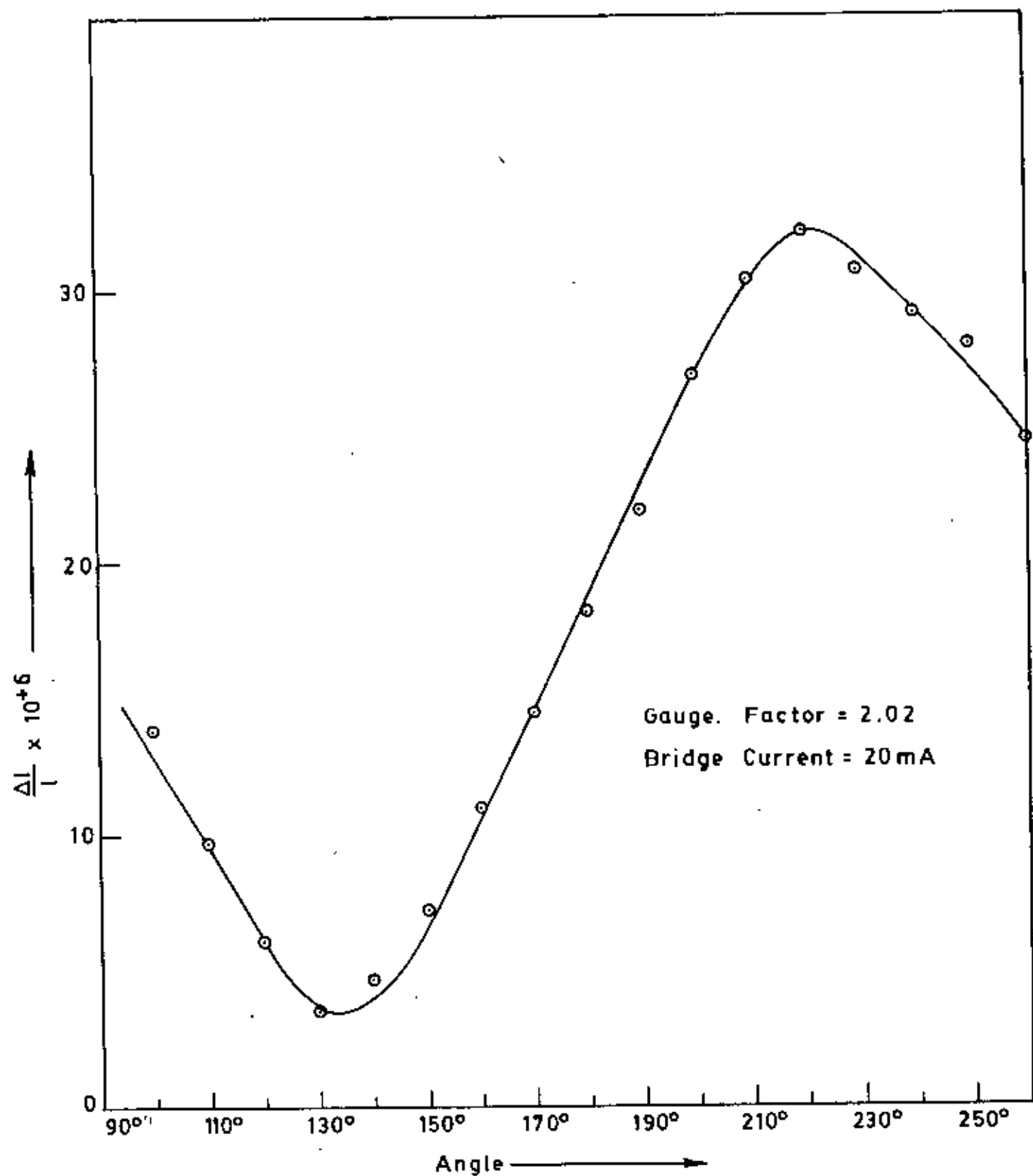


Fig. 9.4 Magnetostriction vs. angular position of field.

Table - 9.4

Variation of the magnetostriction VS angular position of the field.

Bridge current = 20 mA

Gauge Factor = 2.02

Nano voltmeter per deflection $\frac{\Delta R}{R} \times 10^5 = 4.215$

$$\begin{aligned} \therefore \frac{\Delta I}{I} &= \frac{1}{G} \cdot \Delta R/R \\ &= 2.436 \times 10^{-6} \end{aligned}$$

Angle position	Nano Voltmeter reading	magnetostriction $\frac{\Delta I}{I} = \frac{1}{G} \Delta R/R$
100°	5	12.182 × 10 ⁻⁶
110°	4	9.745 "
120°	2.5	6.091 "
130°	1.5	3.655 "
140°	2	4.873 "
150°	3	7.309 "
160°	4.5	10.964 "
170°	6	14.618 "
180°	7.5	18.273 "
190°	9	21.928 "
200°	11	26.801 "
210°	12.5	30.455 "
220°	14	34.109 "
230°	13.5	32.891 "
240°	12	29.237 "
250°	11.5	28.019 "
260°	10	24.365 "

9.4 MEASUREMENTS OF MAGNETOSTRICTION

The experimental determination and analysis of magnetostriction of amorphous iron boron ribbon with composition $Fe_{82} B_{18}$ is presented. The problem associated with strain gauge technique as applied to thin iron boron ribbons with composition $Fe_{82} B_{18}$ are discussed. Magnetostriction measurement as a function of applied field are evaluated. The contribution to net magnetostriction due to this rotation of the domains may have positive sign as that due to 90° domain wall movement. This explained the increase in the positive magnetostriction in our graph shown in Fig.(9.5). In actual process the rotation of the 90° domains may begin before the completion of the 180° domain wall movements depending on anisotropy energy and the hindrance to the domain walls movements. Thus the interpretation of the graph indicating magnetostriction as a function of field is only qualitative except at the saturation magnetostriction, observed value of which is 31.86×10^{-6} .

Magnetostriction is also evaluated for its dependence on annealing temperature and the duration of annealing to see the effect of heat treatment on the domain structure

of ...
 ...
 ...

effecting magnetostriction. The effect of annealing on magnetostriction has also been measured using strain gauge. A systematic decrease in magnetostriction from its maximum value of 31.86×10^{-6} is observed. The magnetostriction vs magnetic field curves were obtained Fig.(9.6) for samples of $Fe_{82}B_{18}$. The annealing time was constant and was 2.5 hours for each sample but the temperatures were different i.e $50^{\circ}C$, $100^{\circ}C$, $150^{\circ}C$, $200^{\circ}C$, $250^{\circ}C$ and $300^{\circ}C$ respectively. The result for the different samples explained in terms of atomic ordering and domain reorganization effect. The saturation magnetostriction linearly decreases with annealing temperatures. The saturation magnetostriction versus annealing temperature with constant annealing time 2.5 hours curves are shown in Fig.(9.7).

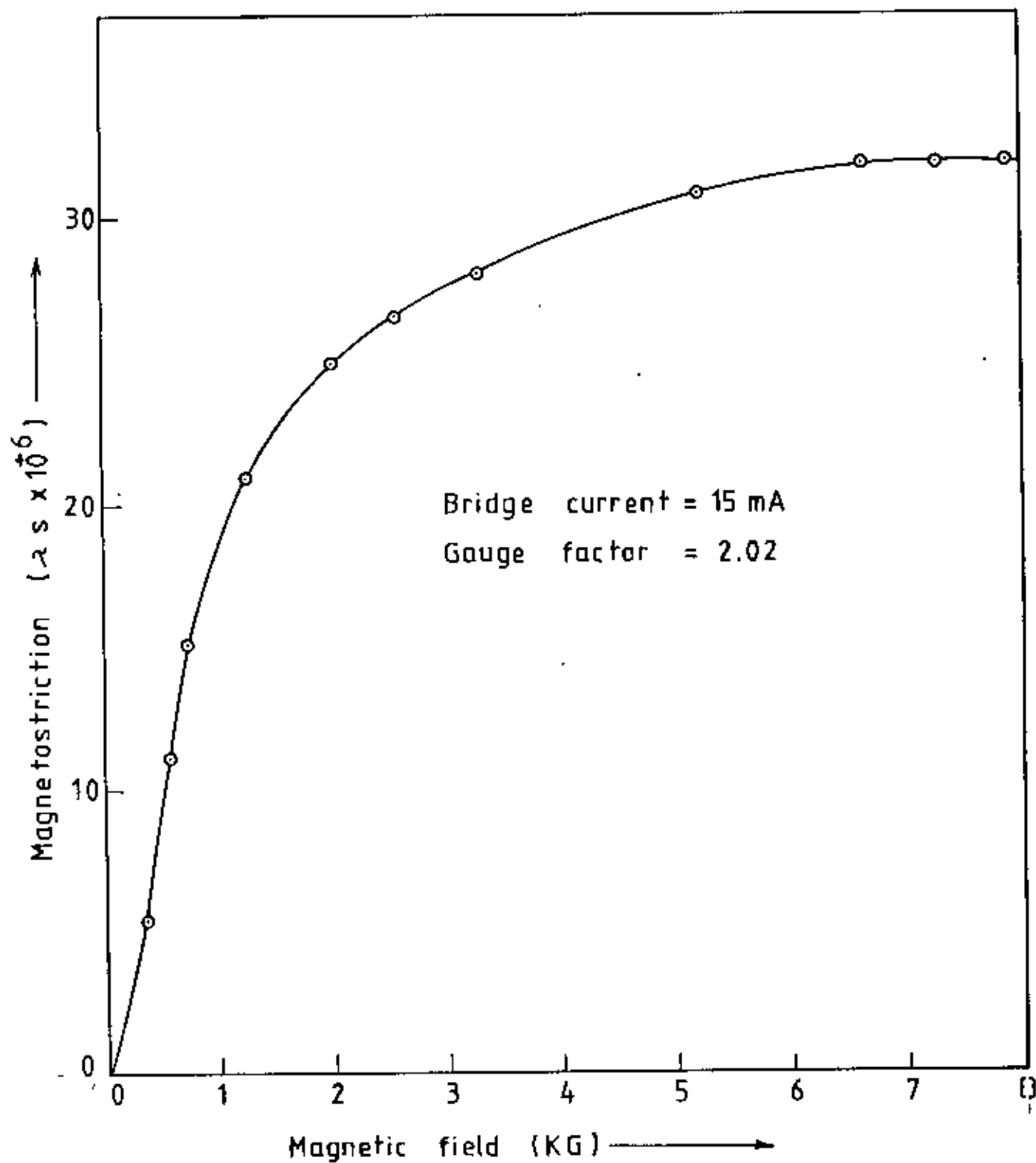


Fig. 9.5 Magnetostriction vs. magnetic field at room temperature for Fe₈₂B₁₈ ribbon.

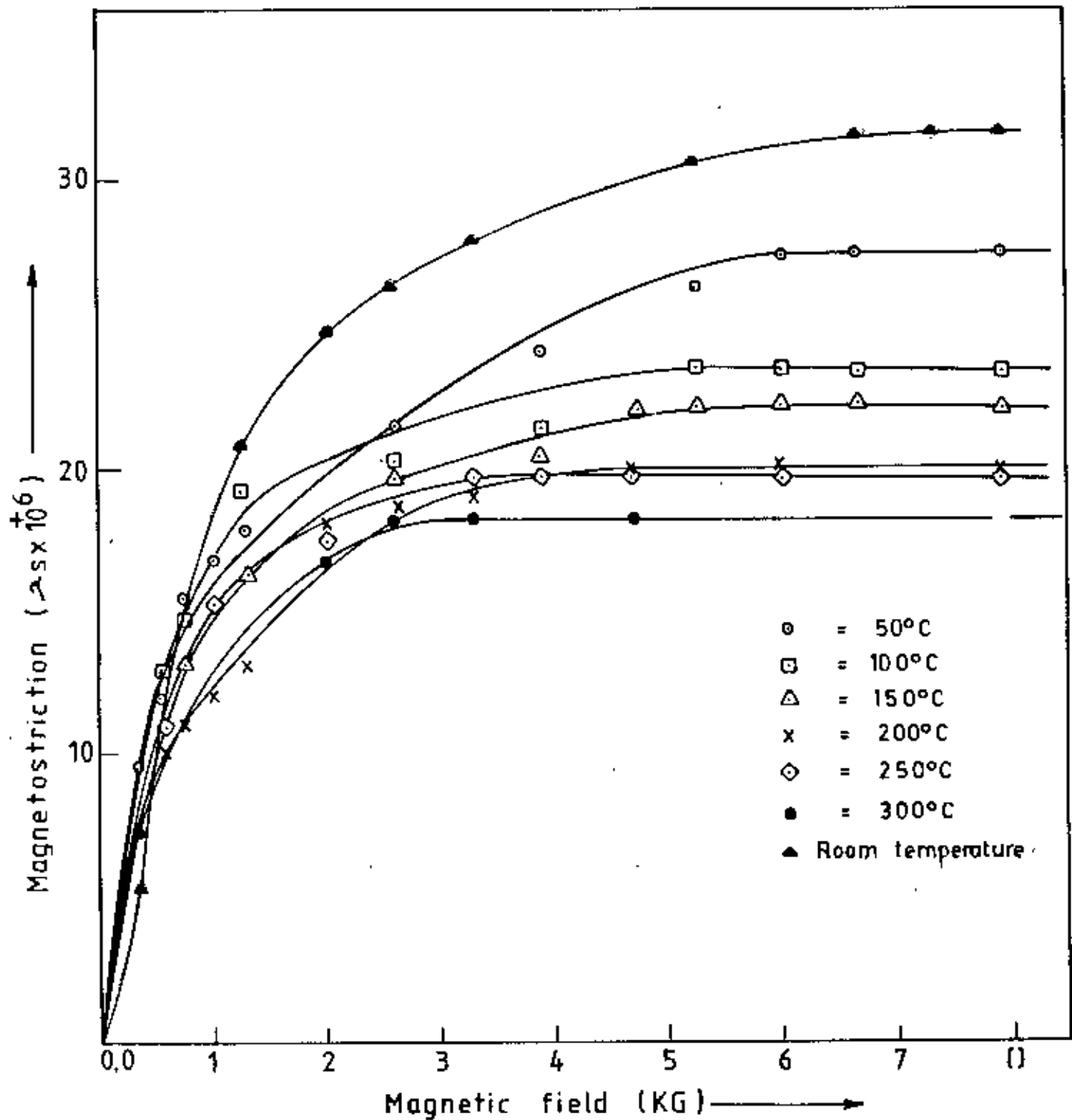


Fig. 9.6 Magnetostriction vs. magnetic field for different annealing temperature for $Fe_{82}B_{18}$ ribbon.

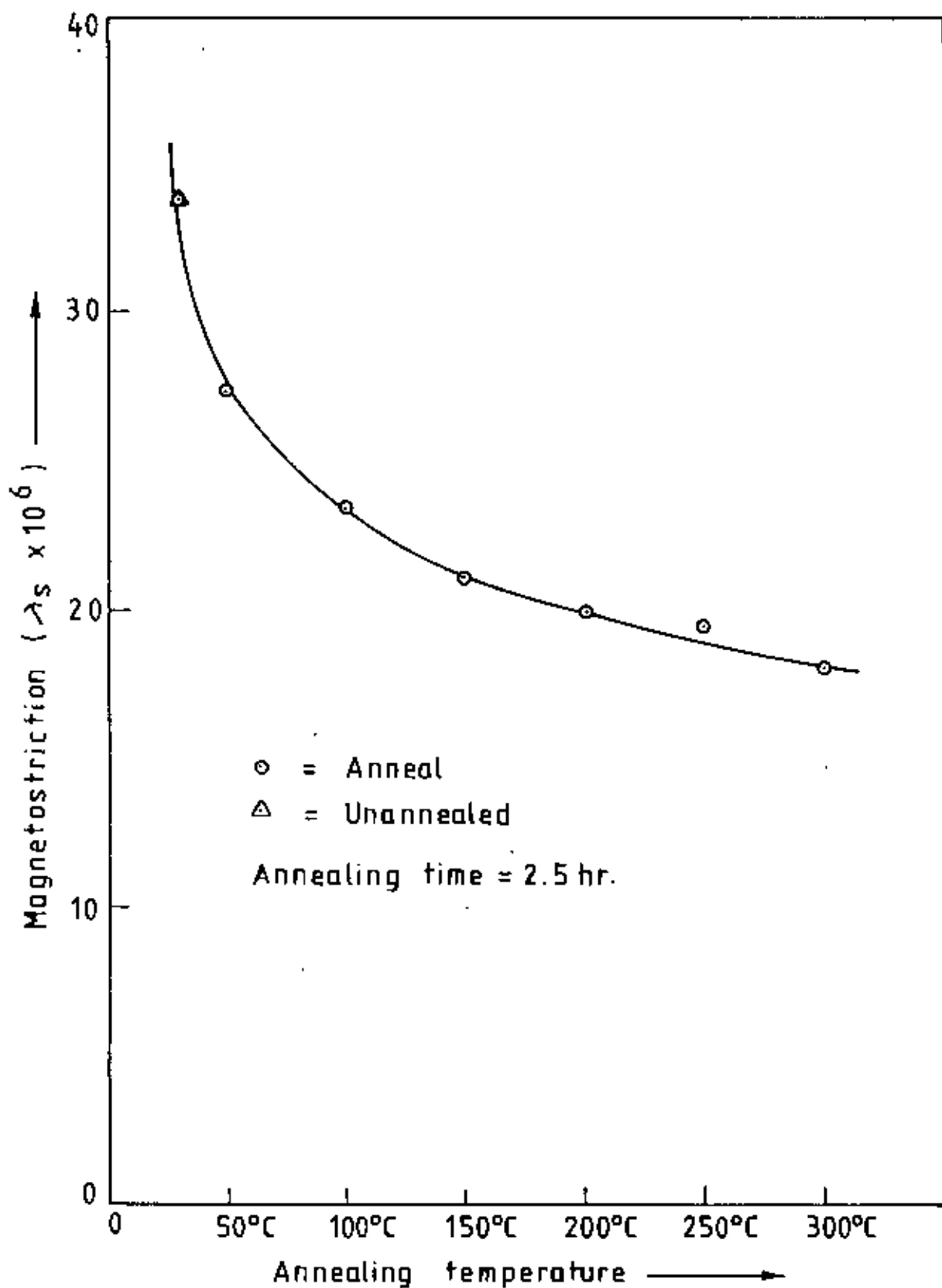


Fig. 9.7 Magnetostriction vs. annealing temperature for Fe₈₂B₁₈ ribbons.

TABLE - 9.5

Variation of magnetostriction with magnetic field for iron born ribbon with composition $Fe_{82} B_{18}$ at room temperature.

Bridge current = 15 mA

Gauge Factor = 2.02

Sensitivity per deflection $\Delta R/R = -7.19 \times 10^{-6}$

Field current (Amp)	Magnetic Field strength (Gauss)	$\Delta R/R$	Magnetostriction $= -\frac{2}{3G} \left(\frac{\Delta R}{R} \right)$
0.4	350	-1.6789×10^{-5}	$+ 5.541 \times 10^{-6}$
0.8	550	-3.3581 "	11.083×10^{-6}
1.0	750	-4.6174 "	15.239 "
2.0	1325	-6.2963 "	20.78 "
3.0	2000	-7.5559 "	24.937 "
4.0	2600	-7.9750 "	26.322 "
5.0	3300	-8.3952 "	27.707 "
8.0	5250	-9.2348 "	30.478 "
10.0	6650	-9.6545 "	31.863 "
11.0	7300	-9.6545 "	31.863 "
12.0	7800	-9.6545 "	31.863 "

TABLE - 9.6

Variation of magnetoresistion with magnetic field
for amorphous annealed sample Fe₈₀B₁₈.

Bridge current = 15 mA

Gauge factor = 2.02

Sensitivity per deflection $\frac{\Delta R}{R} = -6.1915 \times 10^{-6}$

Annealed temperature = 50°C

Annealed time = 2.5 hours.

Field current (amp)	Magnetic Field strength (Gauss)	$\Delta R/R$	Magnetoresistion $= -\frac{3G}{2} \left(\frac{\Delta R}{R} \right)$
0.4	350	-2.8918×10^{-5}	$+ 9.5438 \times 10^{-6}$
0.8	550	-3.6146	11.9297
1.0	750	-4.6991	15.5087
1.4	1000	-5.0607	16.702
2	1300	-5.4222	17.895
4	2600	-6.5066	21.474
6	3900	-7.2294	23.8595
8	5250	-7.9523	26.2454
9	6000	-8.3138	27.4384
10	6650	-8.3138	27.4384

TABLE - 9.7

Variation of magnetostriction with magnetic field
for amorphous Annealed sample $Fe_{80}B_{18}$.

Bridge current = 15 mA

Gauge Factor = 2.02

Sensitivity per deflection $\frac{\Delta R}{R} = -6.4615 \times 10^{-6}$

Annealed temperature = $100^{\circ}C$

Annealed time = 2.5 hours.

Field current (Amp)	Magnetic Field strength (Gauss)	$\Delta R/R$	Magnetostriction $= \frac{-2}{3G} \frac{\Delta R}{R}$
0.4	350	-2.9076×10^{-5}	$+ 9.596 \times 10^{-6}$
0.8	550	-3.8769 "	12.795 "
1.0	750	-4.523 "	14.9275 "
1.4	1000	-5.1692 "	17.06 "
2	1300	-5.8153 "	19.1925 "
4	2600	-6.1384 "	20.2588 "
6	3900	-6.4615 "	21.3251 "
8	5250	-7.1076 "	23.4575 "
9	6000	-7.1076 "	23.4575 "
10	6650	-7.1076 "	23.4575 "

TABLE - 9.8

Variation of magnetostriction with magnetic field
for amorphous Annealed sample $Fe_{80}B_{18}$.

Bridge current = 15 mA

Gauge Factor = 2.02

Sensitivity per deflection $\frac{\Delta R}{R} = -4.923 \times 10^{-6}$

Annealed temperature = $150^{\circ}C$

Annealed time = 2.5 hours.

Field current (Amp)	Magnetic Field strength (Gauss)	$\Delta R/R$	Magnetostriction $= -\frac{2}{3G} \left(\frac{\Delta R}{R} \right)$
0.4	350	$- 2.4615 \times 10^{-5}$	$+ 8.1239 \times 10^{-6}$
0.8	550	- 2.9539 "	9.7487 "
1.0	750	- 3.9385 "	12.9982 "
1.4	1000	- 4.4308 "	14.623 "
2	1300	- 4.9231 "	16.2478 "
4	2600	- 5.9077 "	19.4973 "
6	3900	- 6.1536 "	20.309 "
7	4650	- 6.3999 "	21.122 "
8	5250	- 6.3999 "	21.122 "

TABLE - 9.9

Variation of magnetoresistion with magnetic field for amorphous annealed sample Fe₈₀P₁₈.

Bridge current = 15 mA

Gauge factor = 2.02

Sensitivity per deflection $\frac{\Delta R}{R} = -6.052 \times 10^{-6}$

Annealed temperature = 200°C

Annealed time = 2.5 hours.

Field current (Amp)	Magnetic Field (Gauss)	$\Delta R/R$	Magnetoresistion $(\frac{\Delta R}{R}) (\frac{3G}{2})$
0.4	350	-2.1182 x 10 ⁻⁵	+ 6.9907 x 10 ⁻⁶
0.8	550	-3.026	9.9867
1.0	750	-3.3286	10.9854
1.4	1000	-4.2364	13.9814
2.0	1300	-4.539	14.9801
3.0	2000	-5.4467	17.976
5.0	3300	-5.7494	18.9748
6.0	3900	-6.0519	19.9734
7.0	4650	-6.0519	19.9734

TABLE - 9.10

Variation of magnetostriction with magnetic field for amorphous Annealed sample $Fe_{80}B_{18}$

Bridge current = 15 mA

Gauge Factor = 2.02

Sensitivity per deflection $\frac{\Delta R}{R} = -6.6065 \times 10^{-6}$

Annealed temperature = 250°C

Annealed time = 2.5 hours.

Field current (Amp)	Magnetic Field strength (Gauss)	$\Delta R/R$	Magnetostriction = $-\frac{2}{3G}(\frac{\Delta R}{R})$
0.4	350	-2.3123×10^{-5}	$+ 7.6313 \times 10^{-6}$
0.8	550	-3.9639 "	13.0822 "
1.0	750	-4.6246 "	15.2626 "
1.4	1000	-4.9549 "	16.3528 "
3.0	2000	-5.2852 "	17.4429 "
4.0	2600	-5.9459 "	19.6233 "
5.0	3300	-5.9459 "	19.6233 "

TABLE - 9.11

Variation of magnetostriction with magnetic field
amorphous Annealed sample $Fe_{82}B_{18}$.

Bridge current = 15 mA

Gauge Factor = 2.02

Sensitivity per deflection $\frac{\Delta R}{R} = -4.215 \times 10^{-6}$

Annealed temperature = $300^{\circ}C$

Annealed time = 2.5 hours.

Field current (Amp)	Magnetic Field strength (Gauss)	$\Delta R/R$	Magnetostriction $= -\frac{2}{3G} \left(\frac{\Delta R}{R} \right)$
0.4	350	-2.1075×10^{-5}	$+ 6.9554 \times 10^{-6}$
0.8	550	-2.9505 "	9.7376 "
1.0	750	-3.5827 "	11.8242 "
1.4	1000	-4.6365 "	15.302 "
3.0	2000	-5.058 "	16.693 "
4.0	2600	-5.4795 "	18.084 "
5.0	3300	-5.4795 "	18.084

CHAPTER - X

DTA RESULTS FOR AMORPHOUS IRON BORON RIBBON

DTA RESULTS FOR AMORPHOUS IRON-BORON RIBBON

The study of DTA results for the amorphous thin Iron Boron ribbon was taken to find the anomalies in the temperature vs time curve. The sample with compositions $Fe_{80}B_{20}$ and $Fe_{82}B_{18}$ was chosen for DTA to look at the curie temperature, glass transition temperature and crystallization phase transformation temperature.

The formation and resultant stability of amorphous alloys are important topics, both theoretically and technologically. The theoretical analysis of the factors controlling the ease of formation and the stability of the resultant amorphous alloys have been reviewed and discussed in many previous reviews, for example in the extensive general review by Jones^(10.1) from the thermodynamic view point by Turnbull^(10.2) and most recently by Takayama^(10.3). The ability of an alloy to be quenched into the glassy state is generally measured by the magnitude of the quantity,

$$\Delta T_g = T_m - T_g .$$

Where T_m and T_g are the melting and glass transition temperature respectively. In similar manner the stability of the glass after formation is generally measured by the magnitude of the quantity,

$$\Delta T_x = T_x - T_g .$$

Where T_x is the temperature for the onset of crystallization. Laborsky^(10.4) has clearly shown that the end-of-life, as for magnetic applications are concerned, corresponds to the onset of crystallization. At the onset of crystallization, the coercive force and losses increase and the remanence and permeability decrease, all at a very rapid rate for a small increase in temperature. The effect of alloying elements on the crystallization temperature has been studied by Naka^(10.5) in the series $Fe_{80-x}M_xP_{13}C_7$ and by Laborsky^(10.6) in $Fe_{80-x}Ni_xP_{14}U_6$ and $Fe_{80-x}Ni_xB_{20}$ alloys. Calorimetric measurements were made at a heating rate of 5 deg/min and 40 deg/min respectively; to determine T_x the temperature for the beginning of the crystallization exotherm. Laborsky found the glass transition temperature of $Fe_{80}B_{20}$ to be $441^{\circ}C$.

The DTA traces so obtained in Fig.(10.1) and Fig.(10.2), are all accompanied with exothermic Peaks. The temperature of the reference substance, which is thermally inactive, rises uniformly when heated, while the temperature of a sample changes anomalously when there is physical or chemical change of the active substance at a particular temperature, when there is an exothermic reaction.

For example, there is a peak in the temperature Vs time curve at the temperature of exothermic reaction and there is a (trough) in the temperature Vs time curve when there is endothermic

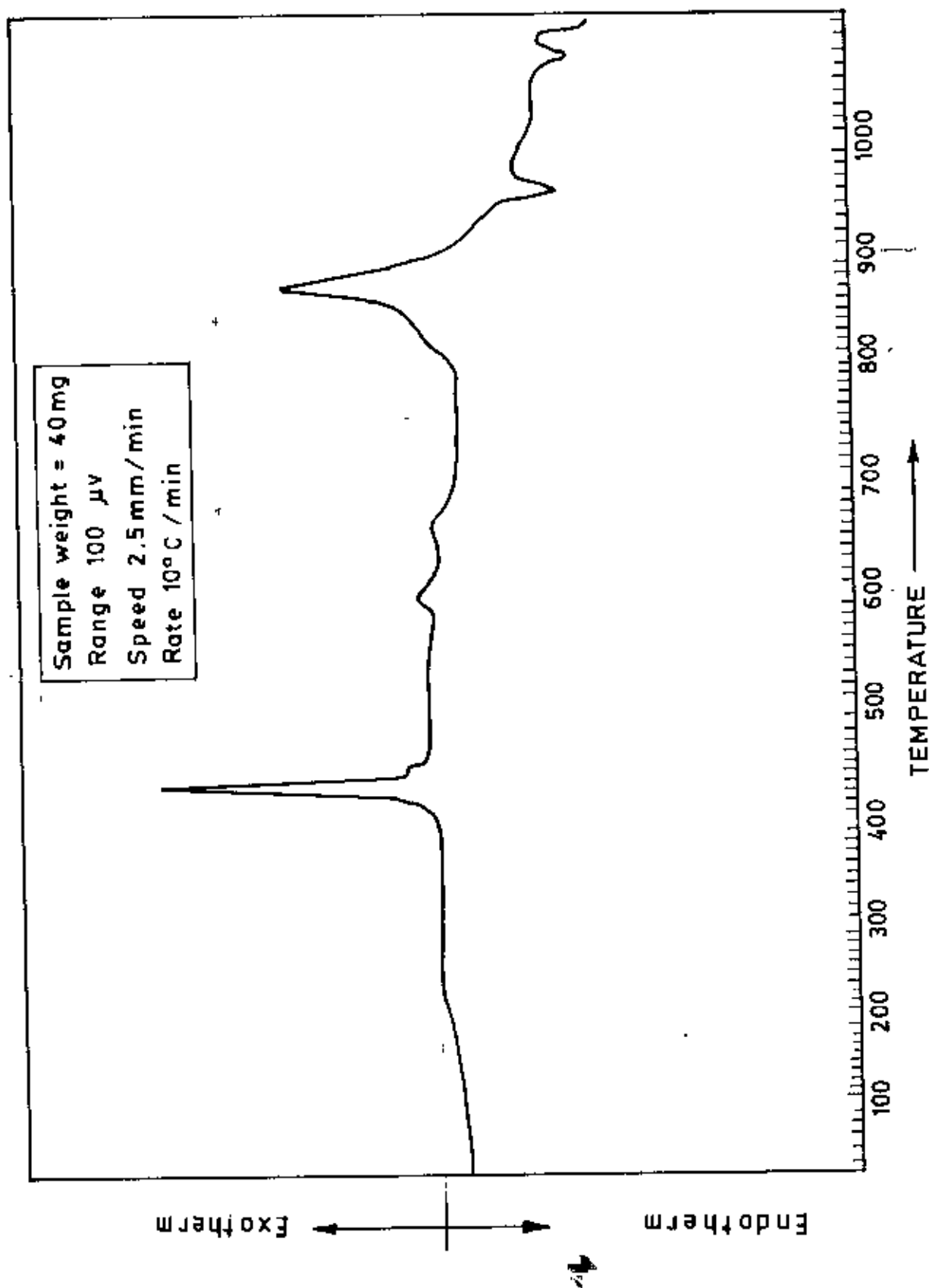


Fig. 10.1 DTA Trace of amorphous iron-boron ribbon (Fe₈₀B₂₀)

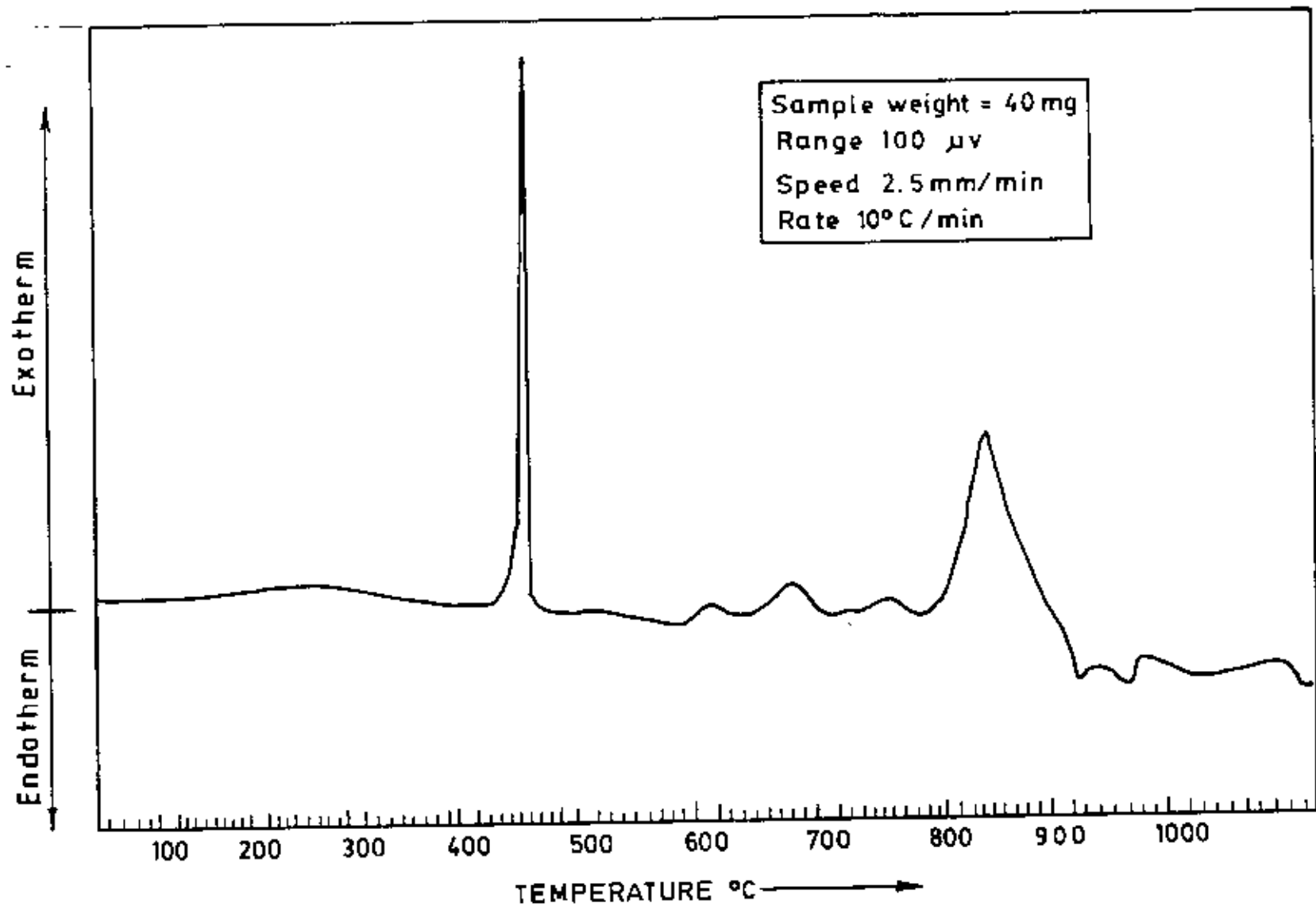


Fig.10.2 DTA Trace of amorphous iron - boron ribbon ($\text{Fe}_{82}\text{B}_{18}$)

reaction. In our case we too expected anomalies in the temperature Vs time curve, were observed. Compositions for both the $Fe_{82} B_{18}$ and $Fe_{80} B_{20}$. The DTA trace of amorphous iron-Boron ribbon of $Fe_{82} B_{18}$ are showed in Fig.(10.2). The two anomalies observed in the temperature Vs time curve were at $448^{\circ}C$ and $834^{\circ}C$ respectively. Similarly DTA Trace of amorphous iron-Boron ribbon of $Fe_{80} B_{20}$ are shown in Fig.(10.1), the anomalies in the temperature Vs time curve observed in this case where at $435^{\circ}C$ and $870^{\circ}C$ respectively. Both the anomalies showed peaks, which corresponds to release of heat at these temperatures due to crystallographic ordering of the atoms. We identify the first peak as glass transition temperature, which means the ribbons were transforming from Amorphous state to crystalline state. The second peak is considered to be due to the formation of multiphase poly crystalline material. In addition to these peaks we expected a very low minute truf corresponding to ferromagnetic transition. However, the low value of this anomaly could not be observed very clearly because of the relatively low sensitivity of the DTA system. Also the heating rate of 10 deg/min was too high for this observation.

Compositions	First peak glass transition temperature	Second peak crystallization phase transformation temperature
$Fe_{82} B_{18}$	$448^{\circ}C$	$834^{\circ}C$
$Fe_{80} B_{20}$	$435^{\circ}C$	$870^{\circ}C$

CHAPTER - XI

CONCLUSIONS

CONCLUSIONS

Amorphous Iron-Boron ribbon is a metastable form of condensed alloy, which has a great potential as a soft magnetic material. This material is magnetically soft having no magnetocrystalline anisotropy due to the absence of crystalline structure. This is also corrosion resistant because there is no grain and hence no grain boundary.

Since this material is obtained in the form of thin ribbons, it needs no further mechanical processing for the reduction of thickness, as in the case of silicon iron transformer core material, for high frequency use. However, since iron Boron is a metastable material its stability is affected by thermal and other agencies. This is a very important factor to be considered for its technological use.

Although this material is supposed to be isotropic due its glassy character, there is an induced anisotropy in the ribbon due to the preparation conditions. As a result, there is some induced magnetostriction in amorphous ribbons that determine the magnetic softness and the magnetization process of this material.

The present work is thus devoted to the study of the stability, change of magnetization and magnetostriction as caused by annealing at different temperatures. In general,

annealing causes the removal of local low instability in the amorphous ribbon by providing thermal vibrational energy to the atoms to overcome the small potential barriers, without crystallization. The removal of these strains, which are produced in the ribbons during preparation, causes change in the initial magnetization curves and also induced anisotropy and magnetostriction.

The study of magnetization, stability and magnetostriction in amorphous ribbons due to annealing is therefore, considered to be very important for future development and technological use of these materials. The preparation and characteristics of amorphous ribbons as a background information is thus described in the beginning of this thesis.

Three basic measurements have been done on amorphous iron-boron ribbons. These are differential thermal analysis, measurements of magnetization and measurements of magnetostriction.

Differential Thermal Analysis (DTA) is done by the standard DTA equipment to look for ferromagnetic transition and glass transition temperatures and stability. Since the specific heat anomaly for these alloys at the ferromagnetic ordering temperature is very small, these were not clearly manifested in the DTA. Accurate specific heat measurement

around curie temperature can only quantify these values. But high temperature specific heat measurement is a difficult task, and equipment for this measurement is not available in our laboratory at present. However, the DTA curves clearly show the glass transition temperature by peaks at 448°C for composition $\text{Fe}_{82}\text{B}_{18}$ and at 435°C for composition $\text{Fe}_{80}\text{B}_{20}$. There are also secondary peaks at 834°C for composition $\text{Fe}_{82}\text{B}_{18}$ and at 870°C for composition $\text{Fe}_{80}\text{B}_{20}$. These are interpreted as arising from phase separations.

Magnetization has been measured by vibrating sample magnetometer (V.S.M.) as a function of field for the compositions $\text{Fe}_{82}\text{B}_{18}$, $\text{Fe}_{81}\text{B}_{19}$ and $\text{Fe}_{80}\text{B}_{20}$. The measurements have been confined to room temperature only because of the unavailability of high temperature oven and low temperature cryostat. Specific magnetization is observed to be $183.26 \text{ Am}^2/\text{Kg}$ for iron boron ribbon with composition $\text{Fe}_{82}\text{B}_{18}$ at room temperature. Magnetization has also been measured for iron boron ribbon with composition $\text{Fe}_{82}\text{B}_{18}$ for different annealing temperatures from 50°C to 300°C . As is expected theoretically this annealing changes the initial magnetization curves, due to the change in domain wall stiffness, but does not change the saturation magnetization at high field. After annealing saturation magnetization is slightly changed and observed to be $190.64 \text{ Am}^2/\text{Kg}$ for $\text{Fe}_{82}\text{B}_{18}$ at annealing temperature 300°C .

Saturation magnetostriction has been measured by strain gauge-technique and observed to be 31.86×10^{-6} for composition $Fe_{82} B_{18}$ at room temperature. The effect of annealing on magnetostriction has also been measured using strain gauge and a systematic decrease of saturation magnetostriction is observed from its maximum value of 31.86×10^{-6} to 18.08×10^{-6} with increasing annealing temperature. This result is quite consistent with theoretical expectation, where magnetostriction is interpreted as arising due to the rotation of strain axes of the amorphous regions having induced technical anisotropy.

From the observations of magnetization and magnetostriction values after annealing at $300^{\circ}C$ it is concluded that the iron boron ribbon can be used over a long time at elevated temperature with out crystallization. Naturally, when used at a lower temperature the metastable state will sustain for much longer time.

Since the specimens are very thin, the free distortion of the specimens associated with domain wall rotations are constrained by the stiffness of the bonded strain gauge. Results obtained for magnetostriction therefore, are likely to be slightly lower than the actual values.

The other limitation is that the temperature variation of the magnetostriction values could not be measured for reasons mentioned earlier.

In future the continuation of this work with varied composition and varied temperatures will, therefore, be very useful for a deeper understanding of the mechanism of magnetostriction and its variation with annealing.

-oOo-

REFERENCES

CHAPTER - I

- 1.1 Soshim Chikazumi, 2nd printing, June, 1966,
in physics of magnetism.
- 1.2 M.A. Asgar, Vol.7(1984) Mechanical Engineering
Research Bulletin., BUEP, p.1.
- 1.3 F.E. Luborsky, Ferromagnetic materials, Vol.1
North-Hall and company, p-451 (1980)
- 1.4 B.d. Cullity, in Introduction to magnetic material.
- 1.5 D.U. Martin, 1967, in Magnetism in solids.
- 1.6 Fujimori, H., H. Morita, Y. obi and S. Ohta, 1977,
in Amorphous magnetism-II (eds. R.A. Levy and
R. Haseguwa) (plenum press, Newyork) p.393.
- 1.7 Chatelir H.Le. Bull. Soc. franc. mineral, 1887
10, 204.
- 1.8 M.A. Aggar, ph.D. Thesis, University of Southampton
(1970).

CHAPTER - II

- 2.1 Gubanov, A.I. 1960, FIZ. Tver. Te1.2, 502
- 2.2 Brenner, A.D.E. Couch and E.K. Williams, 1950, J Res,
Nat. Bureau standards. 44, 109.
- 2.3 Duwez, P.R.H. Willens and W. Klem ml, Jr, 1960,
J, Appl. phys. 31, 1136.
- 2.4 Miroshnichenko, L.S. and I.V. Sallii., 1959, Ind.Lab.
25, 1463 (in English) Fran Zavodskaya Lab, 25, 1398(1959)
- 2.5 Mader, S. and A.S. Nowick, 1965, Appl. phys. Lett. 7, 57
- 2.6 Pond. R. Jr. and R. Maddin, 1969, Trans. Met. Soc.
ALME 245, 2475.

- 2.7 Simpson, A.W. and D.R. Brambley, 1971. *Phys. Stat. Sol.(b)* 43, 291.
- 2.8 Sherwood, R.C., E.M. Gyorgy, H.S. chen, S.D. Ferris, G.Norman and H.J. Leamy 1975, *AIP Conf. Proc.* 24, 745.
- 2.9 Arai, K., N. Tsuya, A. Yamada, H. Shirae, H. Fujimori H.Saito and T. Masumoto, 1976, in *Rapidly quenched metals*, section 1 (eds. N.J. Grant and B.C.Giessen) (MIT Press, Cambridge, Mass.) p.489.
- 2.10 O'Hadley, R.C. 1977, in *Amorphous magnetism* (eds. R.A. Levy and R. Hasegawa) (plenum press, New York) p.379.
- 2.11 A.A. Asgar. Vol.7(1984) *Mechanical Engineering Research Bulletin.* (BUET) p.1.
- 2.12 Alben, R., J.I. Budnick and G.S.Cargill III, 1977, in *Metallic glasses*(eds. H.S. Leamy and J.J. Gilman) (American Society for metals, Metals Park, Ohio) Ch.12.
- 2.13 Felsch, W., 1970, *Z. Angew. Phys.* 29, 218.
- 2.14 Shimada, Y. and H. Kojima, 1976, *J. Appl. phys.* 47, 4156.
- 2.15 Wright, J.G., *IEEE Trans. Magnetics* MAG-12, 95.
- 2.16 Becker, J.J. E.E. Luborsky and J.L. Walter, 1977, *IEEE Trans. Magnetics* MAG-13, 988.
- 2.17 Durand, J. 1977, in *Amorphous magnetism II* (eds. R.A.Levy and R.Hasegawa) (Plenum Press, NewYork)p.305.
- 2.18 Durand, J. and M. Yung. 1977, in *Amorphous magnetism II* (eds. R.A. Levy and R.Hasegawa) (Plenum Press, New York) p.275.
- 2.19 Mizoguchi, T.K. Yamauchi and H. Miyajima 1973, in *Amorphous magnetism* (eds. H.O. Hooper and A.M. De Graff) (Plenum, New York) p.325.

- 2.20 Fujimori, H.H. Morita, Y. obi and S. Ohta. 1977, in *Amorphous magnetism II* (eds. R.A. Levy and R. Hasegawa) (Plenum Press, New York) p.393.
- 2.21 Mizoguchi, T, 1976 ALP Conf. Pr g. 34,286.
- 2.22 Haris, R.M. Plischke and M.J. Zuckerman 1973. *Phys. Rev. Lett.* 31,160.
- 2.23 Gubernatis, J.E. and P.L. Taylor, 1973. *Phys. Lett.* A43, 211.
- 2.24 Handrich, K. 1969 *Phys. Stat. SOL.* 32,K55.
- 2.25 Kobe, S. 1977. in *Amorphous Magnetism II* (eds. R.A. Levy and R. Hasegawa) (Plenum Press New York) pp.529-534.
- 2.26 Montgomery, C.G. J.I. Krugler and R.M. Stubbs,1970.*Phys. Rev. Lett.* 25,669.
- 2.27 Kaneyoshi, T. 1973, *J. Phys. C.*6,LI9.
- 2.28 Richter, J.K. Handrich and J. Schreiber 1975 *Phys. Stat. SOL(b)* 68,K61 .
- 2.29 Yamada, H. and E.P. Wohlfarth, 1975, *Phys. Lett.* 51A,65.
- 2.30 Chatelier, H.Le. *Bull. Soc. franc. mineral* 1887, 10,204.
- 2.31 Na Kamura, H.H and Attal, L.M. *Proc. fourth carbon conf.* Pergamon Press, London 1960,625.
- 2.32 Brook J.D. ad Taylor G.h. 1 65 carbon 3,185.
- 2.33 Dubois J, Agace C and white J.L. 1970,*J. Metallography.* 3,337.
- 2.34 Honda H, Kimura H. and Sanada, Y.1971 carbon,9.695.
- 2.35 Marsh H, Foster, J.M. Hermon G and Iley M.1973, *Fuel*, 52,234.

CHAPTER - III .

- 3.1 Cargill III, G.S. 1975a, *Solid state physics* 30, 227.
- 3.2 Cargill III, G.S. 1976, in *Rapidly quenched metals*, Section 1 (eds, N.J. Grant and B.C. Giessen) (MIT Press, Cambridge, Mass) p.293.
- 3.3 M.A. Asgar, VOL (1984) *Mechanical Engineering Research Bulletin (BUET)* p.1.
- 3.4 Brenner, A. *Electrodeposition of alloys* Academic Press New York (1963)
- 3.5 B.C. Giessen and C.N.J. Wagner, *Liquid Metals, chemistry and physics*, New York 633(1972)
- 3.6 Brenner A. D.E. Couch and E.K. Williams *J.Res. Nat. Bureau Standards* 44, 109,(1950)
- 3.7 Duwez, P.R.H. Willens and W. Klement, Jr. *J. Appl. physics*, 31,1136(1960).
- 3.8 Poud, R.Jr. and R. Maddin, *Trans. Met. Soc. AIME* 245, 8475(1969)
- 3.9 D.Kavesh, 'Metallic glasses' *ASI*(275,1970).
- 3.10 F.E. Luborsky, *Ferromagnetic materials Vol., North-Hall and Company*, p-451(1980)

CHAPTER - IV

- 4.1 Mizoguchi, T.K. Yamauchi and H.Miyajima 1973, in *Amorphous magnetism* (eds, H.O.Hooper and A.M. De Graff) (Plenum, New York) p.325.
- 4.2 Mizoguchi, T.K. Yamauchi and H. Miyajima, 1974, *Proc. Int. Conf. Magnetism, Vol.2 (Moscow Aug.1973)* (Nauka, Moscow).

- 4.3 Gubanov, A.I. 1960, Fiz. Tver. Tel.2.502
- 4.4 Felsch, W, 1970, Z. Angew. Phys. 29,218.
- 4.5 Wright, J.G. 1976, IEEE Trans. Magnetics MAG-12,95.
- 4.6 Shimada, Y. and H. Kojima, 1976. J. Appl. phys.47,4156
- 4.7 Becker, J.J., F.E. Luborsky and J.L. Walter, 1977, IEEE Trans. Magnetics MAG-13,988.
- 4.8 Fujimori, H., H. Morita, Y. Ichi and S.Ohta, 1977, in Amorphous magnetism II (eds. R.A. Levy and R. Hasegawa) (Plenum Press, New York) p.393.
- 4.9. W.P. Wolf: phys. Rev. 108, 1152(1957)
- 4.10 Dwight, K., N. Menyuk and D.O. Smith, 1958, J. Appl. phys. 29.491.
- 4.11 M.A. Mazid and M.A. Chowdhury, "Design and construction of a Foner type vibrating sample Magnetometer, AECD/MMD/1. June, 1986 (Bangladesh).
- 4.12 S.Foner, Rev. Sci. Instr. 27. 548(1956)
- 4.13 S. Foner, Bull. Am. phys. Soc. Ser.II.2,128(1957).
- 4.14 Van Dosterhout, G.W., 1965, Appl.Sci. Res.B6 101
- 4.15 S.Foner, 1959, Rev. Sci. Instr. 30. 548
- 4.16 Pacyna, A.W., 1982 General theory of the signal induced in a vibrating magnetometer. J.phys.E:Sci., Instrument Vol-15,1982,page.663.
- 4.17 Zijlstra, H., Experimental Methods in Magnetism Vol-2; (Wiley New York 1967).
- 4.18 A. Arrott and J.E. Goldman, Rev. Sci. Instr.28,99(1957).
- 4.19 D.K.Stevens and J.H. Crawford, Jr. phys.Rev.92, 1065(1953).
- 4.20 S.Foner and J.O. Artman, J.Appl. phys. 29,443(1958).

CHAPTER - V

- 5.1 M.A. Asgar, Proceeding of the international Conference on physics and energy for developmet, Dhaka, 26-19 Jan. 1985, 153p.
- 5.2 J.H. Van Vleck *phys. Rev.* 52, 1178(1938).
- 5.3 L. Neel, *Ann de physique*, 3, 137(1948).
- 5.4 W.P. Mason and J.A. Lewis, *Phys. Rev.*, 94, 1439(1954).
- 5.5 J.E. Goldman, *phys. Rev.* 72, 529(1947).
- 5.6 M.A. Asgar, ph.D. Thesis, University of Southampton (1970).
- 5.7 H. Nagaoka, *Phil. Mag.* 37, 131(1894).
- 5.8 H.P. Rooksby and J.F.M. Willis, *Nature*, 172, 1054(1953).
- 5.9 R.M. Bozorth and R.W. Hamming, *phys. Rev.* 83, 1239(1921).
- 5.10 E.W. Lee and M.A. ASGAR, *PHYS. Rev. Letters* 22, 1436(1969).
- 5.11 R.C. O'Handley and C.P. Chou, *J. Appl. phy.* 49, 1659(1978).
- 5.12 E.R. Callen and H.B. Callen, *phys. Rev.* 129, 578(1963).
- 5.13 Sherwood R.C. Gyorgy Ef, Chen HS, Ferris SD, Norman-G and Leamy HJ 1974 AIP Conf. Proc. 24, 745-6.
- 5.14 Luborsky EE 1976 AIP Conf. Proc. 29, 209-10 - 1977 *Mater, Sci. Engng* 28, 139-44.
- 5.15 N. Von Akaiov, *ZS.F. Physics*, 57, 249(1928).
- 5.16 C. Kittel and J.H. Van Vleck, *Phys. Rev.* 118(No.5), 1231(1960).
- 5.17 L. Neel, *Proc. Int. Conf. on Theoretical physics Tokyo 1954*, p.701.

- 5.18 E.W. Lee, Proc. phys. Soc. 84, 093(1964).
- 5.19 R.R. McLintock, Rev. Sci. Inst. 30,715(1959).
- 5.20- R.D. Greenough, ph.D. Thesis, Sheffield University, 1960.
- 5.21 R.Birss and E.W.Lee, J. Sci. Inst. 37,225(1960).
- 5.22 H. Wilkinga, De Ingenieur, 73, 103(1961)(in Dutch).

CHAPTER - VI

- 6.1 Chatelier, H.Le., Bull. Soc. franc. mineral, 1887, 10,204.
- 6.2 Nokamura, H.H. and Atlas, L.M., Proc. fourth carbon conf., Pergamon Press, London, 1960, 625.
- 6.3 Hossain. T. and Dollimore J., 1981, Chemical Engineering Research Bulletin BUET,Dhaka,5,25.
- 6.4 Hossain. T., 1983, J. Bangladesh Academy of Science, 7 (No.1 and 2),8.
- 6.5 Hossain,T, and Jahan, T.S. 1986, Indian Journal of Physics.
- 6.6 Podder, J. A.Phil thesis, BUET,Dhaka,1986.
- 6.7 Graham, S.G. ph.D. Thesis, Salford University, England, 1974.
- 6.8 Dubois J, Agace C and White J.L.,1970, J. Metallography, 3,337.
- 6.9 Lewis, I.C. and Edstrom, T., J.org. Chem, 1963,28,2050.

CHAPTER - VII

- 7.1 A. Arrot and J.E. Goldman, Rev. Sci. Instr.28, 99(1957).
- 7.2 D.K. Stevens and J. II Crawford, Jr. phys. Rev.92. 1065(1953).

- 7.3 S. Foner and J.O. Artman, *J. Appl. Phys.* 29, 413(1958).
- 7.4 M.A. Mazid and M.A. Chowdhury, "Design and Construction of a Foner type vibrating sample magnetometer, AECD/MMD/1, June, 1986(Bangladesh).
- 7.5 Van Oosterhout, G.W. 1965, *Appl. Sci. Res.* B6 101
- 7.6 S. Foner 1955, *Rev. Sci. Instr* 27. 578.
- 7.7 M.A. Asgar, ph.D. Thesis, university of Southampton (1970).
- 7.8 R.D. Greenough, ph.D. Thesis, University of Sheffield (1966).
- 7.9 E.W. Lee and M.A. Asgar *Proc. Roy. Soc. London* A326, 73(1970).
- 7.10 Y. Shirakawa and I.Oguma, *Sci. Rep. Tohoku University* A188, 532(1966).
- 7.11 *Neel Ann. de physique* 3, 137(1948).
- 7.12 Pearson *Proc. phys. Soc.* 74, 505(1959).
- 7.13 Pearson, Private Communication to slonczewski) 1961.
- 7.14 Pearson and Harbour Private Communication to Solonczewski, 1961.
- 7.15 Dr. M.D. Wilding, Private Communication.
- 7.16 Dr. H. Harper, Private Communicaton.
- 7.17 H. Wilkinga, *De. Ingenieur*, 73, 103(1961)(in Dutch).

CHAPTER - VIII

- 8.1 M.A. Mazid and M.A. Chowdhury, "Design and Constructon of a Foner type vibrating sample magnetometer, AECD/MMD/1, June, 1986(Bangladesh).

- 8.2 Bd. Cullity, in *Introduction to magnetic material*.
- 8.3 Soshim Chika Zumi, 2nd printing, June, 1966, in *Physics of magnetism*.
- 8.4 O. Wight, K.N. Menyuk, and D.O. Smith, 1958, *J. Appl. phys.* 29, 491..
- 8.5 Mizoguchi, J.K. Yamauchi and H. Miyajima, 1974, *Proc. Int. Conf. Magnetism, Vol. 2 (Moscow Aug. 1973) (Nauka, Moscow)*.
- 8.6 Zij Istra, H., *Experimental Methods in magnetism Vol-2; (Wiley New York 1967)*.
- 8.7 S. Foner, *Bull. Am. phys. Soc. Ser. II.* 2, 128(1957).
- 8.8 W.P. Wolf: *phys. Rev.* 108, 1152(1957).

CHAPTER - IX

- 9.1 M.A. Asgar, ph.D. Thesis, University of Southampton (1970).-
- 9.2 E.W. Lee and M.A. Asgar, *phys. Rev. Letters* 22, 1436(1969).
- 9.3 Lubornky EE 1976 AIP Conf. Proc. 29, 209-10-1977 *Mater, Sci. Eng.* 28, 139-44.
- 9.4 R. Birss and E.W. Lee, *J. Sci. Inst.* 37, 225, (1960).
- 9.5 J.E. Goldman, *phys. Rev.* 72, 529(1947).
- 9.6 R.M. Bozorth and J.G. Walker, *phys. Rev.* 88, 1209(1952).
- 9.7 E.W. Lee and R.R. Birass, *Proc. Phys. Soc.* 78, 391(1961).
- 9.8 H.P. Rooksohy and B.T.M. Willis, *Nature* 172 1054(1953).
- 9.9 Soshim Chika Zumi, 2nd printing, June, 1966, in *physics of magnetism*.
- 9.10 B.D. Cullity in *Introduction to magnetic material*.

CHAPTER - X

- 10.1 Jone's, H., 1973, Rep. Prog. phys. 36,1425.
- 10.2 Turnbull. D., 1974, J. de. physique 35,c4-1.
- 10.3 Takayama, S., 1976, J. Materials Sci. 11, 164.
- 10.4 Luborsky, F.E. and J.L. Walter, 1977a, IEEE Trans. Magnetism MA3-13, 953.
- 10.5 Naka, A., S. Tomizawa, T. Watanabe and T. Masumoto, 1976, in Rapidly quenched metals, section 1 (eds. N.J. Grant and B.C. Giessen)(MIT Press, Cambridge, Mass.) p.273.
- 10.6 Luborsky, F.E., 1977a Materials Sci.Eng.28,139.
- 10.7 Chen, H.S, R.C. Sherwood, H.J. Leamy and E.M.Gyorgy, 1976, IEEE Trans. Magnetism MAG-12,933.
- 10.8 Masumoto, T. and Y. Waseda, H. Kimura and A. Inoe. 1976, Sci. Repts. Res. Insts. Tohoku University A2b,21
- 10.9 Coleman.E., 1976, Materials Sci. Eng. 23,161.

